Synthesis, characterization and testing of nano-structured particles for effective impact modification of glassy amorphous polymers

BY

Andries Jakobus Petrus van Zyl

Dissertation presented for the Degree of Doctor of Philosophy

(Polymer Science)

at the

University of Stellenbosch

Promoter:
Bert Klumperman

Co-promoter:
Ronald D. Sanderson

Stellenbosch
December 2003

Declaration

I, the undersigned, hereby declare that the work contained in this dissertation is my own original work and that I have not previously in its entirety or in part submitted it at any university for a degree.

Abstract

The synthesis of structured nanoparticles, in particular core/shells, is of great technological and economical importance to modern materials science. One of the advantages of structured particles is that they can be synthesized with either a solid core (albeit soft or hard) or a liquid core (of varying viscosity). This adds to the versatility of structured particles and their relevance to a majority of industrial and commercial end-applications.

The synthesis of core/shell particles with liquid cores was investigated for the effective impact modification of glassy amorphous polymers. Polybutyl acrylate was chosen as the shell due to its rubbery nature. Hexadecane functioned as the core oil and facilitated osmotic stability by being a suitable hydrophobe for the miniemulsion synthesis. Polymer synthesis was preceded by the prediction of particle morphology by using thermodynamic prediction models.

Core/shell particles with liquid cores were synthesized via miniemulsion polymerization. This resulted in the direct introduction of core-oil and monomer into the miniemulsion droplets. Polymerization was achieved *in situ*, resulting in the formation of particles with the desired morphology. For additional strength, stability and matrix mixing capabilities, methyl methacrylate (MMA) was grafted onto the initial core/shell particles. The obtained morphology was in contradiction with the predicted morphology, thus pointing to strong kinetic influences during the polymerization process. These influences could be attributed to surface anchoring of polymer chains due to the initiator (KPS) used, the establishment of the polymerization locus as well as the increase in viscosity at the polymerization locus. To test these influences a surface-inactive initiating species (AIBN) and an interfacial redox initiating species (cumyl hydroperoxide/Fe^{2+}) were used. Use of the former resulted in the formation of solid polymer particles due to homogeneous polymerization throughout the droplet, thus leading to an inverse core/shell morphology as a result of thermodynamic considerations.

The redox initiator promoted kinetic influences as a result of fast polymerization kinetics at the droplet/water interface. This, as well as the increase in viscosity, facilitated the production of core/shell particles.

To obtain core/shell particles with the desired size, the influence of surfactant concentration was investigated. Capillary hydrodynamic fractionation (CHDF) was used to determine the particle size of the initial core/shell particles as well as the size of the MMA-grafted core/shell particles. The area stabilized per surfactant molecule was calculated stoichiometrically and compared to "classical" miniemulsion results, i.e. data generated from the synthesis of polymeric latexes in the presence of a hydrophobe, but at a much lower hydrophobe:monomer ratio than was used here. The influence of methanol as well as the possibility of scaling-up the process was also investigated.

The study was further expanded to the investigation of living miniemulsion polymerization techniques to control the molecular architecture of synthesized core/shell latexes. The influence of different RAFT agents, initiators and monomers were investigated on the core/shell formation properties of the investigated systems. The combined effects of establishing the polymerization locus as well as increased polymerization kinetics, thus increasing the viscosity at the polymerization locus, lead to the successful formation of liquid-filled core/shell particles.

To conclude, the ability of the synthesized core/shell particles to induce impact modification in glassy amorphous polymers was investigated. Results showed that incorporation of these particles could effectively modify the intrinsic properties of the investigated polymers, resulting in a brittle-to-ductile transition. Improved impact results of the investigated glassy matrix were obtained.

Keywords: core/shell, liquid-filled, RAFT, miniemulsion, impact modification

Opsomming

Die sintese van gestruktureerde nano-partikels, meer spesifiek kern/skil partikels, is van onskatbare tegnologiese en ekonomiese belang vir moderne materiaalkunde. Een van die voordele van hierdie tipe partikels is dat sintese kan geskied met 'n soliede kern (hard of sag) of vloeistofkern (met wisselende viskositeit). Dit dra by tot die veelsydigheid van gestruktureerde partikels en dus tot grootskaalse aanwending in industriële en kommersiële toepassings.

Die sintese van kern/skil partikels met vloeistofkerne is ondersoek met die oog op effektiewe slagsterkte modifikasie van glasagtige amorfe polimere. Polibutielakrilaat is gekies as skil-polimeer op grond van sy rubberige voorkoms. Heksadekaan moes funksioneer as die kern-olie, maar het ook bykomende osmotiese stabiliteit verleen tydens die miniemulsie-polimerisasie proses. Dit is as gevolg van die gepaste hidrofobiese eienskappe van heksadekaan. Polimeer sintese is voorafgegaan deur die voorspelling van partikel morfologie met behulp van termodinamies gebaseerde voorspellingsmodelle.

Kern/skil partikels is gesintetiseer deur middel van 'n miniemulsie-polimerisasie reaksie wat die direkte inkorporering van kern-olie en monomeer in die miniemulsie-druppel teweeg bring. Polimerisasie vind *in situ* (*lat.* vir in die oorspronklike plek, m.a.w. binne-in die druppel) plaas en lei tot die vorming van partikels met die gewenste morfologie. Metielmetakrilaat is ge-ent op die oorspronklike kern/skil partikels om addisionele sterkte, stabiliteit en vermenging met die matriks polimeer te bewerkstellig. Die verkrygde morfologie is teenstrydig met die voorspelde morfologie, wat dus die teenwoordigheid van sterk kinetiese invloede aandui. Hierdie invloede kan toegeskryf word aan die oppervlak-aktiewe afsetter (KPS, kaliumpersulfaat) wat gebruik is, die daarstelling van die polimerisasie lokus asook die toename in viskositeit by die lokus van polimerisasie. Om hierdie invloede te toets is 'n oppervlak-onaktiewe afsetter (AIBN, asobisisobutironitriel) en intervlak redoks-afsetter (kumielhidroperoksied/Fe^{2+}) gebruik.

Gebruik van eersgenoemde het die vorming van soliede partikels teweeg gebring. Dit is as gevolg van homogene polimerisasie in die druppel en dus die ontstaan van omgekeerde kern/skil partikels weens termodinamiese oorwegings. Die redoks-afsetter het egter die kinetiese oorwegings bevoordeel as gevolg van vinnige polimerisasie-kinetika by die druppel/water intervlak. Dit, tesame met die toename in viskositeit, maak die produksie van kern/skil partikels moontlik.

Vir die verkryging van kern/skil partikels met die gewenste partikelgrootte is die invloed van die seep konsentrasie ondersoek. CHDF (*eng.* capillary hydrodynamic fractionation) is gebruik om die partikelgrootte van die oorspronklike kern/skil partikels, sowel as dié ge-ent met metielmetakrilaat, te bepaal. Die area gestabiliseer per seepmolekule is bereken d.m.v. stoichiometrie en vergelyk met "klassieke" miniemulsie data, d.i. data verkry deur die sintese van latekse in die teenwoordigheid van 'n hidrofoob, maar teen 'n baie laer hidrofoob:monomeer-verhouding as wat hier gebruik is. Die invloed van metanol, asook die moontlikheid om die reaksie op te skaal, is ondersoek.

Die studie is verder uitgebrei om die invloed van lewende miniemulsie-polimerisasie tegnieke in te sluit, om sodoende beheer uit te oefen oor die molekulêre argitektuur van die gesintetiseerde latekse. Die invloed van verskeie RAFT (*eng.* reversible addition-fragmentation chain transfer) agente, afsetters en monomere op die kern/skil vormingsmoontlikhede van die bestudeerde stelsels, is ondersoek. Die gesamentlike effek van die daarstelling van die polimerisasie lokus en dus die verhoging van die viskositeit by die lokus, lei tot die suksesvolle vorming van vloeistof-gevulde kern/skil partikels.

Laastens is die invloed van die gesintetiseerde kern/skil partikels op die slagsterkte van glasagtige amorfe polimere ondersoek. Resultate dui daarop dat die insluiting van hierdie partikels kan lei tot die effektiewe verandering van die intrinsieke eienskappe van die bestudeerde polimere, en dus 'n oorgang van bros na rekbaar kan veroorsaak. 'n

Verbetering in die slagsterkte resultate van die bestudeerde glasagtigte matriks is ook waargeneem.

Sleutelwoorde: kern/skil, vloeistof-gevulde, RAFT, miniemulsie, slagsterkte

To Susan

But we in it shall be remember'd;
We few, we happy few, we band of brothers;
(William Shakespeare, King Henry V, Act IV, Scene III)

Acknowledgements

Writing acknowledgements should be an easy task but the fear of forgetting (athazagoraphobia) to acknowledge someone, upsets the triviality of the matter. Therefore, I need to start off with the persons that were inadvertently left out. I'm very sorry, but nevertheless very thankful. You have to keep in mind that my path crossed with numerous persons during the past four years, which makes it impossible for me to list everyone that was involved. For the rest, here goes!

The most important person in this study is, without a doubt, my promoter Bert Klumperman. Thank you very much for this opportunity, your guidance as well as organizing necessary meetings and project funds. I have learned a great deal from you during the past four years, not only on a scientific level, but also on a personal level. It always amazed me how calm you could be, even though I felt as if nothing was going my way. My main sponsor, the Dutch Polymer Institute (DPI), is also gratefully acknowledged for the financial contribution to the project.

I would like to thank the numerous persons that I was involved with during my visits to the Netherlands. A special word of thanks goes out to Cor and Henelia Beyers, Madri and Marcelle, whose hospitality knew no ends. For TEM analysis I have to thank Joachim Loos, especially for being able to help me at very short notice. Then Jules Kierkels and Bernard Schrauwen are acknowledged for help in preparing and testing samples at the Faculty of Mechanical Engineering, Technical University of Eindhoven. Also to Rutger "Tulptoeter" Bosch a special word of thanks for spending time in South Africa and working on the project.

Closer to home I would like to thank my co-promoter, Prof Ron Sanderson. Thank you very much for the opportunity to study at this world-class institution. The staff at Polymer Science, Aneli, Calvin, Erinda, Johan and Margie, is sincerely thanked for their help and assistance. Deon de Wet-Roos is thanked for his invaluable discussions and

ideas, which definitely made a difference to the project. The Division of Polymer Science as well as the NRF are also thanked for additional funding during my project.

Mohamed Jaffer of the University of Cape Town is thanked for the many hours spent doing TEM analyses. Although results were sometimes few, I always enjoyed the company and the friendly chats we had while staring into the glow of the TEM. Chris Ferguson of the Key Centre for Polymer Colloids, University of Sydney, is acknowledged for CHDF analysis.

Then I would also like to acknowledge Cynthia Dixon from MegaVision for granting me permission to use the image on the cover of the thesis. The image was taken by Richard Salas with a MegaVision T32 digital back mounted on a Sinar 4x5 view camera.

On a more personal note I would like to thank all my friends, especially those whom I have closely worked with during the past four years. There was never a dull moment, always strong competition and definitely a lot of friendly bantering between us all. However, there were always encouraging words in desperate times. Mention must be made of my special friends Ewan and Tanya, Chantel, Charl, Dessi, Jaco, James, Jasper, Jerrie, Malan, Martina, Matthew, Peter, Sven and Valerie. Thanks for all the enjoyable times and encouragement.

To my parents, many thanks for providing me with all the opportunities and guidance. Then last, but definitely not least, I want to thank my wife, Susan. Thank you for your endless support, encouragement, tons of love and for being you!

Table of contents

Chapter 4: The role of surfactant in controlling particle size and stability in the miniemulsion polymerization of polymeric nanocapsules

Glossary

Abbreviations

AFM	atomic force microscopy
AIBN	2,2'-azobis(isobutyronitrile)
ATRP	atom transfer radical polymerization
BMA	butyl methacrylate
BzA	benzyl acrylate
CDB	phenyl 2-propyl dithiobenzoate (cumyl dithiobenzoate)
CHDF	capillary hydrodynamic fractionation
CHP	cumyl hydroperoxide
CMC	critical micelle concentration
CVADTB	4-cyano-4-((thiobenzoyl)sulfanyl)pentanoic acid
D	decane
DCA	dynamic contact angle
DCM	dichloromethane
DDI	distilled deionized
DIBTC	S-1-dodecyl-S'-(R,R'-dimethyl-R-acetic acid) trithiocarbonate
DIPB	1,3-diisopropenylbenzene
EDTA	ethylenediaminetetraacetic acid, disodium salt
EGDMA	ethylene glycol dimethacrylate
HD	hexadecane
iniferter	initiator-transfer agent-terminator
Is	impact strength
KOH	potassium hydroxide
KPS	potassium persulfate
MeOH	methanol
MMA	methyl methacrylate
NMP	nitroxide-mediated polymerization

NMR	nuclear magnetic resonance
O	1-octanol
OO	olive oil
PBA	poly(butyl acrylate)
PBMA	poly(butyl methacrylate)
PC	polycarbonate
PDI	polydispersity
PET	polyethylene terephthalate
PMMA	poly(methyl methacrylate)
PO	paraffin oil
PPPDTA	phenyl 2-propyl phenyl dithioacetate
PS	polystyrene
PVOH	polyvinyl alcohol
RAFT	reversible addition fragmentation chain transfer
RVE	representative volume element
SANS	small-angle neutron scattering
SAXS	small-angle x-ray scattering
SDS	sodium dodecyl sulfate
SEC	size-exclusion chromatography
SEM	scanning electron microscopy
SFS	sodium formaldehyde sulfoxylate
SMBS	sodium metabisulfite
SO	silicone oil
Sty	styrene
TEM	transmission electron microscopy
THF	tetrahydrofuran

Notations

k_p^1	propagation rate coefficient for the leaving group (R) to monomer
$\bar{M}_n$	number average molar mass

$\bar{M}_{n,\,theory}$	theoretical number average molar mass
$\bar{M}_w$	weight average molar mass
$\bar{n}$	average number of radicals per particle
$[chains]$	number of polymer chains produced
$[I]$	initiator concentration
$[I]_0$	initial initiator concentration
$[I]_w$	initial concentration of initiator in the aqueous phase
$[M]$	monomer concentration
$[M]_0$	initial monomer concentration
$[M]_w$	monomer concentration in the aqueous phase
$[radical]$	radical concentration
$[RAFT]$	RAFT concentration
$[RAFT]_0$	initial RAFT concentration
$[SR]$	concentration of the transfer agent
A	area
A_{surf}	area per surfactant molecule
C_m	concentration of monomer in particles
C_p	concentration of the leaving free radical in the particle
C_{tr}	transfer constant
C_w	concentration of the leaving free radical in the aqueous phase
D	diameter
D	diffusion coefficient of a low molar mass species in a semi-dilute polymer solution
d	relevant diffusion distance
Da	Damköhler number
D_L	diffusion coefficient for long free radicals
D_S	diffusion coefficient for short free radicals
D_w	diffusion coefficient in water
E	total interfacial energy
E_0	interfacial energy

f	aperture radius (Chapter 3)
f	efficiency factor (Chapter 5)
F	force at zero immersion depth
f_{entry}	efficiency for entry
f_I	initiator efficiency for addition of initiator radicals to monomer
FW_M	molar mass of the monomer
FW_{RAFT}	molar mass of the RAFT agent
G	surface free energy
ID	interparticle distance
k_{add}	addition rate coefficient
k_{-add}	reverse addition rate coefficient
k_d	dissociation rate constant
k_{dm}	coefficient for desorption of a monomeric free radical (exit) from a particle
k_{frag}	fragmentation rate coefficient
k_p	propagation rate coefficient
k_p(BA)	propagation rate coefficient of butyl acrylate
k_p(Sty)	propagation rate coefficient of styrene
$k_{p,aq}$	propagation rate coefficient in the aqueous phase
k_t	termination rate constant
$k_{t,aq}$	termination rate coefficient in the aqueous phase
k_{tLL}	rate coefficient for termination between two long free radicals
k_{tr}	transfer rate coefficient
k_{tSL}	rate coefficient for termination between short and long free radicals
k_{tSS}	rate coefficient for termination between two short free radicals
k_β	fragmentation rate coefficient
$L(r,t)$	concentration of long free radicals
M	monomer
$M(r,t)$	concentration of the monomer
M_{surf}	molar mass of the surfactant

N_A	Avogadro's number
N_p	number of particles
$N_{surf\ chains}$	number of surfactant chains
o/w	oil/water
p	perimeter of the sample
$P(exit)$	probability of exit
$P^{\cdot}$	propagating polymeric radicals
R	droplet radius
r	radius
$R^{\cdot}$	low molar mass radicals
R_h	hydrodynamic radius of droplet
R_p	propagation rate
r_s	swollen radius of particle
R_{tr}	transfer rate
S	surfactant to monomer weight ratio
$S(r,t)$	concentration of short free radicals
S_i	spreading coefficient
t	time
T_g	glass transition temperature
V	volume
V_f	volume fraction of inclusions
W_m	weight of monomer
W_{surf}	weight of surfactant
x	fractional conversion
Z	chain length at which short chains become long chains
z	lowest number of monomer units required for the oligomer to be surface active
Π	osmotic pressure
α	constant for the stacking of rubber spheres in a matrix
ε_b	strain to break
γ	surface/interfacial tension

γ_l	surface tension of the liquid
γ_{sl}	solid/liquid interfacial tension
γ_{sv}	solid/vapor interfacial tension
λ	strain
θ	angle
θ_c	contact angle
θ_{op}	contact angle between the oil and polymer
θ_{ow}	contact angle between the oil and water
ρ	average density of a droplet
ρ_m	short-chain radical concentration
σ_t	stress
σ_Y	yield stress
υ_P	fractional value of polymer P
υ_Q	fractional value of the core polymer

List of figures

List of schemes

List of tables

Chapter 1

Introduction

1.1 General introduction

The world, as we see it, is becoming bigger, better and faster every single day and thus requires improved materials to keep up with increasing technological demands. However, it is not only technological evolution but also ecological regress that necessitates the search for alternative materials which will facilitate conservation of precious resources. One way of doing this is to strengthen existing materials or to modify their properties, thereby allowing more expensive strong materials (*e.g.* metals) to be replaced. A quick look at what is currently happening on the research front reveals the following: biopolymers are being used in functional tissue engineering of cardiovascular substitutes;[1] nanotubes, which are stronger than steel and able to conduct electricity, are being synthesized;[2] and polyLEDs are being actively researched by Philips as possibilities for high-tech displays and conventional electronic devices,[3] to name but a few. Although such research is very costly, tremendous cost cuts in the end products should be realized with further development, refinement and acceptance (by the consumer market) of these endeavours.

The term "nano", roughly translated from Greek as "extremely small" (or, in scientific terms, 10^{-9}), has recently taken the scientific community by storm. As this author can rightfully quote from a recent issue of C&EN[4] "These days, you can't swing a dead cat without hitting something with the word "nano" on it.". This will probably become the next catchphrase after Richard Feynman's[5] much quoted (and therefore not repeated here) historical words back in 1959. But regardless of the fact that scientists see this "little" word as a selling point for obtaining precious project funds, the reality is that there is much more to it than bargaining power. By being able to modify material

properties microscopically (or on the nanoscale) it is also possible to modify the macroscopic properties of that material.

This concept has been extensively investigated by the Faculty of Mechanical Engineering, Materials Technology, at the University of Eindhoven.[6] Through the introduction of complex models it was possible to study and predict the outcome of deformation behavior in heterogeneous polymer systems, i.e. polymeric systems modified by inclusions, albeit polymeric, rubbery or a combination. This research group was particularly interested in investigating the low strain to break and toughness of polymers, which would result in the intrinsic brittleness of certain polymers when compared to others. What was common practice up to then was to introduce heterogeneity to avoid the formation of crazes. Their studies concluded, however, that further strengthening was possible by influencing the intrinsic post-yield behavior.[6] This could effectively be done by lowering the strain softening, i.e. reducing the localization phenomenon, or by increasing the strain hardening, which stabilizes the deformation. The improvement of toughness was proved by pre-deformation and the addition of heterogeneities, which altered intrinsic strain softening in the glassy polymeric samples, as well as crosslinking, pre-orientation and blending, which altered the intrinsic strain hardening. It was also found that blending should be done with pre-cavitated rubber or particles which have easily cavitating inclusions (*e.g.* core/shell particles with a soft rubber core and relatively hard rubber shell) in order to reduce the triaxial stress. Knowing this, a representative volume element was modeled. The model consisted of inclusions (voids and core/shell particles) of which the amount, shell thickness and morphology could be modified to study the macroscopic effects, i.e. tensile and impact toughness. Results suggested using a nano-sized modifier, which resembles the representation in Figure 1.1 and possesses the following properties:

1. easily-cavitating core material with modulus < 3 MPa,
2. the core material should be encapsulated with a rubber shell with modulus of 300 MPa,
3. the particle diameter (core and shell) should be roughly 30 nm.

It was therefore suggested that inclusion of the above-proposed modifier particles would result in the toughening of a glassy amorphous polymer. The glassy polymer, or matrix, must have a modulus of 3000 MPa and 2-5 wt% of the modifier should be used for effective modification.

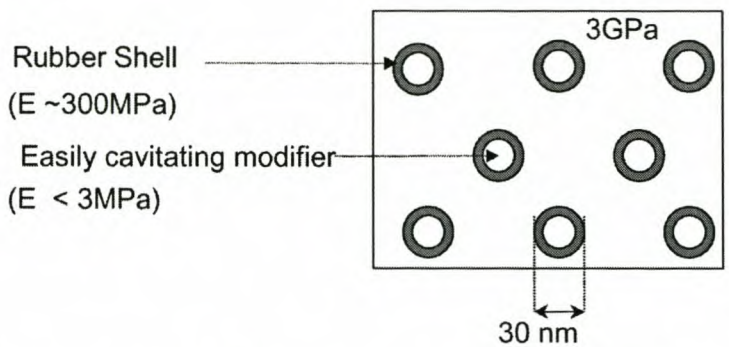

Figure 1.1: Proposed core/shell structure of nano-sized modifier particles, which should improve toughness of glassy polymers.[6,7]

1.2 Objectives

As a result of the above discussion and consequent proposal, the overall objective of this thesis was therefore to synthesize and evaluate nano-structured particles with well-defined core/shell morphology. The particles should resemble the representation in Figure 1.2, thus consisting of a low modulus core-oil (hexadecane), which resembles a cavity (i.e. pre-cavitation for effective impact modification), covered by a poly(butyl acrylate) rubber shell.

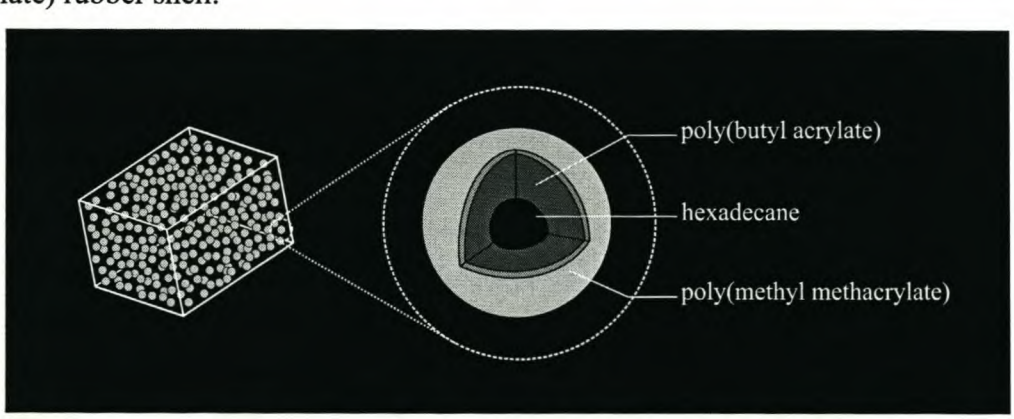

Figure 1.2: Particle morphology and composition, as proposed by this research initiative, to increase toughness of a glassy amorphous polymer.

To improve matrix mixing capabilities, the initial core/shell particles should be covered with a secondary poly(methyl methacrylate) shell. The secondary shell will also give structural stability to the initial particle, thereby enhancing processing capabilities as well as allowing analysis by destructive analytical techniques. Synthesis will be preceded by the evaluation of possible polymer/oil combinations to check their suitability for core/shell formation. This will be achieved by using well-known particle morphology prediction models. Free-radical chemistry will be used to prepare the particles *in situ*, i.e. as a one-step synthesis in a miniemulsion polymerization reaction. The miniemulsion conditions will facilitate the production of nano-scaled particles. The processes involved in establishing core/shell morphology during the *in situ* polymerization step will be studied, i.e. thermodynamic and kinetic considerations, and the morphology and particle size will be extensively characterized by various analytical techniques.

Furthermore, the particle size and stability of the synthesized core/shell latex will be evaluated as a function of the surfactant concentration and the presence or absence of a short-chain alcohol, and compared to "classical" miniemulsion data. The possibilities of a scale-up (to a volume 2.5 times that of the original) will also be investigated by comparing particle size and morphology data of the relevant experiments.

The possibility to synthesize structured particles with well-defined morphologies and characteristics of a living/controlled polymerization will be investigated on model compounds (styrene as shell material and isooctane as core material). This will be achieved by looking at the influence of different initiators and RAFT (reversible addition fragmentation chain transfer) agents on the outcome of particle morphology. The investigation will be extended to include the chemical precursors, i.e. butyl acrylate and hexadecane, needed to synthesize core/shell particles with impact modification possibilities, as originally intended.

To conclude, the mechanical properties of the synthesized core/shell modifier particles incorporated into a glassy polymeric matrix will be studied. This will be preceded by looking at the visual clarity of the moulded samples as well as the success of

compounding. The influence of the core/shell modifier particles on the outcome of the tensile and impact behavior will be investigated, as well as the influence of defects, which is inherent to the sample preparation method.

1.3 Thesis layout

This thesis consists of seven chapters, four of which are experimental. Chapter 2 provides a brief insight into, and historical overview of, the synthesis of structured particles. Chapter 3 describes the investigation of morphology prediction models based on thermodynamic considerations. The deviation between the observed and predicted morphologies, which is a result of the interplay between kinetics and thermodynamics in the *in situ* miniemulsion polymerization process used, is discussed. Hypotheses are proposed to investigate this and visual results are presented. The addition of a secondary glassy shell is also discussed.

Chapter 4 describes the miniemulsion process and its complexity and discusses the influence of the surfactant on obtaining the desired particle size. As a result of the complex nature of the miniemulsion process, the stability of the synthesized core/shell particles are investigated by making use of stoichiometrical calculations as based on "classical" miniemulsion experiments. The success of secondary shell addition, as discussed in Chapter 3, is evaluated by making use of various analytical techniques to obtain the particle size of the grafted material. Furthermore, the addition of a short-chain alcohol and the possible scale-up of the experiment are discussed. The effects of these two parameters on the characteristics of the final latex are compared with initial results.

In Chapter 5 the results of the previous two chapters are combined to create a novel technique to synthesize core/shell particles with liquid cores and living and controlled characteristics. This technique includes the use of a living free radical polymerization mechanism in which a RAFT agent is used. The influence of various RAFT agents and initiating species was investigated on a model system consisting of styrene as shell polymer and isooctane as core liquid, and their influences documented by various

analytical techniques. The investigation was expanded by changing the monomeric species from styrene to butyl acrylate and the oil species from isooctane to hexadecane, to revert back to the system used in Chapter 3. This was done to determine whether it is possible to effectively synthesize core/shell particles with the desired morphology, dimensions and properties, while the constituting polymer shows living and controlled characteristics. This also created the opportunity to investigate chain extensions on the obtained particles.

Chapter 6 considers the ability of the synthesized particles to be compounded with a suitable matrix polymer and the consequent outcome. Results are presented as visual and TEM images. The influence of the modifier particles on the intrinsic behavior of the matrix polymer under tensile and impact conditions is also described.

Chapter 7 is an epilogue which summarizes the main conclusions on all the previous chapters and discusses some recommendations for future research.

References

(1) Baaijens, F. In *Inside DPI*; Buskes, H., Ed.; Communicabus: Eindhoven, February 2003; Vol. 2, pp 18-21.

(2) Buskes, H. In *In search of the ultimate properties*; DPI Annual Report 2002, 2002; pp 16-17.

(3) Buskes, H. In *Bright future for polymer electronics*; DPI Annual Report 2002, 2002; pp 22-23.

(4) Wilson, E. K. In *Chemical and Engineering News*, 2003; Vol. 81, pp 27-29.

(5) Feynman, R. P. In *There's Plenty of Room at the Bottom*, Annual Meeting of the American Physical Society at the California Institute of Technology, 1959.

(6) Smit, R. J. M. *Toughness of Heterogeneous Polymeric Systems: A Modeling Approach*, Technische Universiteit Eindhoven, Eindhoven, 1998, 103.

(7) Jansen, B. J. P. *Toughening of Glassy Amorphous Polymers via Chemically-induced Phase Separation*, Technische Universiteit Eindhoven, Eindhoven, 1998, 104.

Chapter 2

Structured particles: A brief insight and historical overview

Abstract

Relevant scientific achievements in structured particle synthesis, particularly core/shell, are discussed, including the numerous synthesis routes currently available. The end-applications of these tailored particles and, hence, the importance of this study are mentioned.

2.1 Introduction

The development of modern materials science has presented numerous new and interesting challenges. One of these is the construction of nano-structured colloidal particles with distinct geometry, which is of great technological and economic importance. The technology used for the design and synthesis of structured particles can be referred to as "particle engineering". This is probably the best way to summarize the intricate process used to create particles with the desired morphology as it entails the modification of particle surfaces through tailoring of surface properties. This can be achieved either by coating the primary particles or encapsulating them with a selected material. Not only does this process engineers the physical shape, dimensions and constitution of the resulting materials, but also physical properties are completely re-engineered to suit desired end-applications.

Due to the versatility of this process, numerous structures can be designed to meet rigorous molecular and colloidal requirements. This is made possible by the vast number of monomers and different polymerization techniques available, which can successfully be employed in the production of these particles. This results in numerous structured particles with various end-uses. Improved impact toughness and architectural and automotive coatings are only three examples of the myriad of high-value-added products offered by the inclusion of core/shell particles.[1]

Another important genre of core/shell particles is obtained by the ability to synthesize hollow or voided particles. This is usually achieved through removal of the inner core polymer to produce a cavity, which can again be filled, thus further increasing the number of tailored products that can be synthesized. These particles can be used to encapsulate drugs, cosmetics, dyes, inks as well as toxic substances and solvents, with the added advantage that controlled release of encapsulated substances can be engineered if deemed necessary. This is achieved by controlling process parameters, which will consequently lead to different shell properties.

This research endeavor focuses on the synthesis of stable core/shell particles with liquid cores. This chapter therefore provides a brief historical insight into structured particles and highlights different synthesis routes. Not only is this necessary to understand the intricate process of core/shell synthesis, but also to emphasize and understand the novel aspects achieved through this study.

2.2 Core/shell particles – synthesis routes and historical highlights

A number of techniques can be used to synthesize core/shell particles. The oldest, introduced in 1929 by Kruyt *et al.*,[2] is the preparation of microcapsules/microspheres by coacervation, which is the encapsulation of the core material by a coacervate. The coacervate can be either aqueous or nonaqueous, where this refers to the polymer solution or wall-forming polymer, and not the core material. For aqueous coacervation the core material must be compatible with the excipient polymer and must be insoluble in the coacervation medium.[3] Bachtsi *et al.*[4] used the coacervation method to encapsulate silicon oil with a crosslinked polyvinyl alcohol. In this instance the oil was dispersed in the aqueous polymer solution for a predetermined time after which the formation of a polymer-rich phase occurred at the onset of the particular cloud point temperature. The polymer-rich phase will adsorb on the surface of the hydrophobic oil, thus leading to the formation of a shell polymer. Again the focus area of this method is the pharmaceutical field as shown by Rabiskova *et al.*[5]

Similar to the above is the formation of core/shell polymers by means of heterocoagulation[6,7] where two ionically different polymeric species are prepared separately and then emulsified together, thus leading to preferential encapsulation of the one species by the other.

The most well-known method for the synthesis of a core/shell polymer is the polymerization of a second-stage monomer in the presence of seed latex particles, otherwise known as a two-stage synthesis.[8] Here the seed particles can be synthesized beforehand and redispersed for addition of the shell polymer, or, they can be synthesized

in situ, resulting in a layered heterogeneous structure. However, processing variables can cause deviation from the desired core/shell morphology thereby resulting in some intermediate morphology (for additional information see Chapter 3). This method is still extensively used as is evident from the wealth of literature available.[9-13] However, this new method of synthesizing structured particles sparked a few debates of which the mechanism of particle growth was one of them. Grancio and Williams[14,15] proposed the non-uniform "core-shell" theory in which they stated that the seed particles are not homogeneously swollen with monomer and that there would be no concentration gradient of monomer from the centre of the particle to its surface. They suggested that the growing particles consisted of an expanding polymer-rich core surrounded by a monomer-rich shell, which serves as major locus of polymerization. Keusch and Williams[16] adapted this theory slightly by stating that at equilibrium saturation of seed particles with monomer, the seed particles would be encapsulated by a sheath of nearly pure monomer, thus proposing a polymer segment density gradient: high in the central region of the particle, dropping to a low value in the peripheral region. They concluded that the encapsulation phenomenon was probably controlled by molecular thermodynamic considerations.

Napper[17] proposed an alternative hypothesis, stating that surface active oligomers, formed by the addition of water-soluble initiator to monomer, will adsorb onto the particle surface and become incorporated in the particles by adding new monomer. Diffusion restrictions of the large polymer radicals in the viscous media, relative to the monomer molecules, results in the newly formed polymer remaining closer to the particle surface.

Preparation of microcapsules by suspension-crosslinking was introduced in the late 1960s by Rhodes *et al.*[18] and is similar to suspension polymerization. It involves the formation of a stable droplet suspension of the polymer solution as well as the dissolved or dispersed substance, which will ultimately form the core material, in an immiscible liquid, followed by gradual hardening of the droplets by covalent crosslinking.[19] In order to establish core/shell morphology with this technique it is quite important for the core

material to have a high affinity for the droplet phase rather than for the suspension media. This technique was successfully used by Konishi *et al.*[20] to synthesize hollow polydivinylbenzene particles. This was achieved after suspension polymerization of divinylbenzene/toluene droplets in which polystyrene was dissolved. Crosslinking of the divinylbenzene lead to the formation of a hard polymeric shell, ultimately resulting in the formation of microcapsules.

The synthesis of hollow core/shell particles (also known as microspheres and microcapsules) based on solvent extraction or evaporation can be traced back to the late 1960s. This technique involves the dispersion of an already formed polymer in water (also called a pseudo latex) by dissolving the polymer in a suitable solvent, followed by emulsification of the resulting organic solvent solution ("oil") to form an oil-in-water (o/w) emulsion. Upon removal of the organic solvent, as well as a fraction of the water, microcapsules will form. This technique is used extensively in medical applications where the formed capsules, which will facilitate sustained or slow-release drug delivery, are loaded with bioactive material.[21-32] The structure of the microsphere surface layer can be modified, which will strongly influence the rate and amount of drug release, thus allowing the capsules to be tailored for their end-applications. Variables that will strongly influence the surface layer properties are the pH of the aqueous phase as well as the composition of the polymer phase, which is employed as shell, as this will influence the density of the polymer matrix.[33]

The gradual removal of solvent during the solvent extraction will result in a decrease in volume and increase in the viscosity of the individual droplets. This will result in a violation of the conditions to maintain the steady-state droplet size equilibrium, which will ultimately lead to coalescence.[34] However, this can be overcome by the use of surfactant/cosurfactant combinations, which will reduce the number of effective collisions, and thus coalescence, between droplets.

Another preparation method for microcapsules is by interfacial polycondensation.[35-39] This method was extensively used during the 1980s although the idea of a

polycondensation reaction between two different phases was already conceived in 1959.[40,41] The formation of microcapsules by interfacial polymerization involves the reaction of various reactants at the interface of two immiscible liquid phases. The reactants are dissolved in their corresponding phases, i.e. aqueous and organic, and emulsified upon which the reactants diffuse together and rapidly polymerize at the interface to form a film of polymer.

With the major synthesis techniques for core/shell particles, albeit hollow or filled, already established by the mid-1980s, further research was focused on the mechanisms involved as well as using, for example, the two-stage method, which is usually used to prepare core/shell particles with seed cores and solid shells, to synthesize hollow or liquid-filled particles.[42-44]

In 1985 Cho and Lee[45] reported on the poly(methyl methacrylate)-seeded emulsion polymerization of styrene. They showed that the desired core/shell morphology of a hydrophobic monomer encapsulating a hydrophilic polymer can be achieved by controlling process parameters such as the type of initiator, type of surfactant as well as the viscosity of the polymerization loci. The latter can be dictated by the addition of a chain transfer agent. Further work by Chen *et al.*[46] confirmed this by evaluating the role of surfactant in composite latex particle morphology. They also found a correlation between conversion (and thus viscosity) and the change from predicted to observed morphology. In 1992 Lee and Rudin[47] studied the effect of core/shell inversion in a two-stage latex. A more hydrophilic polymer was synthesized first, followed by a more hydrophobic polymer in the second stage. This resulted in phase inversion to the thermodynamically preferred state, as long as viscosities of the phases allowed sufficient mobility to do so.

Encapsulation of an oil is becoming increasingly more important especially due to the vital significance of these particles in the pharmaceutical industry, as mentioned earlier.[48] In 1989 Berg *et al.*[49] encapsulated emulsified oil droplets by *in situ* vinyl polymerization. Although at that stage very little was known about *in situ* formation of an encapsulating

polymer, they still saw the need to investigate the possibilities to encapsulate a core oil. They concluded that free radical polymerization does not automatically guarantee polymer formation at the oil/water interface and that the ability to encapsulate hydrocarbon oils, via free radical chemistry, depends to a large extent upon the type and amount of surfactant used. They suggested, however, that the type of initiator has no effect on the outcome of morphology for their system as long as it does not alter the interfacial tension.

In a communication in 1991 Muscato and Sundberg[50] stated that the mechanism for phase separation and morphology control in particles produced from *in situ* polymerizations are still not completely understood. They studied the same polymer/oil system as Berg *et al.*[49] and concluded that the developments of morphology and phase separation are caused by a thermodynamic driving force.

In 2000 McDonald *et al.*[51] encapsulated a nonsolvent with polystyrene without the necessity of a high shear dispersion. According to them, the influence of the water-soluble thermal initiator plays an important role in adsorbing oligomeric radicals to the surface of the dispersion, which will then become the primary site for polymerization. The development of molar mass was an important factor which they considered, as an initially low molar mass polymer would result in the formation of particles with a hollow structure. This resulted in the use of chain transfer agents to allow for an optimum core/shell formation molar mass < 50 000 g/mol as well as the use of a water-miscible alcohol to decrease the molar mass. An equilibrium model was developed on the basis of the Flory-Huggins theory, which was successful in characterizing initial and final stages of the process. However, the model was oversimplified, ignoring some key components (effects of initiator, acid comonomers and alcohol) necessary to unify kinetics and thermodynamics.

Tiarks *et al.*[52] reported in 2001 on the formation of nanocapsules via a one-step synthesis (*in situ*) in miniemulsion. MMA and Sty were used as monomers and hexadecane as the hydrocarbon oil to be encapsulated. Influences of the type of

surfactant, volume of hydrocarbon oil and type of monomer were discussed. According to them no polystyrene capsules could be synthesized with a surface active initiator (KPS) and anionic surfactant (SDS), which, according to previously mentioned literature, should improve the possibilities of forming a core/shell polymer.

Other, less frequently used methods of synthesizing core/shell particles include the following.

Composite particles can also be prepared via block copolymers or self-assembly.[53-56] In 2000 Nah *et al.*[57] synthesized a triblock copolymer based on poly(γ-benzyl-L-glutamate) as the hydrophobic part and poly(ethylene oxide) as the hydrophilic part. The copolymers associated in water to form polymeric micelles at which point the bioactive agents could be added. Due to the hydrophobic nature of these agents they preferentially oriented in the core of the nanoparticles. Similarly, in 2002 Jang and Ha[44] synthesized triblock copolymers consisting of poly(oxyethylene) and poly(oxypropylene). Upon micelle formation MMA was added to form the core polymer, followed by crosslinked styrene as shell. By using a suitable solvent, organic core etching was used to remove the PMMA core, thus producing hollow spheres.

Templating approaches have also been followed to establish polymer nanocapsules.[58,59] The mechanism involves the formation of a polymer shell around a preformed template particle with subsequent removal to form the container particle.

2.3 Conclusions

From this brief historical introduction it is clear that much has been achieved in the field of core/shell synthesis during the last century. However, although core/shell particles are synthesized and applied in numerous fields, it follows from this historical journey that certain aspects concerning the synthesis mechanism remain unsolved. The balance between thermodynamics and kinetics is not yet fully understood and, due to new techniques being developed, the number of parameters associated with these terms is

increasing at an alarming rate. In the following chapters the influence of kinetic aspects on the outcome of particle morphology will be demonstrated and explained further, which will hopefully enlighten the reader as to the importance of this predicament. The solution still lies in the ability to model the mechanism involved in forming structured particles; the only problem being the inability to qualify and quantify the different processes involved in the kinetic and thermodynamic components.

References

(1) McDonald, C. J.; Devon, M. J. *Adv. Colloid Interface Sci.* **2002**, *99*, 181-213.

(2) Bungenberg de Jong, H. G.; Kruyt, H. R. *Proc. Koninkl. Nederland Akad. Wetenschap* **1929**, *32*, 849.

(3) Arshady, R. *Polym. Eng. Sci.* **1990**, *30*, 905-914.

(4) Bachtsi, A. R.; Boutris, C. J.; Kiparissides, C. *J. Appl. Polym. Sci.* **1996**, *60*, 9-20.

(5) Rabiskova, M.; Song, J.; Opawale, F. O.; Burgess, D. J. *J. Pharm. Pharmacol.* **1994**, *46*, 631-635.

(6) Okubu, M.; Lu, Y.; Wang, Z. *Colloid Polym. Sci.* **1998**, *276*, 833-837.

(7) Ottewill, R. H.; Schofield, A. B.; Waters, J. A.; Williams, N. S. J. *Colloid Polym. Sci.* **1997**, *275*, 274-283.

(8) Hughes, L. J.; Brown, G. L. *J. Appl. Polym. Sci.* **1961**, *V*, 580-588.

(9) Pérez, N.; Whitcombe, M. J.; Vulfson, E. N. *J. Appl. Polym. Sci.* **2000**, *77*, 1851-1859.

(10) Kim, H.-B.; Wang, Y.; Winnik, M. A. *Polymer* **1994**, *35*, 1779-1786.

(11) Okubo, M.; Murakami, Y.; Tsukuda, Y. *Chemistry Express* **1993**, *8*, 253-256.

(12) Ha, J.-W.; Park, I. J.; Lee, S.-B.; Kim, D.-K. *Macromolecules* **2002**, *35*, 6811-6818.

(13) Park, J. M. *Korea Polymer Journal* **2001**, *9*, 51-65.

(14) Grancio, M. R.; Williams, D. J. *J. Polym. Sci., Part A-1* **1970**, *8*, 2617-2629.

(15) Grancio, M. R.; Williams, D. J. *J. Polym. Sci., Part A-1* **1970**, *8*, 2733-2745.

(16) Keusch, P.; Williams, D. J. *J. Polym. Sci.: Polym. Chem. Ed.* **1973**, *11*, 143-162.

(17) Napper, D. H. *J. Polym. Sci., Part A-1: Polym. Chem.* **1971**, *9*, 2089-2091.

(18) Rhodes, B. A.; Zolle, I.; Wagner, N. H. *Clin. Res.* **1968**, *16*, 245.

(19) Arshady, R. *Polym. Eng. Sci.* **1989**, *29*, 1746-1758.

(20) Konishi, Y.; Okubo, M.; Minami, H. *Colloid Polym. Sci.* **2003**, *281*, 123-129.

(21) Juni, K.; Ogata, J.; Nakano, M.; Ichihara, T.; Mori, K.; Akagi, M. *Chem. Pharm. Bull.* **1985**, *33*, 313-318.

(22) Gurny, R.; Boye, T.; Ibrahim, H. *J. Controlled Release* **1985**, *2*, 353-361.

(23) Krause, H.-J.; Schwarz, A.; Rohdewald, P. *Int. J. Pharm.* **1985**, *27*, 145-155.

(24) Cavalier, M.; Benoit, J. P.; Thies, C. *J. Pharm. Pharmacol.* **1986**, *38*, 249-253.

(25) Lemoine, D.; Préat, V. *J. Controlled Release* **1998**, *54*, 15-27.

(26) Lemos-Senna, E.; Wouessidjewe, D.; Lesieur, S.; Duchêne, D. *Int. J. Pharm.* **1998**, *170*, 119-128.

(27) Scholes, P. D.; Coombes, A. G. A.; Illum, L.; Davis, S. S.; Vert, M.; Davies, M. C. *J. Controlled Release* **1993**, *25*, 145-153.

(28) Jeffery, H.; Davis, S. S.; O'Hagan, D. T. *Pharm. Res.* **1993**, *10*, 362-368.

(29) Sheorey, D. S.; Shastri, A. S.; Dorle, A. K. *Int. J. Pharm.* **1991**, *68*, 19-23.

(30) Ogawa, Y.; Yamamoto, M.; Okada, H.; Yashiki, T.; Shimamoto, T. *Chem. Pharm. Bull.* **1988**, *36*, 1095-1103.

(31) Bodmeier, R.; Chen, H. *J. Controlled Release* **1990**, *21*, 223-233.

(32) Bodmeier, R.; Chen, H. *J. Pharm. Pharmacol.* **1988**, *40*, 754-757.

(33) Bodmeier, R.; McGinity, J. W. *Pharm. Res.* **1987**, *4*, 465-471.

(34) Arshady, R. *Polym. Eng. Sci.* **1990**, *30*, 915-924.

(35) Yan, N.; Zhang, M.; Ni, P. *J. Membr. Sci.* **1992**, *72*, 163-169.

(36) Frère, Y.; Danicher, L.; Gramain, P. *Eur. Polym. J.* **1998**, *34*, 193-199.

(37) Pensé, A. M.; Vauthier, C.; Benoit, J. P. *Colloid Polym. Sci.* **1994**, *272*, 211-219.

(38) Alexandridou, S.; Kiparissides, C.; Fransaer, J.; Celis, J. P. *Surf. Coat. Technol.* **1995**, *71*, 267-276.

(39) Arshady, R. *J. Microencapsulation* **1989**, *6*, 13-28.

(40) Morgan, P. W. *J. Polym. Sci.* **1959**, *40*, 299-327.

(41) Wittbecker, E. L.; Morgan, P. W. *J. Polym. Sci.* **1959**, *40*, 289-297.

(42) Schellenberg, C. *Nanostrukturierte Polymermaterialien auf der Basis von Kern-Schale Dispersionen*, Universität Potsdam, Golm, 2000, 113.

(43) Schellenberg, C.; Akari, S.; Regenbrecht, M.; Tauer, K.; Petrat, F. M.; Antonietti, M. *Langmuir* **1999**, *15*, 1283-1290.

(44) Jang, J.; Ha, H. *Langmuir* **2002**, *18*, 5613-5618.

(45) Cho, I.; Lee, K.-W. *J. Appl. Polym. Sci.* **1985**, *30*, 1903-1926.

(46) Chen, Y. C.; Dimonie, V.; El-Aasser, M. S. *J. Appl. Polym. Sci.* **1992**, *45*, 487-499.

(47) Lee, S.; Rudin, A. *J. Polym. Sci., Part A: Polym. Chem.* **1992**, *30*, 865-871.

(48) Romero-Cano, M. S.; Vincent, B. *J. Controlled Release* **2002**, *82*, 127-135.

(49) Berg, J.; Sundberg, D.; Kronberg, B. *J. Microencapsulation* **1989**, *6*, 327-337.

(50) Muscato, M. R.; Sundberg, D. C. *J. Polym. Sci., Part B: Polym. Phys.* **1991**, *29*, 1021-1024.

(51) McDonald, C. J.; Bouck, K. J.; Chaput, A. B. *Macromolecules* **2000**, *33*, 1593-1605.

(52) Tiarks, F.; Landfester, K.; Antonietti, M. *Langmuir* **2001**, *17*, 908-918.

(53) Ali, M. M.; Stöver, H. D. H. *Macromolecules* **2003**, *36*, 1793-1801.

(54) Meier, W. *Curr. Opin. Colloid Interface Sci.* **1999**, *4*, 6-14.

(55) Hotz, J.; Meier, W. *Langmuir* **1998**, *14*, 1031-1036.

(56) Nardin, C.; Hirt, T.; Leukel, J.; Meier, W. *Langmuir* **2000**, *16*, 1035-1041.

(57) Nah, J.-W.; Jeong, Y.-I.; Cho, C.-S.; Kim, S.-I. *J. Appl. Polym. Sci.* **2000**, *75*, 1115-1126.

(58) Meier, W. *Chem. Soc. Rev.* **2000**, *29*, 295-303.

(59) Möhwald, H. *Colloids Surf., A* **2000**, *171*, 25-31.

Chapter 3

Core/shell particles containing liquid cores: morphology prediction of the required system, synthesis and characterization

Abstract

The ability to synthesize core/shell particles with distinct geometries is becoming more important due to their potential applications. In this study structured particles with liquid cores and polymeric shells were synthesized by an in situ miniemulsion polymerization reaction. The resulting materials were used to evaluate existing morphology prediction models based on thermodynamic considerations. Results showed that thermodynamic models are inadequate for the morphology prediction of in situ polymerized species. For particles prepared in this way, kinetic influences, e.g. anchoring effects, chain mobility and viscosity, play a significant role in defining the end-morphology of the particles.

Reproduced from:

Core/Shell Particles Containing Liquid Cores: Morphology Prediction, Synthesis and Characterization

André J.P. van Zyl, Ron D. Sanderson, Deon de Wet-Roos, Bert Klumperman, **Macromolecules**, 2003, 36, 8621-8629.

3.1 Introduction

Core/shell particles can be prepared via various routes. A two-stage seeded emulsion polymerization was the first general method developed by which to prepare latex particles featuring this unique structure.[1,2] Here the second stage monomer is polymerized in the presence of the core seed latex, which can either be prepared beforehand in a separate step (so-called "dead" or inactive seeding) or *in situ* during the emulsion polymerization (so-called "live" or active seeding). Other methods soon followed, such as suspension cross-linking,[3] coacervation,[4] interfacial polymerization,[5] solvent evaporation[6] and vesicle template polymerization.[7]

The synthetic route for the preparation of core/shell particles with liquid cores is slightly different from the conventional emulsion polymerization systems because of the high hydrophobicity and low water solubility of the core oil. In conventional emulsions no transport of the core liquid into micelles will take place. This ultimately results in an oily layer being present at the end of the reaction, which is undesirable. Miniemulsion polymerizations, however, have proved to be a suitable method for the preparation of systems involving large amounts of hydrophobe.[8] By subjecting the oil/water/surfactant/cosurfactant system to high shear, the oil, which consists of the core liquid and monomer, will form droplets, from which structured particles will develop during polymerization (see Scheme 3.1). In addition, phase separation can take place upon polymerization with consequent formation of particles with the desired morphology. High shear fields, required for the miniemulsification process, can be created by devices such as ultrasonicators, homogenizers and microfluidizers.

Depending on the polymerization parameters and conditions, the miniemulsion polymerization reaction can yield particles with various morphologies, ranging from core/shells, via acorn or hemispheres, to heteroaggregates or inverted core/shells. These morphologies can be characterized by means of well-established characterization techniques such as TEM,[9] SEM or AFM[10,11] and also via less well-known ones, *e.g.* solid-state NMR,[9,12] SAXS[13] and dielectric analysis.[14]

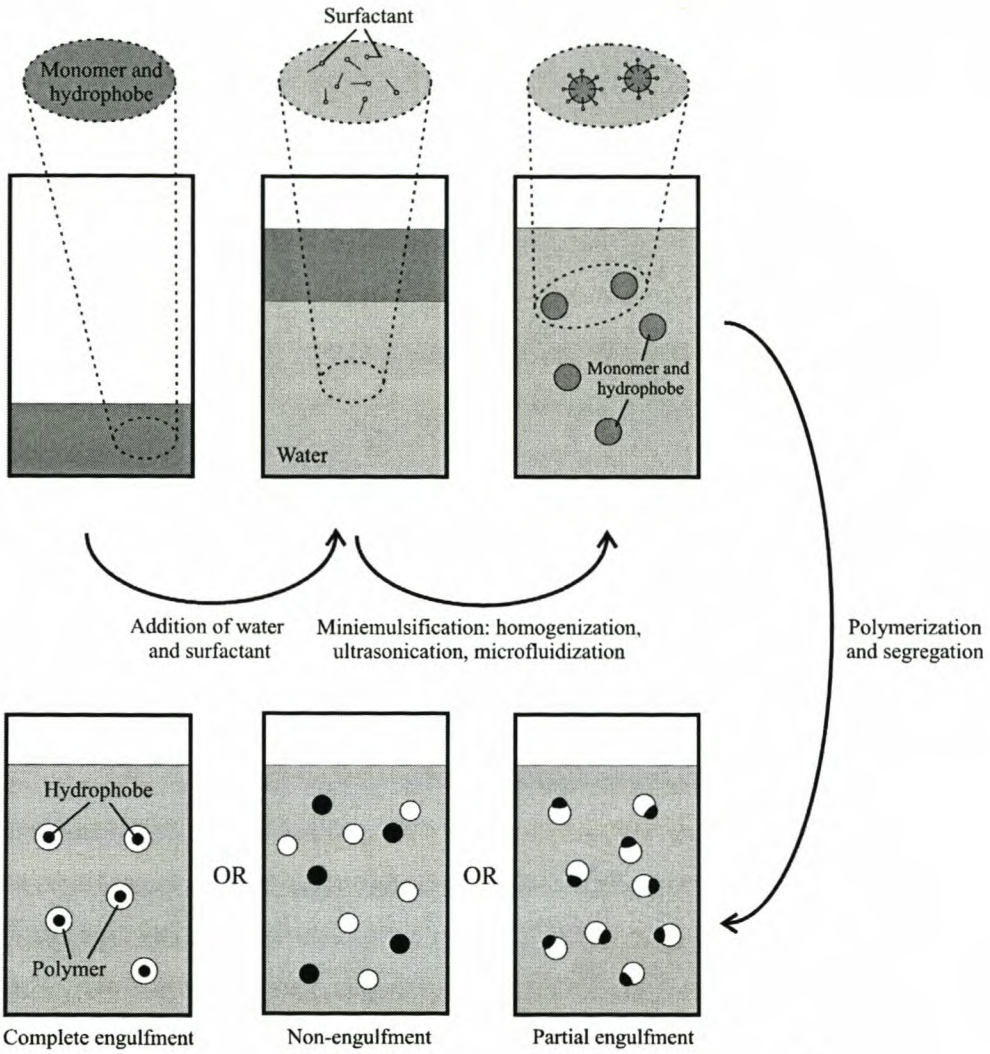

Scheme 3.1: Schematic representation of the miniemulsion process.[15]

In this chapter core/shell latexes based on poly(butyl acrylate) (PBA) and poly(butyl methacrylate) (PBMA) as shell, and hexadecane (HD) as core liquid, are studied. Different combinations of low viscosity core liquids and polymers are evaluated in terms of surface and interfacial tensions, followed by morphology predictions for the different permutations. The core oils were selected on the basis of their different hydrophobicities. PMMA was chosen to act as a second (glassy) shell around the initial rubbery shell to increase the particle strength and stability during analysis. The particles were synthesized using a miniemulsion polymerization process, followed by a redox-grafting polymerization step to accomplish the secondary shell formation.

3.2 Theoretical background

In 1970 Torza and Mason[16] reviewed the interactions of three phases in shear and electric fields. In their study they considered two immiscible liquid drops, designated as phase 1 and phase 3, which were suspended in a mutually immiscible liquid phase, phase 2. If equilibrium is considered when these two immiscible liquid drops are brought into contact in the third liquid phase of equal density, then the minimum surface free energy

$$G = \sum \gamma_{ij} A_{ij} \tag{3.1}$$

can be equated if it is assumed that the final equilibrium state is solely determined by the three interfacial tensions $\gamma_{ij}\left(i \neq j \neq k = 1,2,3\right)$, where A_{ij} is the area of the ij^{th} interface in the configuration.[17] Similarly, the three spreading coefficients can be considered,

$$S_i = \gamma_{jk} - \left(\gamma_{ij} + \gamma_{ik}\right) \tag{3.2}$$

which yields the same result as that based on minimizing G. By adopting the convention of designating phase 1 to be that for which $\gamma_{12} > \gamma_{23}$ it follows that $S_1 < 0$. By inspection of Equation 3.2 it is clear that only three possible sets of values can exist for S_i:

$$S_1 < 0, S_2 < 0, S_3 < 0 \tag{3.3}$$

$$S_1 < 0, S_2 < 0, S_3 > 0 \tag{3.4}$$

$$S_1 < 0, S_2 > 0, S_3 < 0 \tag{3.5}$$

These three sets correspond to the three possible equilibrium configurations which can be termed: complete engulfment, partial engulfment and non-engulfment of the core phase. A schematic view of the different configurations with the assigned spreading coefficients is shown in Figure 3.1.

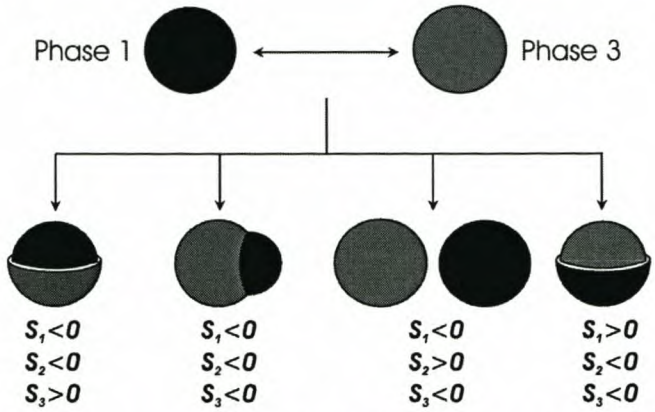

Figure 3.1: Schematic representation of different morphological configurations with the assigned spreading coefficients.

Note that a fourth possible morphology has been added. In the event of phases 1 and 3 being reversed, i.e. if initial conditions ($\gamma_{12} > \gamma_{23}$) are not met, then an inverse core/shell morphology is possible. Torza *et al.*[16] showed that their theory holds for a number of systems, including three-phase emulsions, by inducing interaction between droplets via shear and electric fields. As a result of this work they were also able to study the mechanism of engulfment by using high-speed cinematography.

Although the above applied to a system consisting of three liquids, the theory still holds true for systems consisting either of two polymers or a polymer/oil combination. However, in such cases the morphology is influenced by complex variables, as established by Berg *et al.*[18] They investigated the influence of both formulation and process variables on the morphological characteristics of a polymer/oil composite by studying the *in situ* vinyl polymerization of methyl methacrylate in the presence of n-decane or hexadecane. This allowed them to show the relationship between the type of emulsifier used and the outcome of the morphology, as well as the effect of the type of initiator used.

Sundberg *et al.*[19] remarked on the diffusive restrictions, i.e. polymer chain mobility, on the outcome of particle morphology and related this to the viscosity of the polymeric phase. They showed that it is possible to achieve non-equilibrium morphologies, i.e.

there may exist a number of states of phase separation, and therefore different morphologies may co-exist which are not thermodynamically stable morphologies. Sundberg's work was later extended to include morphology development in a three-component emulsion polymer system.[20]

In 1992 Winzor *et al.*[21] reported on the influence of the monomer on interfacial tensions. They showed that the presence of monomer strongly influenced polymer/polymer as well as polymer/water interfaces. This allowed them to incorporate monomer consumption, i.e. monomer conversion, in their morphology predictions, thus allowing for the variation in interfacial areas and interfacial tensions with composition. This provided a method by which to calculate the preferred morphology at any point along the reaction pathway.

Chen *et al.*[22,23] also discussed the influence of processing parameters on the outcome of particle morphology. They supported their reasoning by including the polymerization conversion in their equations for free energy changes. This allowed them to study the particle morphology during the course of seeded emulsion polymerization and allowed them to relate morphological tendencies to diffusion resistance, internal viscosities and the influence of surfactant, as well as the influence of surface polarity as caused by the choice of initiating species.

In 1994 Waters[24,25] reported on the prediction of the thermodynamically-favored surface morphology by quantifying the relative interfacial energies. In his work he studied both engulfment of a non-deforming as well as a deformable sphere, thereby enabling him to define interfacial energy equations, which makes it possible to visualize the variation in interfacial energy as a function of the degree of engulfment. For the engulfment of a non-deformable entity Waters considered a composite particle, as depicted in Figure 3.2, with curved-surface-areas and volumes as shown in Figure 3.3. The composite particle consisted of a non-deformed spherical core polymer (Q) engulfed by a polymer (P).

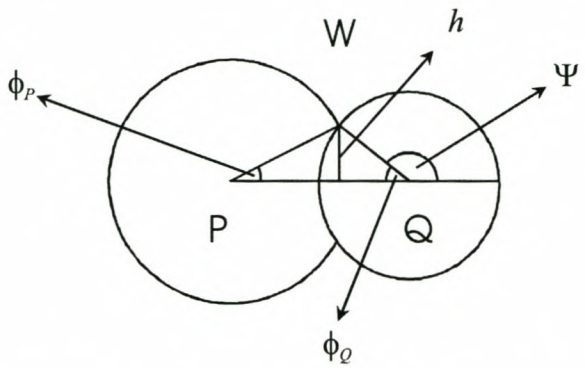

Figure 3.2: Cross-sectioning of a doublet structure of a composite particle consisting of a non-deformable sphere.[25]

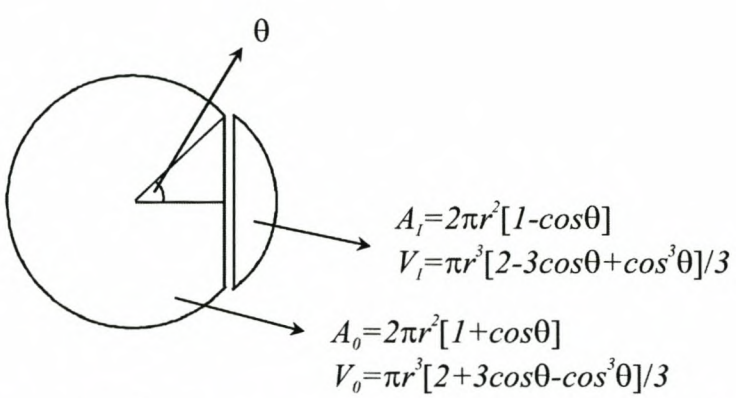

Figure 3.3: Curved-surface-areas and volumes for a truncated sphere.[25]

From Figure 3.3 it follows that the curved area (A_1) subtended by the angle 2θ is given by

$$A_1 = 2\pi r^2[1- \cos\theta] \tag{3.6}$$

and for the opposite area

$$A_0 = 2\pi r^2[1+ \cos\theta] \tag{3.7}$$

From this he could equate the areas of the Q-Wth, P-Qth and P-Wth interfaces, which produced

$$A_{Q-W} = (\pi/2)^{1/3}(3\upsilon_Q)^{2/3}[1+\cos\phi_Q] \tag{3.8}$$

$$A_{P-Q} = (\pi/2)^{1/3}(3\upsilon_Q)^{2/3}[1-\cos\phi_Q] \tag{3.9}$$

$$A_{P-W} = (\pi/2)^{1/3}(3\upsilon_Q)^{2/3}[1+\cos\phi_p]\sin^2\phi_Q/\sin^2\phi_p \tag{3.10}$$

where υ_Q is the fractional value of the core polymer, if a composite particle with unit total volume is assumed. Although the value of ϕ_Q is known $(0 \le \phi_Q \le \pi)$, the value of ϕ_p must be determined through a re-iteration process. This is done by considering the function

$$F(\phi_p) = F(\psi) + 4\upsilon_P/\sin^3(\psi)\upsilon_Q \tag{3.11}$$

where $F(\theta) = (2+3\cos\theta-\cos^2\theta)/\sin^3\theta$ and $\psi = \pi - \phi_Q$ (υ_p is the fractional value of polymer P), followed by a re-iteration process to calculate ϕ_p. The total interfacial energy can be obtained by substituting Equations 3.8-3.10 into Equation 3.1, where γ_{ij} is the interfacial tensions between the P-Wth, Q-Wth and P-Qth interface. This yields

$$\begin{aligned} E &= (\pi/2)^{1/3}(3\upsilon_Q)^{2/3}[\gamma_{P-W}(1+\cos\phi_p)\sin^2\phi_Q/\sin^2\phi_p + \gamma_{Q-W}(1+\cos\phi_Q) + \gamma_{P-Q}(1-\cos\phi_Q)] \\ &= (\pi/2)^{1/3}(3\upsilon_Q)^{2/3}N \end{aligned} \tag{3.12}$$

where

$$N = [\gamma_{P-W}(1+\cos\phi_p)\sin^2\phi_Q/\sin^2\phi_p + \gamma_{Q-W}(1+\cos\phi_Q) + \gamma_{P-Q}(1-\cos\phi_Q)] \tag{3.13}$$

Dividing Equation 3.13 with the interfacial energy (E_0) for the fully engulfed structure (which can be either core/shell or inverted core/shell) the following equation can be obtained:

$$E/E_O = N/\left[2\left(\gamma_{P-Q} + \gamma_{P-W}/\upsilon_Q^{2/3}\right)\right] \tag{3.14}$$

where

$$E_O = 2(\pi/2)^{1/3}3^{2/3}\left[\gamma_{P-W} + \upsilon_Q^{2/3}\gamma_{P-Q}\right] \tag{3.15}$$

Plots of E/E_O vs. ϕ_Q will indicate whether an intermediate morphology has a lower interfacial energy than the engulfed structure; the minimum in the interfacial energy profile indicates the degree of engulfment that yields a stable morphology. The steepness of the curves indicates the magnitude of the thermodynamic driving force for the rearrangement of the morphology. Figure 3.4 shows examples of the energy traces for two systems A and B, respectively. System A follows a gradual reduction in interfacial energy as a function of ϕ_Q, hence pointing to an engulfed system. System B, on the other hand, shows a minimum interfacial energy which is directly followed by an increase in energy, thereby indicating an intermediate doublet as the preferred structure.

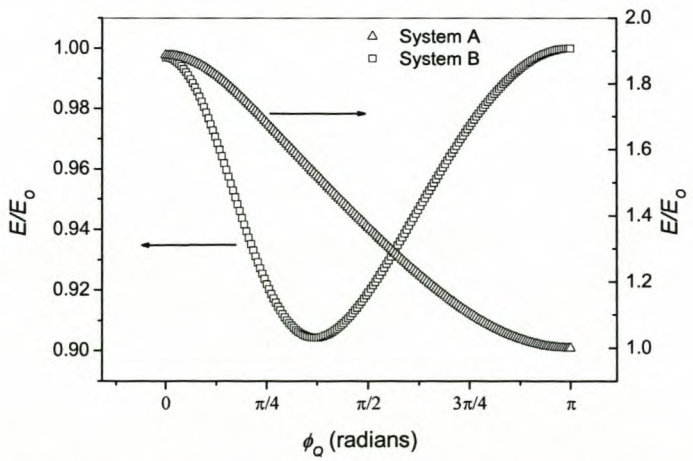

Figure 3.4: Energy curves showing the interfacial energies of two systems, A and B, as a function of degree of engulfment.[24]

For the engulfment of a deformable sphere, Waters[24] considered the structure as depicted in Figure 3.5 and obtained equations for the three interfacial areas.

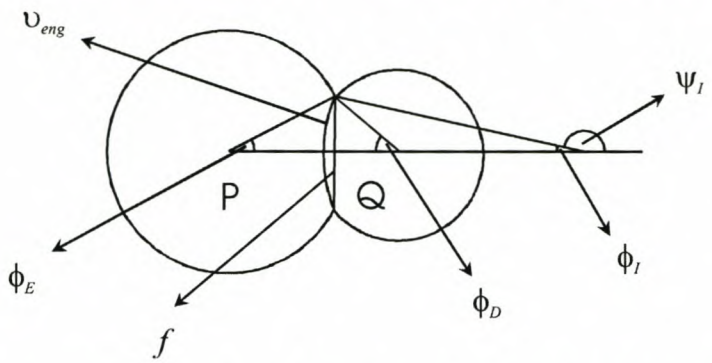

Figure 3.5: Cross-sectioning of a deformable sphere showing the angles which define the structure.[24]

These equations are

$$A_{Q-W} = \frac{2\pi f^2}{\sin^2 \phi_D}(1+\cos\phi_D) \tag{3.16}$$

$$A_{P-W} = \frac{2\pi f^2}{\sin^2 \phi_E}(1+\cos\phi_E) \tag{3.17}$$

$$A_{P-Q} = \frac{2\pi f^2}{\sin^2 \phi_I}(1-\cos\phi_I) \tag{3.18}$$

where f is the aperture radius and ϕ_D, ϕ_E and ϕ_I can be determined through an iteration process. Note that for a non-deformable sphere Q, $\phi_D = \phi_I = \phi_Q$.

In 1998 Loxley and Vincent[26] used the method of Torza and Mason[16] to predict particle morphologies of a PMMA/oil system. By varying the type of surfactant used, the desired core/shell morphology of a PMMA/hexadecane system with poly(methacrylic acid) as aqueous emulsifier was obtained. In 2001 Tiarks *et al.*[15] reported on the

synthesis of nanocapsules by miniemulsion polymerization of different monomers in the presence of large amounts of hydrophobe. They showed the effect of different monomers and monomer mixtures, the type of surfactant and the hydrophobe on the morphological characteristics of the polymer/oil composite particle. They concluded their study by showing that it is possible to produce a range of particle morphologies by simply controlling the above-mentioned parameters.

To summarize, particle morphologies can be predicted by using spreading coefficients as proposed by Torza and Mason.[16] However, care must be taken due to the number of factors that can influence the interfacial energies and hence the outcome of the final particle structure. These factors include: the type and amount of surfactant and type and amount of initiator used, the reaction temperature, the compatibility of the synthesized polymers and the difference in the hydrophilicity of the monomers and polymers.[27-29]

3.3 Experimental

3.3.1 Materials

Butyl acrylate (BA, Hoechst, 99.5%), butyl methacrylate (BMA, Aldrich, 99%) and methyl methacrylate (MMA, ICI Chemicals and Polymers, 99.9%) were all washed with a 0.3M potassium hydroxide (KOH, Associated Chemical Enterprises, 85%) solution, followed by distillation at reduced pressure to remove the inhibitor. Monomers were stored at –12 °C prior to use. Sodium dodecyl sulfate (SDS, BDH, 90%); potassium persulfate (KPS, 99+%), sodium metabisulfite (SMBS, 97%), cumyl hydroperoxide (CHP, 80%), sodium formaldehyde sulfoxylate (SFS), iron(II)sulfate (99+%), ethylene glycol dimethacrylate (EGDMA, 98%) (all Aldrich); toluene (99.9%), tetrahydrofuran (THF, 99.9%) (both Riedel-de Haën); methanol (MeOH, 99.8%), ethylenediaminetetraacetic acid, disodium salt (EDTA, 99%) (both ACROS); polyvinyl alcohol (PVOH, Fluka, 15000 Da); dichloromethane (DCM, 99%) and sodium bicarbonate (99.5%) (both Saarchem), were used as received. Distilled deionized water, obtained from a Millipore Milli-Q purification system, was used. Hexadecane

(HD, 99%), decane (D, 99+%), 1-octanol (O, 98%) (all ACROS), paraffin oil (PO), olive oil (OO, highly refined) (both from Aldrich) and silicon oil (SO) (SA Silicones) were employed as possible core oils. 1,1'-Azobis(cyclohexanecarbonitrile) (Aldrich, 98%) was used as received and 2,2'-azobis(isobutyronitrile) (AIBN, Delta Scientific, 98%) was recrystallized from methanol.

3.3.2 Polymerization of BA, BMA and MMA for surface tension experiments

PBA, PBMA and PMMA were synthesized by free radical solution polymerizations in order to ensure surfactant-free polymers, which would otherwise have a significant influence on surface tension evaluations due to surfactant interaction. Toluene (269 g) and BA (89 g, 6.94×10^{-1} mol) were added into a 500 mL roundbottom flask which was immersed in a heated oil bath. The flask was equipped with a reflux condenser and nitrogen feed. Initiator 1,1'-azobis(cyclohexanecarbonitrile) (0.45 g (1.84×10^{-3} mol) in 2 g toluene) was added and the reaction allowed to continue for 21 hours at 70 °C. In the case of BMA and MMA, toluene was substituted by THF. All quantities remained the same. The molar masses of the synthesized polymers were: 94 561 g/mol for PBA, 196 000 g/mol for PBMA and 168 060 g/mol for PMMA, as measured by SEC relative to PMMA (Section 3.3.7).

3.3.3 Interfacial and surface tension measurements and subsequent spreading coefficient calculations

To be able to predict the morphology of structured particles it is necessary to first evaluate the surface properties of the polymers, oils and surfactant/cosurfactant in question. A torsion balance and a platinum Du Noüy ring were used for surface tension evaluations of the different oils and for interfacial tension measurements of the oil/water combinations. Interactions between the polymer and oils, as well as polymer/water interactions, were evaluated using a Cahn DCA contact angle analyzer. For contact angle evaluations, polymer samples (PBA and PBMA) were prepared by dip-coating nylon strings into a polymer solution and allowing them to dry in a dust-free environment

before analysis (in the case of PMMA, films were cast from solution and used as is). The nylon strings were first cut to size and then soaked in acetone for several minutes to rid them of any oils, which may have resulted from contact by hand. After thorough drying in an oven the strings were subsequently dipped into a PBA or PBMA solution, then allowed to dry overnight, after which they were dipped again. This was repeated the following day. The strings were kept in a desiccator of which the top vent was left open for the THF fumes to escape. After four days the desiccator was degassed to ensure a solvent-free environment. This was done for five hours prior to surface tension determinations.

The contact angle could be calculated from force/immersion depth curves by using the modified Young's equation[30]

$$\theta_c = cos^{-1}\left(\frac{F}{p\gamma}\right) \tag{3.19}$$

where F is the force at zero depth of immersion, p is the perimeter of the sample and γ is the surface tension of the oil. To calculate the force at zero depth of immersion, the point of zero depth of immersion (ZDOI) was located, as shown in Figure 3.6.

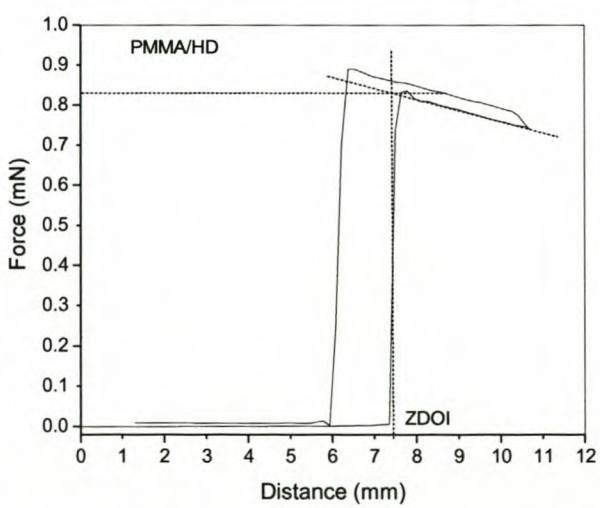

Figure 3.6: Calculating the force at zero depth of immersion from the surface tension hysteresis loop.

A perpendicular line was drawn from this point (from the abscissa) and a straight line was drawn through the advancing data to obtain an intersection point. By drawing a perpendicular line from the ordinate through the intersection, the force at zero depth of immersion was obtained.

For the oil/polymer and polymer/water combinations, Young's equation[31]

$$\gamma_{sl} = \gamma_{sv} - \gamma_l \cos\theta_c \qquad (3.20)$$

was used, where γ_{sl} is the solid/liquid interfacial tension, γ_{sv} is the solid/vapor interfacial tension, γ_l is the surface tension of the liquid and θ_c is obtained from Equation 3.19. The value of γ_{sv} can be obtained from literature or can be calculated.[31,32] Oil/water interfacial tensions and surface tensions of the different liquids (γ_l) were directly obtained with the torsion balance. However, values from literature could also be used.[33] The Du Noüy ring was cleaned in concentrated H_2SO_4 and rinsed with distilled water and acetone before use and also in-between consecutive measurements, to ensure accuracy. For all of the above measurements at least three readings were taken and the mean value was used in further calculations.

As temperature is an important parameter in surface properties of polymers and oils,[34] the laboratory temperature was regulated to be 20.5±1 °C and the humidity was kept constant by conducting experiments in a controlled environment.

3.3.4 Synthesis of PMMA/HD core/shell particles by direct emulsification

PMMA was made as described in Section 3.3.2 and subsequently dissolved in DCM. To this was added the HD as core-liquid. The oil phase was consequently emulsified in a solution of PVOH and distilled deionized (DDI) water and stirred for 2 hours at 700 rpm. The solution was left standing in a fume hood for 3 days to allow for the DCM to

evaporate and the core/shell particles to form. Afterwards the particles were thoroughly washed and dried for SEM analysis.

3.3.5 Synthesis of PBA/HD core/shell particles by miniemulsification - shearing

PBA/HD core/shell particles were prepared by shearing the kettle charge (see Table 3.1) with a Silverson L4R shearer.

Table 3.1: Miniemulsion recipe for the synthesis of PBA/HD core/shell particles.

	(g)	(mmol)
Kettle charge		
SDS	1	3.47
DDI	100	
BA	5.5	42.91
Hexadecane	4.3	18.99
Sodium bicarbonate	0.29	3.45
Initiator solution		
KPS	0.025	0.09
SMBS	0.017	0.09
Purge gas		
N_2		
Crosslinker		
EGDMA	0.19	0.96

The kettle charge consisted of a surfactant/water solution, monomer, core oil and sodium bicarbonate (1:1 molar ratio between SDS and sodium bicarbonate, which is used as buffer). The Silverson was equipped with a special tubular mixing assembly unit designed for volumes between 50 and 500 mL. The shearing was done in a specially designed beaker containing a mantle through which water was continuously pumped. This was done to cool the emulsion to prevent any possibility of thermal initiation. Shearing was continued for 1 hour. After shearing, 70 g of the sheared fluid was added to a reaction flask and the reaction continued by adding KPS initiator and SMBS at 80 °C (1:1 molar ratio between KPS and SMBS, which is used as redox couple). Continuous purging was performed by bubbling nitrogen through the latex solution. EGDMA (3.5 wt% to monomer) was added 1 hour after the start of the reaction to give more stability to

the rubbery shell through crosslinking. The reaction was allowed to continue for 3.5 hours after which it was cooled down.

3.3.6 Synthesis of PBA/HD core/shell particles by miniemulsification - ultrasonication

Butyl acrylate, hexadecane and sodium bicarbonate were premixed with a SDS/water solution for 1 hour after which a miniemulsion was obtained by sonicating the mixture with a Sonics & Materials Inc. Vibracell VCX 750 ultrasonicator for 30 minutes at 90% amplitude (161.69 kJ). During this period the solution was continuously stirred in a jacketed vessel to avoid polymerization due to heating. After miniemulsification the solution was transferred to a 250 mL glass reactor, suspended in a thermostatted oil bath and equipped with a condenser and nitrogen purge. Polymerization was achieved by adding KPS initiator and SMBS at 80 °C. Continuous purging was performed by bubbling nitrogen through the latex solution. EGDMA (30 wt% to monomer) was added 60 minutes after the start of the reaction to give more stability to the rubbery shell through crosslinking. Delayed addition of the crosslinker was significant to allow the formation of the preferred morphology.[10,35-38] The reaction was allowed to continue for 3.5 hours after which it was cooled down to 50 °C.

To add a second shell a redox initiator system consisting of cumyl hydroperoxide/Fe^{2+}/ethylenediaminetetraacetic acid/sodium formaldehyde sulfoxylate (CHP-Fe^{2+}-EDTA-SFS) was used in the grafting of MMA onto the PBA shell. EDTA was used as chelating agent and SFS as reducing agent[39,40] to reduce Fe^{3+} to Fe^{2+} during the redox polymerization. The MMA was fed over a 1.5 hour period. A typical formulation for the above reactions can be seen in Table 3.2.

Table 3.2: Miniemulsion recipe for the synthesis of PBA/HD core/shell particles and subsequent grafting with MMA in the presence of an interfacial redox initiator system.

	(g)	(mmol)
Kettle charge		
SDS	0.7	2.427
DDI	70	
BA	3.85	30.038
Hexadecane	3.01	13.292
Sodium bicarbonate	0.204	2.428
Initiator solution		
KPS	0.0247	0.091
SMBS	0.0174	0.092
Purge gas		
N_2		
Crosslinker		
EGDMA	1.16	5.852
Graft reaction		
MMA	3.85	38.454
CHP	0.25	1.643
$FeSO_4.7H_2O$	0.0104	0.037
EDTA	0.4	1.075
SFS	0.4	2.595

3.3.7 Analytical techniques

Atomic force microscopy (AFM)

One droplet of an undiluted latex solution was deposited on an angularly placed, flat silica surface so that the polymer formed a smooth film consisting of a few monolayers of latex particles. Excess water was removed by blotting with filter paper. AFM experiments were carried out using a Topometrix Explorer with silicon non-contact tips from Nanosensors GmbH (Germany). AFM images were obtained at ambient conditions while operating the instrument in non-contact mode.

Transmission electron microscopy (TEM)

Samples for TEM measurements were prepared following a procedure of Sue *et al.*[41] who proposed a novel staining technique for studying saturated polyacrylate rubbers. Sample preparation was done by precipitating and drying the latex to obtain a fine powder. The powder was subsequently embedded in Spurr's resin and cured at 60 °C for 16 hours. The epoxy resin block was then placed in styrene for 1 hour after which it was washed with water and patted dry. The block was transferred to a glass jar containing 0.5g OsO_4 and left there for 3 days to allow adequate staining by the vapor. To complete the process, the block was left in a fumehood for 24 hours to allow excess OsO_4 to evaporate, after which it was microtomed at ambient temperature with a Reichart Ultracut S (Leica, Vienna, Austria) ultramicrotome, with a diamond knife, to produce slices with a thickness of 100 nm. These slices were placed on a copper grid. Analyses were done on a JEM - 200CX (JEOL Ltd, Tokyo, Japan) TEM.

A non-destructive TEM sample preparation procedure was also followed. For this procedure 2mL of the latex was added to an excess of MeOH to aid precipitation of the particles. The particles were dispersed by shaking and transferred to a copper TEM grid by pipette. The grid was left to dry at ambient temperature before analyses were performed. No staining was applied to the dried particles. Contrast between the core and shell was the result of the combined effects of the different path length and material densities of the constituting materials. This resulted in increased scattering of the incident e^--beam from the wall material, resulting in a darker region on the TEM images. Analyses were done on a JEM - 200CX and 2000FX (JEOL Ltd., Tokyo, Japan) TEM. The copper grids were prepared by the deposition of a thin film of carbon for increased strength and conductivity of the film.

Size-exclusion chromatography (SEC)

Molar mass distributions were measured via size-exclusion chromatography (SEC). Dried latex samples were dissolved in THF (8 mg/mL) and filtered through a 0.45 μm

nylon filter. Analyses were carried out with a SEC system comprising a Waters 610 Fluid Unit, Waters 410 Differential Refractometer at 30 °C, Waters 717_{plus} Autosampler and Waters 600E System Controller. Two PLgel 5 μm Mixed-C columns and a pre-column (PLgel 5μm Guard) were used and the column oven was set at 30 °C. Millennium[32] was used for data acquisition and data analysis. THF was used as solvent and the flow rate was 1.0 mL/min. The volume of the injected samples was 100 μL. The system was calibrated with narrow poly(methyl methacrylate) standards ranging from 2 500 to 898 000 g/mol.

Scanning electron microscopy (SEM)

For SEM analysis the latex sample was pipetted onto a metal stub and allowed to dry, after which it was sputter-coated with gold. A Topcon ABT60 SEM was used.

3.4 Results and discussion

3.4.1 Evaluation of the spreading coefficient prediction model of Torza and Mason, and the synthesis and characterization of PMMA/HD core/shell particles

To evaluate the ability to predict, synthesize and characterize core/shell particles it was deemed appropriate to first synthesize a PMMA core/shell particle containing hexadecane (HD) as core oil. The reason why this was chosen is that PMMA forms a hard shell, which makes analysis much easier. Also, because the particles were synthesized according to the method adopted by Loxley *et al.*,[26] the spreading coefficient calculation procedure and consequent morphology prediction could be evaluated by comparing the results of the present study with their results.

To calculate the interfacial tension value between PMMA and hexadecane, certain surface properties of the respective substrates need to either be known, calculated or obtained experimentally. Interfacial and surface tension measurements were performed according to Section 3.3.3. Results of surface tension, interfacial tension and contact

angle measurements as well as the corresponding literature values,[26] are shown in Table 3.3.

Table 3.3: Surface tension, interfacial tension and contact angle values calculated for a PMMA/HD/SDS system and compared to literature data.[26]

Surface tension (γ_{lv}) Hexadecane		
Literature (mN/m)	Torsion balance (mN/m)	Avg (mN/m)
27.6	27.5 27.3 27.5 27.6	27.48
Interfacial tension (γ_{ll}) Hexadecane/SDS/H_2O		
Literature (mN/m)	Torsion balance (mN/m)	Avg (mN/m)
6.7	6.7 6.2 6.4	6.4
Contact angle (°) PMMA/Hexadecane		
Literature (°)	Cahn DCA (°)	
17.4	15.42	
Interfacial tension (γ_{sl}) PMMA and Hexadecane		
Literature (mN/m)	Young's equation (mN/m)	
14.4	14.6	

From Table 3.3 it is clear that the literature values can be reproduced.

To evaluate methods by which core/shell particles could be characterized, another system from the same literature source[26] was selected, namely poly(methyl methacrylate)/hexadecane/polyvinyl alcohol (PMMA/HD/PVOH). According to the spreading predictions for this system an acorn morphology should be obtained. Particles were synthesized according to Section 3.3.4 and used, as is, for optical microscope studies. Figure 3.7 shows optical microscope images of the synthesized particles. Figures 3.8 and 3.9 shows SEM images of the obtained particles, clearly indicating the acorn morphology obtained.

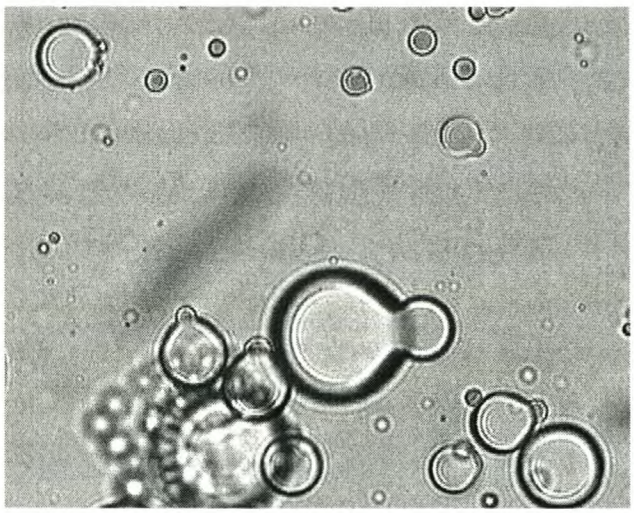

Figure 3.7: Optical microscopy image of PMMA/HD/PVOH particles, showing the existence of acorn morphology.

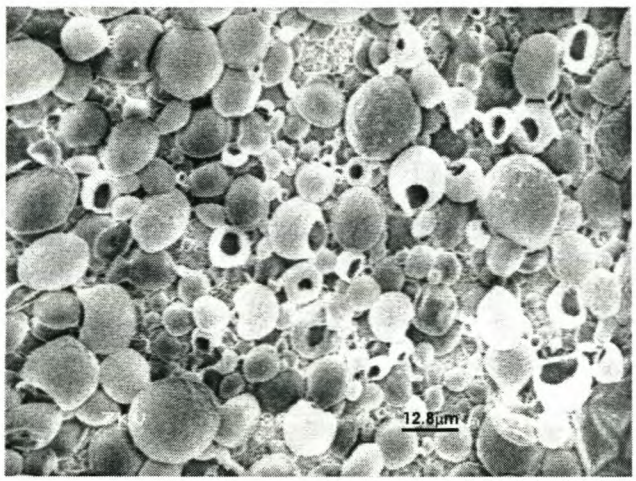

Figure 3.8: SEM image of PMMA/HD/PVOH particles, confirming the existence of acorn morphology.

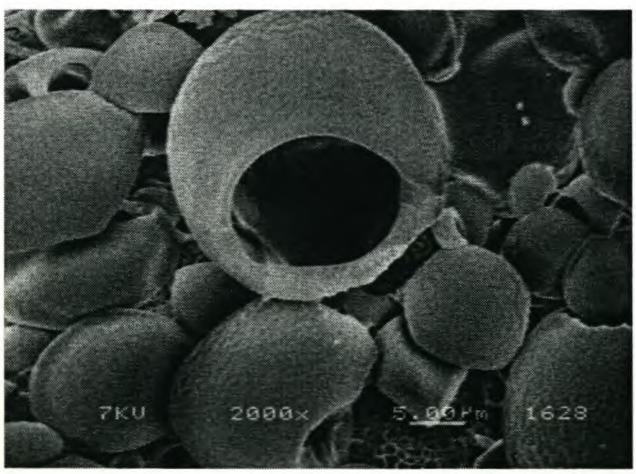

Figure 3.9: Close-up SEM image of a synthesized PMMA/HD/PVOH particle, showing acorn morphology.

By carrying out the above experiments the calculation of the relevant interfacial values and consequent spreading values could therefore be evaluated. This would serve as a basis for the rubber/oil system (PBA/oil and PBMA/oil), which was to be investigated further.

3.4.2 Morphology predictions of poly(meth)acrylate/oil combinations in a surfactant/water system

Values for the γ_{sv} of PBA and PBMA were obtained from literature and were taken as 33.7 and 31.2 $mN.m^{-1}$ respectively.[31] Values for the contact angle between the oil and polymer (θ_{op}), polymer and water (θ_{pw}) as well as the calculated interfacial tensions and spreading coefficients can be seen in Table 3.4.

The influence of hexadecane as costabilizer on the oil/water and oil/polymer interface was also investigated (Table 3.4). This was done to confirm work done by Landfester *et al.*[42] who reported that hexadecane does not act as a surface active agent. The hydrophobe will act as a "super swelling" agent whereas a fatty alcohol, *e.g.* cetyl alcohol, is assumed to influence the rigidity of the oil/water interface or lower the interfacial energy.

However, Table 3.4 shows a small discrepancy between costabilized and non-costabilized oil/polymer interfacial values. The reason for this is that the contact angles are calculated by Equation 3.19. A small error in the observation of the force value (F) (as obtained from force/immersion curves) will result in a large deviation when calculating the contact angle θ_c, hence producing variations between contact angles for costabilized and non-costabilized systems. However, when the interfacial tension values are calculated by Equation 3.20, the discrepancy in contact angle values are again reduced, thus leading to small differences between interfacial tension values, thereby not influencing spreading predictions. In other words, the addition of hexadecane will in no way influence the interfacial tensions and, therefore, the outcome of spreading predictions.

Table 3.4: Interfacial tensions (γ_{ij}) and spreading coefficient (S_i) data and subsequent predicted morphologies of different polymer/oil combinations. (D = decane, HD = hexadecane, SO = silicone oil, OO = olive oil, PO = paraffin oil, O = 1-octanol)

PBA										**Morphology**
Oil	**Costabilizer**	θ_{op}	θ_{pw}	γ_{op}	γ_{pw}	γ_{ow}	S_1	S_2	S_3	**prediction**
D		12.5	73.4	9.3	23.2	7.0	<0	<0	>0	core/shell
D	HD	8.9	73.4	8.8	23.2	6.9	<0	<0	>0	core/shell
HD		48.1	73.4	14.6	23.2	6.7	<0	<0	>0	core/shell
SO		28.3	73.4	13.9	23.2	9.7	<0	<0	<0	acorn
SO	HD	29.6	73.4	14.1	23.2	9.7	<0	<0	<0	acorn
OO		60.8	73.4	16.8	23.2	1.7	<0	<0	>0	core/shell
OO	HD	57.8	73.4	15.3	23.2	1.7	<0	<0	>0	core/shell
PO		59.0	73.4	17.4	23.2	9.1	<0	<0	<0	acorn
PO	HD	54.3	73.4	15.3	23.2	9.2	<0	<0	<0	acorn
O		36.2	73.4	10.1	23.2	1.1	<0	<0	>0	core/shell
O	HD	35.9	73.4	10.1	23.2	1.1	<0	<0	>0	core/shell
PBMA										
D		17.5	71.9	7.4	19.8	7.0	<0	<0	>0	core/shell
D	HD	19.6	71.9	7.4	19.8	6.9	<0	<0	>0	core/shell
HD		13.9	71.9	3.4	19.8	6.7	<0	<0	>0	core/shell
SO		24.9	71.9	10.8	19.8	9.7	<0	<0	<0	acorn
SO	HD	24.2	71.9	10.6	19.8	9.7	<0	<0	<0	acorn
OO		40.6	71.9	4.9	19.8	1.7	<0	<0	>0	core/shell
OO	HD	38.3	71.9	4.1	19.8	1.7	<0	<0	>0	core/shell
PO		31.8	71.9	4.3	19.8	9.1	<0	<0	>0	core/shell
PO	HD	34.6	71.9	5.3	19.8	9.2	<0	<0	>0	core/shell
O		38.9	71.9	8.4	19.8	1.1	<0	<0	>0	core/shell
O	HD	42.9	71.9	9.9	19.8	1.1	<0	<0	>0	core/shell

In the calculation of the spreading coefficients for the investigated system, the continuous phase (water, *w*) was taken as phase 2, the polymer phase (*p*) was assigned to phase 1 and the oil phase (*o*) was assigned to phase 3. The reason for this assignment is

that it fulfills the requirement: $\gamma_{12} > \gamma_{23}$. Figure 3.10 shows the spreading values and consequent predicted morphologies for the different PBA- and PBMA-oil systems.

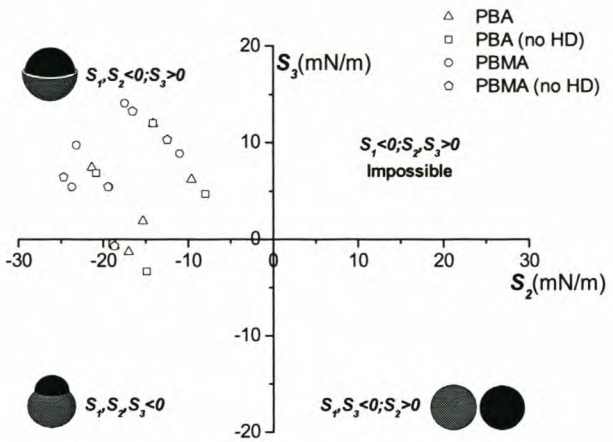

Figure 3.10: Graphical representation of spreading coefficients and predicted morphologies for the different PBA- and PBMA-oil systems.

Although the predictions according to the spreading coefficients return values such as core/shell or acorn, care must be taken with the interpretation of these results. For the spreading predictions to be valid it was taken that $\gamma_{12} > \gamma_{23}$. Phase 12 corresponds to the polymer/water interface and phase 23 to the oil/water interface, hence showing that the interfacial tension between the oil and water is lower than the interfacial tension between the polymer and water. Thermodynamically the driving force will therefore be to form an oil layer between the water and polymer phases because of the drive to lower energies. This becomes clearer when looking at predictions done according to the work of Waters.[24,25] In this instance the engulfing polymer is chosen and the energy is monitored as a function of engulfment. Predictions were performed by substituting the interfacial tension values into Equation 3.12. Plots of E/E_O vs. ϕ_Q will indicate whether an intermediate morphology has a lower interfacial energy than the engulfed structure and the degree of engulfment which corresponds to the lowest energy.

Energy traces for the PBA/PBMA-oil systems are shown in Figures 3.11 and 3.12.

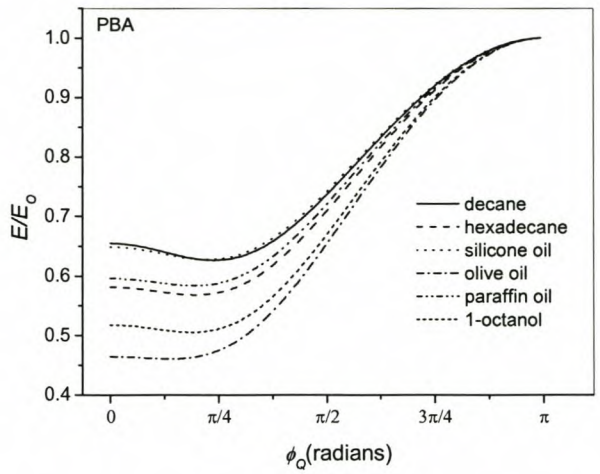

Figure 3.11: Traces showing the change in energy as a function of ϕ_Q (degree of engulfment) for the engulfment of different oils by PBA.

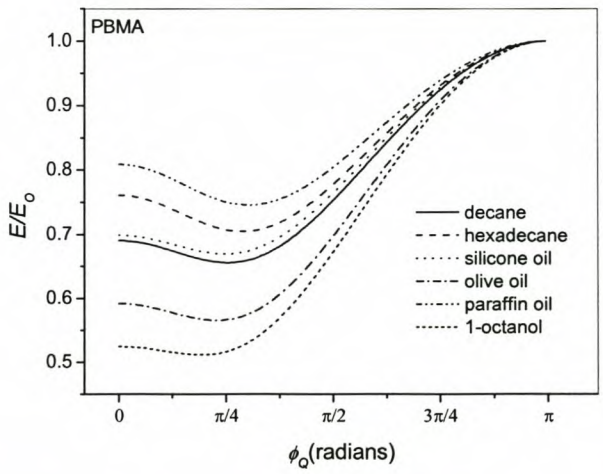

Figure 3.12: Traces showing the change in energy as a function of ϕ_Q (degree of engulfment) for the engulfment of different oils by PBMA.

From this it follows that the energy increases if the oil is used as the engulfed (Q^{th}) phase and the polymer as the engulfing (P^{th}) phase, hence evidently indicating an inverted core/shell morphology. These results suggest that the predictions from Torza/Mason and from Waters both point to an inverted core/shell morphology. Nevertheless, experimental verification of the PBA/HD system was worthwhile.

3.4.3 Formation of stable core/shell latexes

PBA/HD core/shell particles synthesized by miniemulsification - shearing

In the first attempt to synthesize the PBA/HD core/shell particles, an emulsion system was used. However, a continuous oily layer was present on top of the formed emulsion, pointing to the fact that no mechanism was present by which to force the oil into the micelles. To overcome this problem the oil and monomer were forced into the micelles by applying a shear force to the kettle charge as discussed in Section 3.3.5.

Figure 3.13 shows an optical microscopy image which revealed an abundance of particles which were all of the same size (± 1 μm). Excessive Brownian motion of the observed structures confirmed that they were particles and not air bubbles trapped between the microscope slides.

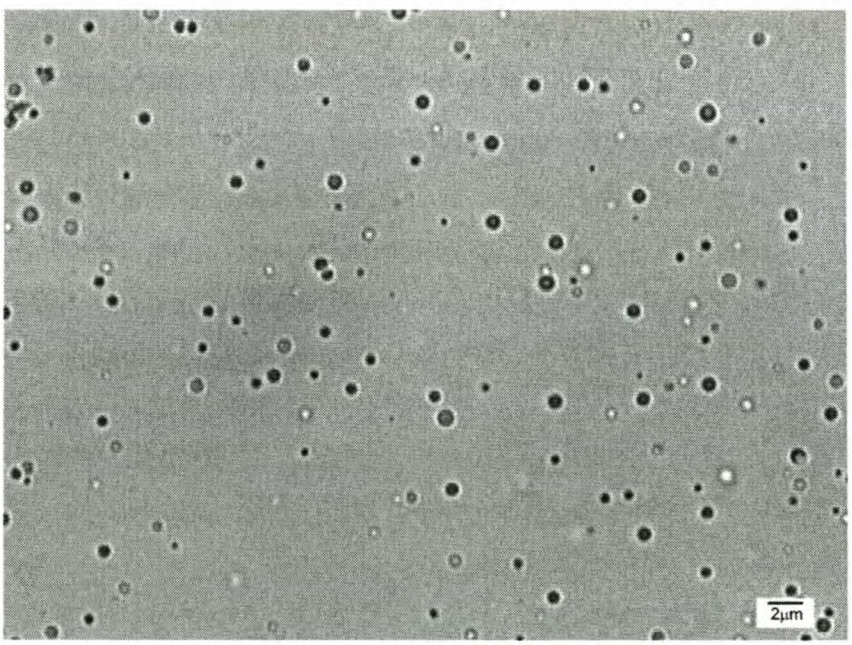

Figure 3.13: Optical microscopy image of PBA/hexadecane particles indicating the formation of core/shell morphologies.

In initial experiments the PBA was lightly crosslinked and no grafting was performed.

Film formation was evaluated after casting of the latex on a silica substrate. AFM images in Figures 3.14 (a.)–(f.) show clearly the effect of film formation at room temperature. Non-crosslinked PBA has a T_g of –55 °C and even a lightly crosslinked PBA will show immediate spreading at room temperature. In Figure 3.14 (b.) the presence of "bumps" and "potholes" can be seen. The bumps represent intact particles while the potholes are representative of collapsed particles, which point to the initial formation of core/shell particles (cavities) (Figure 3.15).

At the end of the film formation no more cavities are left and a smooth surface can be distinguished in Figure 3.14 (f.). Initial AFM images were different to the predictions made. These differences are supported by additional TEM analyses, which will be shown later (Figure 3.19).

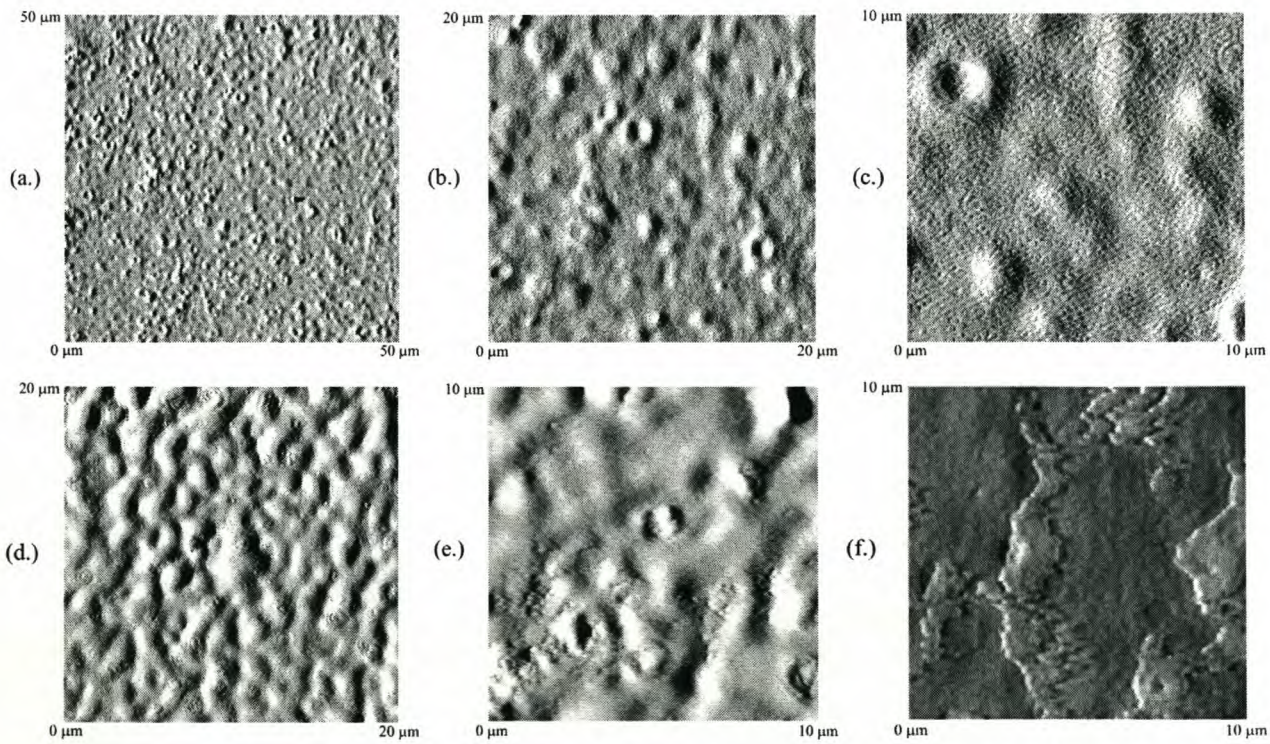

Figure 3.14: AFM images showing the film formation of PBA/HD core/shell particles at room temperature: (a.)-(c.) show different magnifications of the same sample area whereas (b.) and (d.)-(f.), consecutively, show film formation as a function of time.

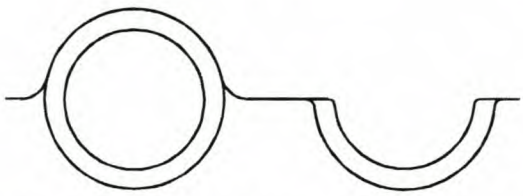

Figure 3.15: Interpretation of "bumps" and "potholes" as seen during AFM analysis of the film formation of PBA/HD core/shell particles.

Interfacial grafting of methyl methacrylate onto polybutyl acrylate in miniemulsion – Initial problems and solutions

As was shown in Figure 3.14, AFM images of the formed latex particles proved the existence of container (liquid-filled) particles to a certain extent. More conclusive evidence, requiring more destructive testing procedures, was however still needed. Due to the nature of the particles, any other technique, besides looking at the film formation properties by AFM, or, using sparse SAXS or SANS beam time, was out of the question. Particle beams in SEM and TEM would instantaneously destroy the sample and it was therefore necessary to find suitable ways to strengthen the particles. Crosslinking of the outer polymer shell was done but this only allowed a slight increase in the T_g, which was still inadequate. The logical step by which to strengthen the particles was to enforce surface grafting of the particles with a glassy polymer. Not only should the glassy nature of the secondary shell polymer provide adequate strengthening, but it would also impart better matrix mixing properties to the formed core/shell particles, when needed, and keep the original morphology intact.

Different techniques exist by which to graft polymers, *e.g.* allowing the secondary monomer to swell the seed latex, feeding the secondary monomer etc. In the present instance the original core/shell structure, i.e. liquid core and rubbery shell, had to be maintained at all costs, thus eliminating swelling of the seed latex. This technique could however be used if additional data on the phase behaviour between the shell polymer and grafting polymer was available. Rather than to complicate matters, it was decided to focus on interfacial grafting of the initial core/shell particles.

To establish surface grafting, the obvious choice was to employ an interfacial initiating system. However, further investigation was needed due to the nature of the shell polymer, PBA, used. PBA does not have any unsaturated groups, unless they are built-in deliberately, but it does possess a hydrogen atom on the PBA-backbone which can easily be removed, thus leaving an active site for grafting. The most suitable initiating system would therefore comprise an interfacial redox initiator system, *e.g.* cumyl hydroperoxide (CHP), as seen in Scheme 3.2.

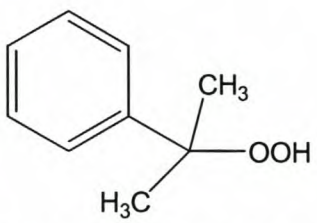

Scheme 3.2: Structure of cumyl hydroperoxide (CHP).

Redox initiators are two- or multi-component systems with varying oxidation and reduction properties.[43-46] Advantages over one-component thermal dissociative initiators include (1.) a lower activation energy, which allows a lower polymerization temperature to be used, (2.) faster dissociation rates and (3.) more hydrophobic radicals produced from CHP will preferentially be in the oil phase, thereby decreasing radical desorption to the aqueous phase and eliminating unwanted secondary nucleation processes.[39] The latter is especially important when grafting in miniemulsions due to the large quantities of surfactant present in the system.

The hydrophobic oxidant (CHP) was used together with a hydrophilic reducing agent (ferrous ion, Fe^{2+}, and sodium formaldehyde sulfoxylate, SFS) and a chelating agent ethylenediaminetetraacetic acid, disodium salt (EDTA). SFS is used to regenerate Fe^{2+} back from Fe^{3+}. EDTA will complex with Fe^{2+} to prevent Fe^{2+} oxidation in the aqueous phase.[40]

For the reaction procedure, three distinct mechanism steps can be highlighted: (1.) diffusion step, (2.) initiation step and (3.) regeneration step. For CHP as radical producer in a latex system, the process can be schematically described as in Scheme 3.3.

1.) Diffusion

$$ROOH + SFS\text{-}EDTA\text{-}Fe^{2+} \longrightarrow ROOH\text{-}Fe^{2+}\text{-}EDTA + SFS$$

2.) Initiation

$$ROOH\text{-}Fe^{2+}\text{-}EDTA \longrightarrow HO^{\cdot}Fe^{2+}\text{-}EDTA + RO^{\cdot}$$

3.) Regeneration

$$HO^{\cdot}Fe^{2+}\text{-}EDTA \longrightarrow {}^{-}HO^{\cdot}Fe^{3+}\text{-}EDTA$$

$${}^{-}HO^{\cdot}Fe^{3+}\text{-}EDTA + SFS \longrightarrow SFS\text{-}Fe^{3+}\text{-}EDTA + OH^{-}$$

$${}^{-}HO^{\cdot}Fe^{3+}\text{-}EDTA + ROOH \longrightarrow ROOH\text{-}Fe^{3+}\text{-}EDTA + OH^{-}$$

$$ROOH\text{-}Fe^{3+}\text{-}EDTA + SFS \longrightarrow SFS\text{-}Fe^{3+}\text{-}EDTA + ROOH$$

$$SFS\text{-}Fe^{3+}\text{-}EDTA \longrightarrow SO_2^{-}\text{-}Fe^{2+}\text{-}EDTA + CH_2O$$

$$SO_2^{-}\text{-}Fe^{2+}\text{-}EDTA + ROOH \longrightarrow ROOH\text{-}Fe^{2+}\text{-}EDTA + SO_2^{-}$$

$$SO_2^{-}\text{-}Fe^{2+}\text{-}EDTA + SFS \longrightarrow SFS\text{-}Fe^{2+}\text{-}EDTA + SO_2^{-}$$

Scheme 3.3: Radical producing process of CHP in the presence of a chelating agent (EDTA), reducing agent ($FeSO_4$) and regenerator (SFS).[40]

On addition of the CHP, the radical producer, being more hydrophobic, will swell the oil phase (in the case of a miniemulsion system, the droplets will be representative of the oil phase). During the diffusion step, the EDTA-Fe^{2+}-SFS complex will diffuse through the aqueous phase and react with the CHP at the droplet/water interface. Initiation will occur with the consequent formation of cumyloxy radicals, which are able to abstract a hydrogen atom from the PBA backbone.[47] In the presence of MMA, polymerization will take place, but only if the regenerator (SFS) is present to allow the reaction to continue to completion.

Scheme 3.4 shows the simplified reaction scheme for the grafting of MMA onto PBA in the absence of a regenerator.

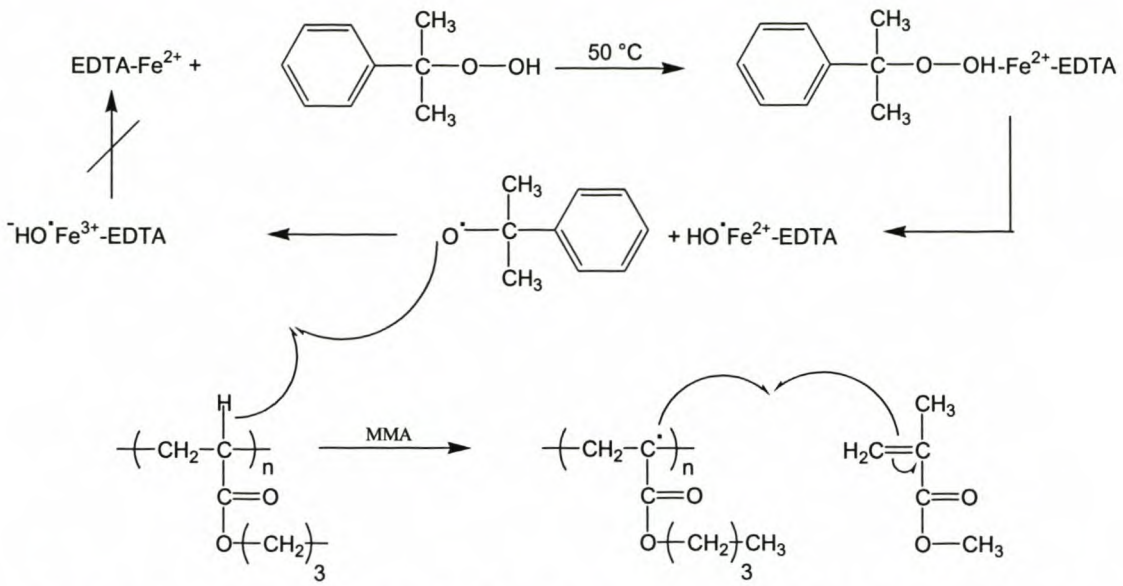

Scheme 3.4: Reaction scheme for the grafting of MMA onto PBA in the absence of a regenerator.

In this instance the regeneration of the Fe^{3+} to the lower valence Fe^{2+} cannot take place, thus causing the initiation to stop as soon as all the Fe^{2+} is used. Even though initial polymerization will be possible, it will not be able to go to completion, thereby leaving the surface of the initial particles partly covered. Results of this are presented in Figure 3.16, which shows an AFM image of agglomerated particles.

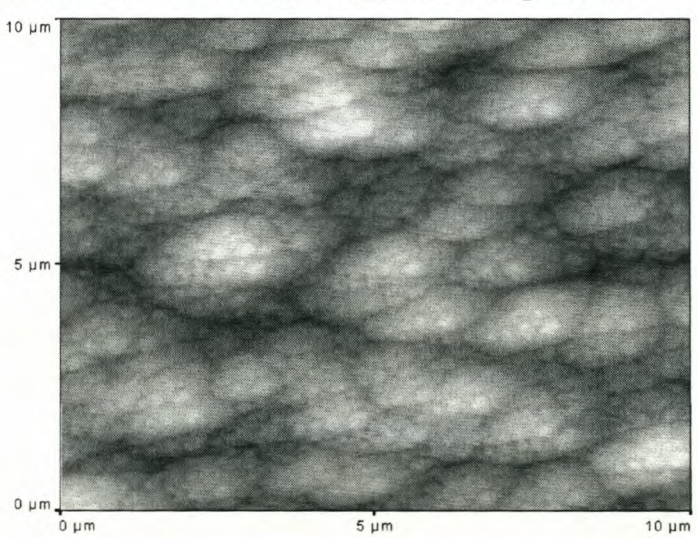

Figure 3.16: AFM image of synthesized core/shell particles illustrating agglomeration during film formation.

The definition between individual particles is not very good, indicating the predominant rubbery nature of the shell. This is reflected by film formation when the latex is precipitated and dried.

In the presence of the regenerator (SFS), polymerization will go to completion (Scheme 3.5). This is illustrated by the AFM image taken of the synthesized particles (Figure 3.17) where the effect of polymerization is clearly shown. Individual particles can be seen and precipitated particles exhibit a powdery nature upon drying.

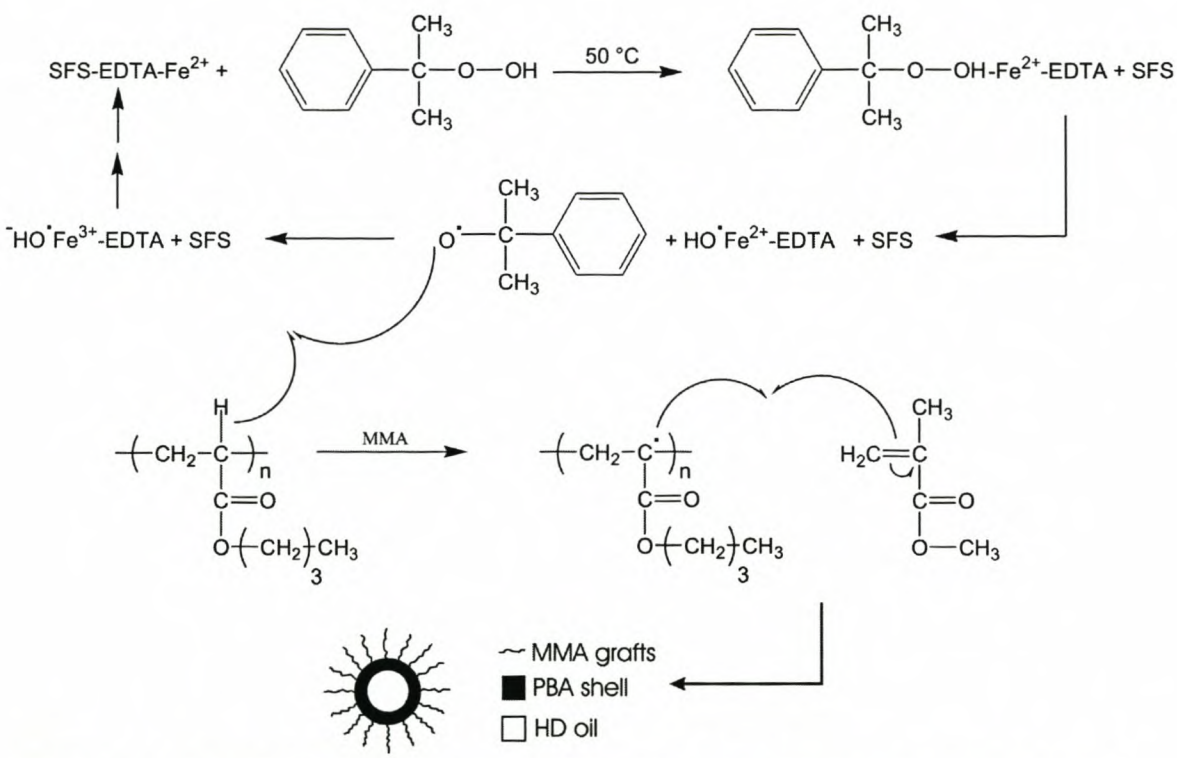

Scheme 3.5: Reaction scheme for the grafting of MMA, showing the mechanism of hydrogen abstraction from the PBA backbone and consequent formation of a secondary glassy PMMA shell.

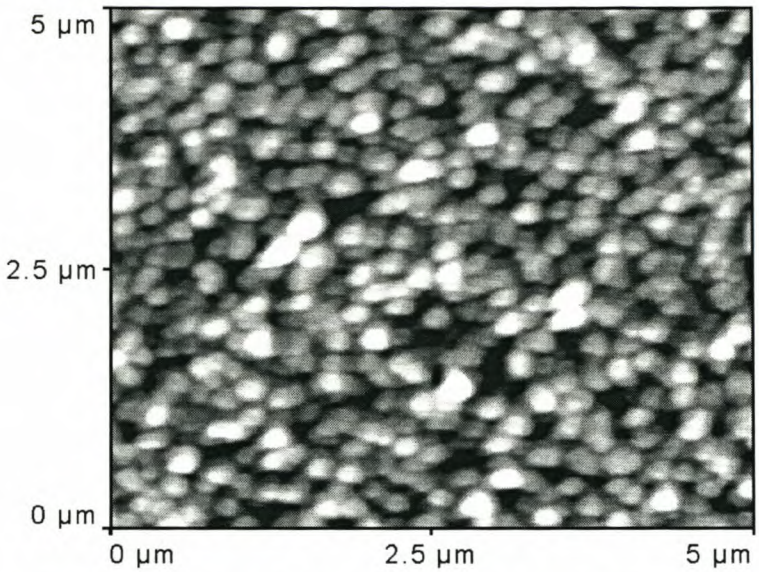

Figure 3.17: AFM image of individual spherical core/shell particles indicating a successful polymerization process and thereby decreasing agglomeration.

PBA/HD core/shell particles synthesized by miniemulsification - ultrasonication

PBA/HD core/shell particles were synthesized by a miniemulsion polymerization reaction as discussed in Section 3.3.6. Conversion curves for the polymerized PBA and added EGDMA are shown in Figure 3.18.

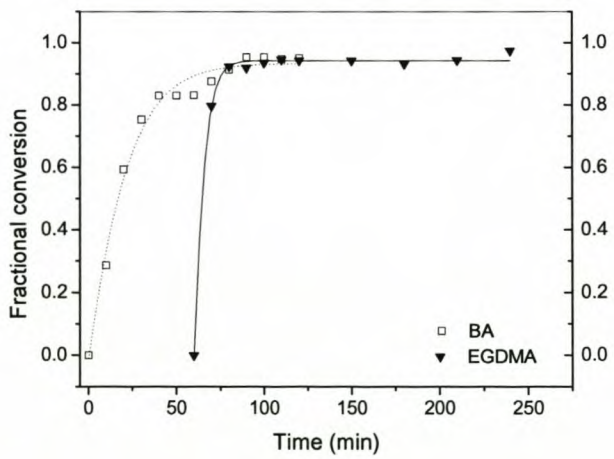

Figure 3.18: Conversion curve for the formation of PBA. The conversion curve for the addition of EGDMA at 60 minutes is also shown.

For TEM analyses the initial PBA shell was strengthened by crosslinking as well as grafting of methyl methacrylate (MMA) onto the primary PBA shell. Strengthening of the particles had to be done for TEM sample preparation. The lack of stability would lead to a destroyed morphology during embedding and curing of the particles in the epoxy resin as well as physical deformation and extraction of the particles when cut with a diamond knife during the ultramicrotoming process. Figures 3.19 (a.)-(d.) show TEM images of the particles, clearly indicating core/shell formation.

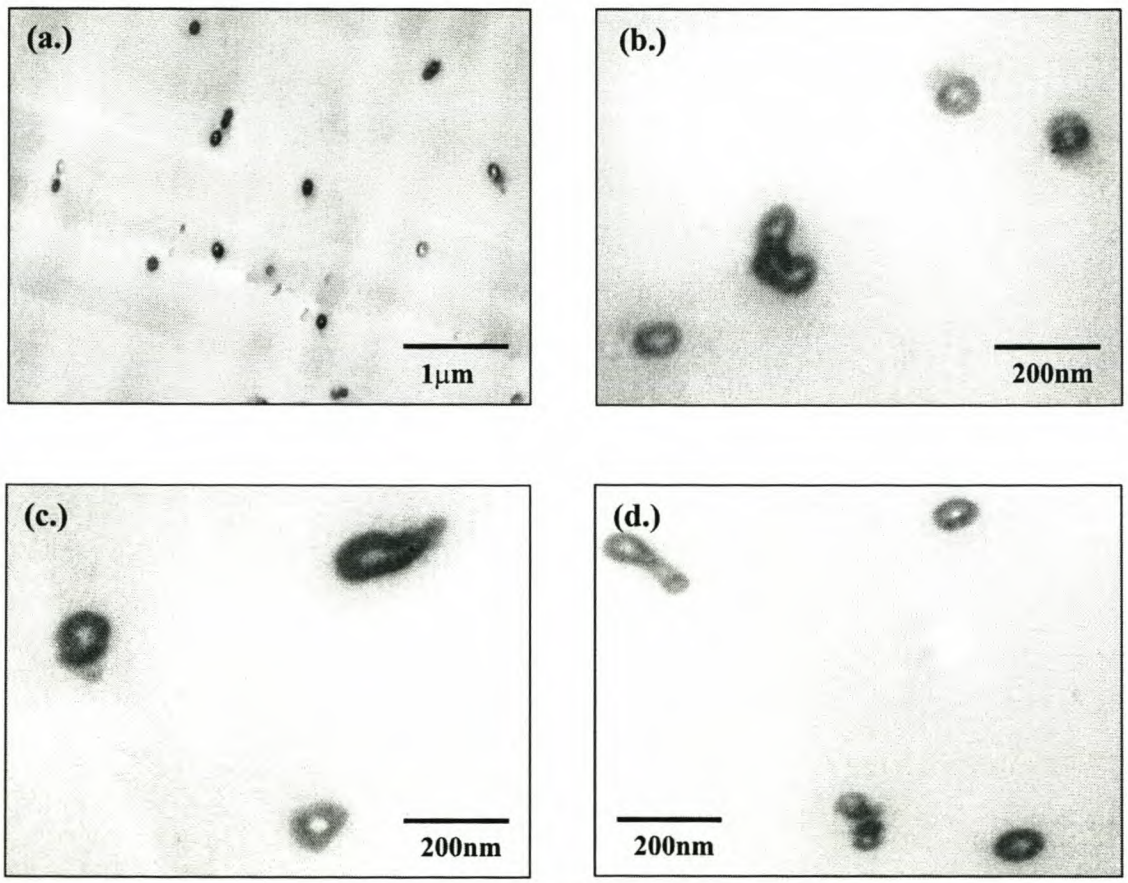

Figure 3.19: TEM images of the synthesized PBA/HD core/shell particles dispersed in Spurr's resin: (a.) is a low magnification TEM of the synthesized particles and (b.)-(d.) are high magnification images of different sections on the microtomed samples.

The stained areas are representative of the poly(meth)acrylates while the lighter areas represent the core oil, which most presumably disappeared due to the high vacuum of the

TEM. It is clear that the morphology predicted does not correspond to the morphology that was obtained experimentally. Clearly other effects contribute to the formation of proper core/shell particles and these effects must overrule the thermodynamic effects.

3.4.4 Thermodynamic vs. kinetic control of particle morphology

Influence of the anchoring effect induced by initiators

Particle morphology can be controlled by two factors, namely thermodynamics and kinetics. Unfortunately the assumption is usually made that the equilibrium morphology of the final latex composite particle is determined by the thermodynamic part of the equation while the kinetic part will only determine the ease with which the equilibrium morphology can be achieved. The work of Torza and Mason[16] can be mentioned as an example where the thermodynamics of the system were the key factor in controlling the equilibrium morphology due to the high mobility of the liquid phases.

In 1985 Cho *et al.*[48] discussed the anchoring effect of ionic terminal groups that are introduced into a sample through the use of an ionic initiator. Other factors that were investigated in their work included swelling time, pH and viscosity at the polymerization loci. This was done to explain the change in particle morphology that takes place during a polymerization reaction. The difference in hydrophobicity of the constituting phases should have an influence on the outcome of the particle morphology. However, Cho *et al.* found that this was not the case, but that morphological changes could rather be related to the type and concentration of initiator used and to the polymerization temperature. In the case of potassium persulfate (KPS) the initiator will fragment into two identical primary radicals, which will initiate polymerization. However, on entering the droplet the terminal $-SO_4^-$ endgroup will anchor itself at the water/oil interface, leading to an anchoring effect and thereby influencing morphology. A graphical representation is shown in Figure 3.20. Due to the surfactant-like nature of the oligomeric radical (polar headgroup, non-polar tail), the anchoring effect will also play an important role in the reduction of the interfacial tension and in increasing the surface polarity of the latex particles.

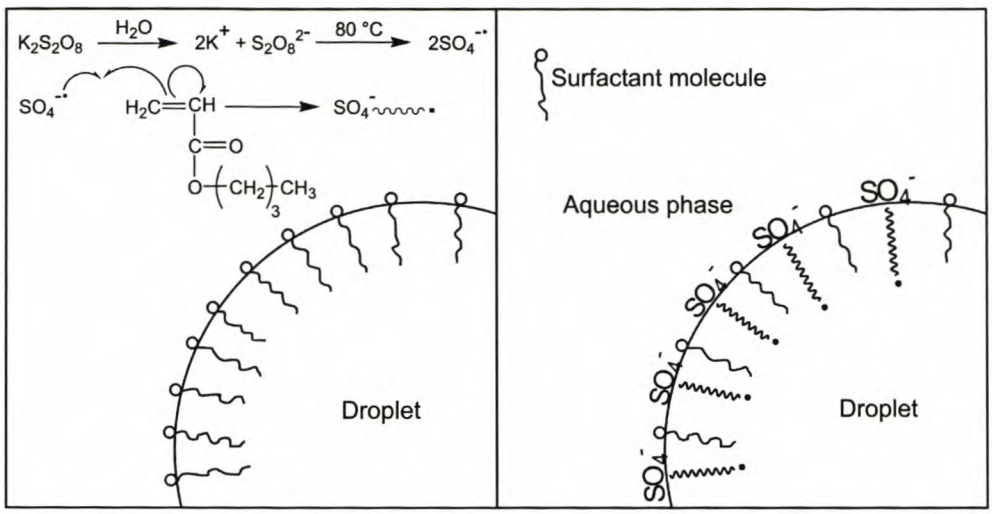

Figure 3.20: The anchoring effect caused by the interaction between entering radicals and surfactant.

Distribution of free radicals in droplets

Due to the fact that the hydrophilic endgroup of the entering oligomeric free radical will preferentially stay at the droplet/water interface, nonuniform distribution of free radicals in the droplet can occur. This will result in the movement of a growing free radical, caused by Brownian motion and/or by a propagation event, to be restricted near the surface of the droplet. Consider two possible short-chain radical concentration profiles (ρ_m) as depicted in Figure 3.21 (analogous to the distribution of free radicals in latex particles as found in emulsion systems by Chern *et al.*[49]). Curve (a.) represents a nearly uniform distribution of free radicals in a droplet whereas curve (b.) is representative of a nonuniform distribution. In the first case only one change in radical flux is present (based on the interplay between radical entry and exit), which is directed towards the aqueous phase. In the case of the nonuniform distribution two radical fluxes are present, one directed towards the inside of the droplet and the other towards the aqueous phase. The distribution of monomer-unit radical species is dependant on the location in which these species formed as well as the viscosity of the system, which will influence the mobility. Note that size of the species formed due to transfer will be similar to those of the monomer units thereby allowing relatively high mobility.

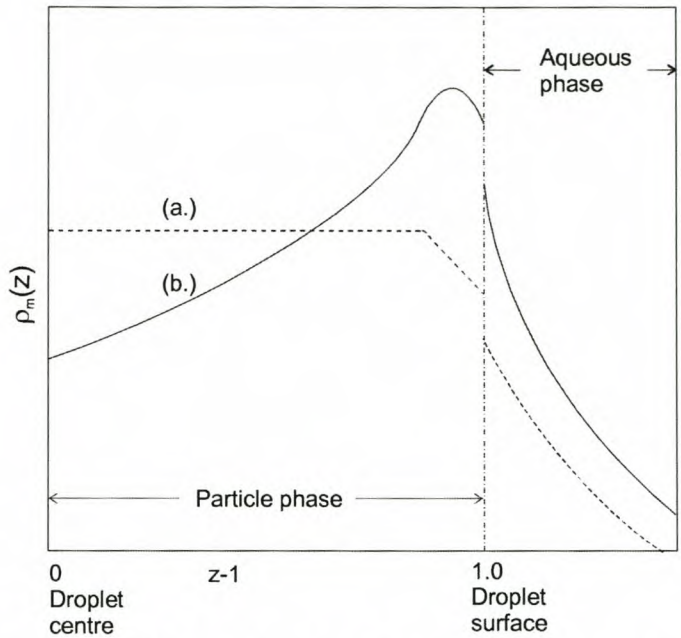

Figure 3.21: Distribution of free radicals in a droplet (analogous to Chern *et al.*[49]).

This only holds true if the viscosity of the system is not too high. For a system corresponding to high mobility species, curve (a.) will be a good approximation for the concentration profile of short-chain radical species present in the system. This profile, however, is strongly dependant on the local concentration of long-chain free radical species within the droplet volume if the viscosity of the system is very high. Chern *et al.*[49] calculated the distribution of free radicals in particles if the entering oligomeric species are anchored to the particle surface. This showed that the population of free radicals is significantly greater near the surface of the particle, thus causing the nonuniform distribution and thereby deviating from previous kinetic studies assuming uniform distribution of free radical species. This has, therefore, a considerable effect on the reaction kinetics and will therefore be able to influence the outcome of particle morphology. A similar situation will exist for droplets in a miniemulsion system.

Influence of viscosity

The rate of morphological change from one situation to the other is dependant on the diffusional resistance (which is related to chain mobility). A low viscosity at the polymerization locus will enhance the mobility of the polymer chains. This will enhance the migration of the two immiscible phases into two different domains, thus being able to adopt thermodynamically favored morphologies. A high local viscosity on the other hand will create a kinetic barrier towards polymer chain diffusion and decrease the degree of phase separation. The competition between phase separation and polymerization kinetics will be the determining factor in the generation of non-equilibrium morphologies, as shown by Cho *et al.*[48] and depicted in Figure 3.22.

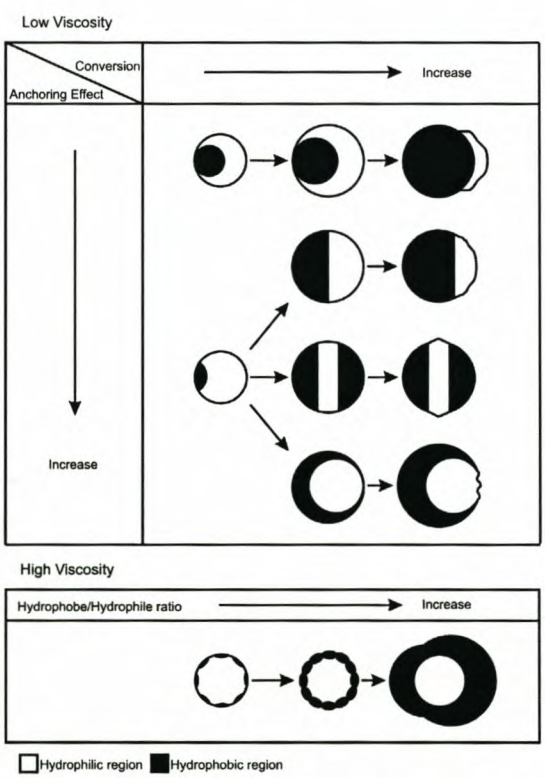

Figure 3.22: The influence of the degree of anchoring, conversion and viscosity on the outcome of particle morphology.[48]

Further evidence of kinetically controlled particle morphology was given in 1990 by Mills *et al.*[50] who considered the dependence of the morphology on various factors

including rate of diffusion, propagation, termination, entry, transfer and exit. In order to do this the monomer and free radical concentrations in particles were calculated as a function of position and time, using "pseudobulk" equations.[51] These equations were extended[50] to take into account diffusion, spatial inhomogeneities as well as the chain length dependant termination kinetics. Instead of only using single free radical species *R(r,t)* (which is the concentration of free radicals as a function of time and position in a particle) long radicals and relatively mobile short radicals were considered. Entering radicals can be seen as long, due to the surface anchoring effect of the hydrophilic endgroup, while exiting radicals must be short to be reasonably soluble in the aqueous phase.

The equations for these conditions are:

$$\frac{\partial L(r,t)}{\partial t} = \frac{1}{r^2}\frac{\partial}{\partial r}\left[r^2 D_L \frac{\partial L(r,t)}{\partial r}\right] - 2k_{tLL}L(r,t)^2 - k_{tr}L(r,t)M(r,t) - k_{tSL}S(r,t)L(r,t) + k_p S(r,t)C_m/Z \tag{3.21}$$

$$\frac{\partial M(r,t)}{\partial t} = \frac{1}{r^2}\frac{\partial}{\partial r}\left[r^2 D_M \frac{\partial M(r,t)}{\partial r}\right] - k_p M(r,t)[L(r,t) + S(r,t)] \tag{3.22}$$

$$\frac{\partial S(r,t)}{\partial t} = \frac{1}{r^2}\frac{\partial}{\partial r}\left[r^2 D_S \frac{\partial S(r,t)}{\partial r}\right] - 2k_{tSS}S(r,t)^2 + k_{tr}L(r,t)M(r,t) - k_{tSL}S(r,t)L(r,t) - k_p S(r,t)C_m/Z \tag{3.23}$$

where *M(r,t)* is the concentration of the monomer, *L(r,t)* and *S(r,t)* the concentrations of the short and long free radicals respectively, k_{tr} is the rate coefficient for transfer to monomer, k_{tLL} is the rate coefficient for termination between two long free radicals, k_{tSL} is the rate coefficient for termination between a short and long free radical, k_{tSS} is the rate coefficient for termination between two short free radicals, D_L and D_S are the diffusion coefficients for long and short free radicals respectively, k_p is the propagation rate coefficient, C_m is the concentration of monomer in the particles, Z is the chain length at

which a short chain becomes a long chain, r is the distance from the centre of the particle and t is the time.

A number of very important deductions were made from these kinetic studies *e.g.* (1.) the probability to produce a core/shell morphology will increase when the rate coefficient of entry of free radicals is sufficiently high (*e.g.* in the case of a redox initiator) and (2.) a higher tendency for core/shell morphology is possible when the rate of termination is high relative to the rate of diffusion.

Influence of the repulsive wall effect

The repulsive wall effect is a result of the decrease in entropy of a polymer chain being confined near the surface of a droplet/particle.[52,53] This is also a thermodynamic effect and can effectively work against surface anchoring by repelling the growing polymer away from the droplet surface. However, studies by Mills *et al.*[54] found that entropic driving forces of polymeric chains away from the particle surface are negligible and do therefore not contribute significantly to establishing the morphology. The effect of surface anchoring is, therefore, still the dominant contributor

The deviation from thermodynamically controlled particle morphology has been mentioned by many other authors including Jönsson *et al.*,[55] Stubbs *et al.*,[56] Shen *et al.*[57] and Muscato *et al.*[58]

Additional evidence for kinetically controlled particle morphology

A further study into the effect of chain mobility on the obtained morphology was undertaken by changing the initiation system. Two aspects of the initiation system were taken into consideration: first, the anchoring effect, which is present in the case of a charged primary radical (*viz.* KPS) and, second, the locus of generation of primary radicals. In this study the initiator was changed from KPS to AIBN as well as to a redox initiator.

For the redox initiator, cumyl hydroperoxide with Fe^{2+} was chosen. This system is the same as was used for the grafting of the PMMA onto the initial PBA shell (Section 3.3.6). CHP is oil soluble and will enter the droplets when added to the miniemulsified system. However, CHP only dissociates at an appreciable rate in conjunction with the transition metal complex (Fe^{2+}/EDTA), which is water soluble. Therefore, the primary radical producing reaction can only take place at the oil/water interface. Hydrophobic radicals produced from the redox reaction between CHP and Fe^{2+} will initiate the butyl acrylate monomer to form oligomer radicals ($P_i^{\cdot}$) at the surface of the monomer droplets. Butyl acrylate and CHP gradually diffuse out to supply the monomer and initiator consumption at the outer layer of the droplet. Initial polymerization therefore starts in the outer layer, thus causing an increase in viscosity of this region with monomer conversion. As viscosity increases, the CHP and BA diffusion rate will slow. The concentration of CHP and BA in the outer layer will therefore be lower compared to the concentration in the inner layer, gradually tapering off as the reaction proceeds. Figure 3.23 represents the expected concentration distribution of each of the reagents present.

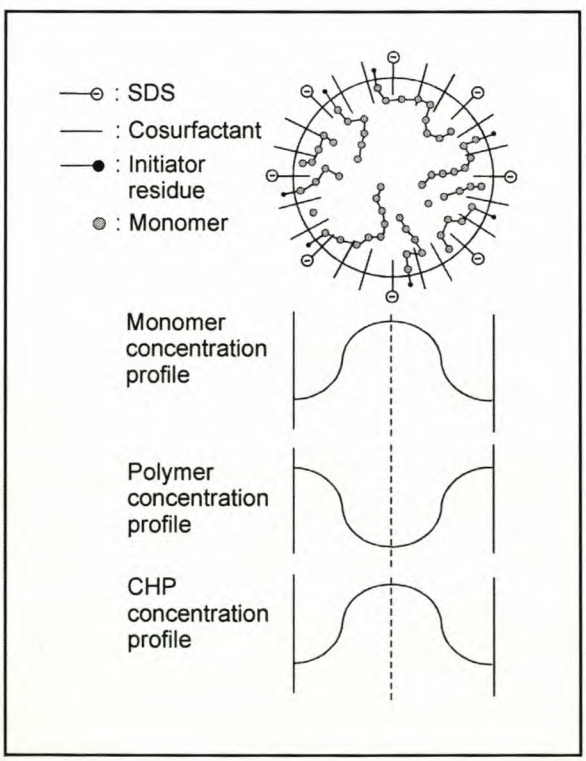

Figure 3.23: Concentration distribution of each of the reagents present in a redox initiated system.[40]

Results of the experiment with redox initiation can be seen in Figure 3.24.

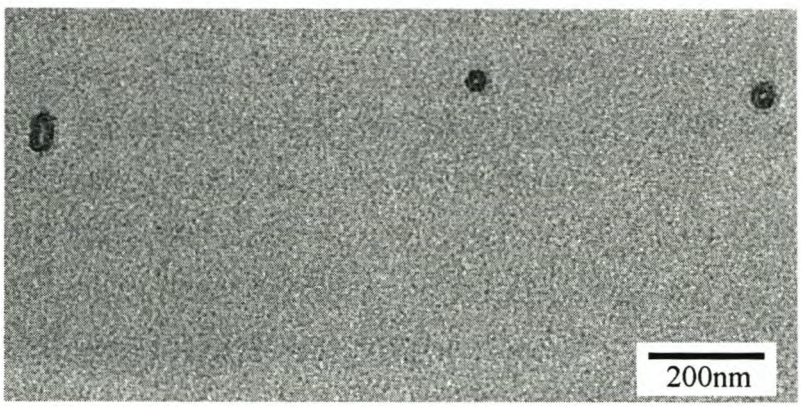

Figure 3.24: TEM image of core/shell particles synthesized with the use of a redox initiator.

AIBN was used as an oil-soluble initiator that will generate primary radicals throughout the organic phase. AIBN has no ionic group that can establish surface anchoring and shows slightly higher rates of dissociation compared to KPS.[59] Thus, although AIBN has a degree of water phase initiation,[60-62] the entering radicals will not be able to anchor themselves at the water/droplet interface, and primary radicals will also be created in the interior of the latex particle. The result of the AIBN initiated polymerization can be seen in Figure 3.25.

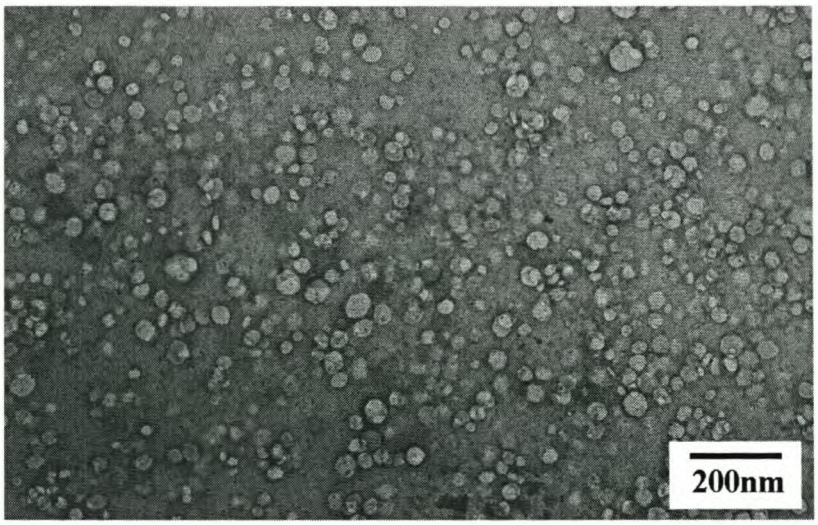

Figure 3.25: TEM image of solid particles synthesized with the use of an oil-soluble initiator (AIBN).

The main difference between the AIBN initiated system and the KPS or CHP/Fe^{2+} initiated systems is the solid particles obtained in the former, and the core/shell particles obtained in the latter case. KPS leads to surface anchoring as discussed above. However, both CHP and AIBN yield oil-soluble primary radicals that do not seem to have a particular preference for the oil – water interface. As mentioned, AIBN and CHP/Fe^{2+} differ in their locus of primary radical generation. The essential question then is: how fast is initiation/propagation compared to diffusion; more specifically, is a primary radical or short chain oligomer able to diffuse throughout the particle before it has grown to a chain length that virtually immobilizes it? An accurate assessment of diffusivity *versus* polymerization kinetics is quite complicated. Therefore, we limit the assessment to an order of magnitude estimation of the so-called Damköhler number (Da).[63] This is a dimensionless number that indicates whether a reaction is diffusion-controlled or chemically controlled. The Damköhler number is defined as follows:

$$\mathrm{Da} = \frac{k_p \cdot [M]}{\mathrm{D}/\mathrm{d}^2} \qquad (3.24)$$

where D is the diffusion coefficient of a low molar mass species in a semi-dilute polymer solution, k_p is the propagation rate constant of a growing radical (or initiation rate constant of a primary radical), $[M]$ is the monomer concentration at the locus of polymerization, and d is the relevant diffusion distance. Typical values for these quantities are: $D = 10^{-9}$ m^2s^{-1}, $k_p = 10^4$ L $mol^{-1}s^{-1}$, $[M] = 5$ mol L^{-1}, $d = 10^{-8}$ m. This would result in $Da = 5\times10^{-3}$ which is indicative of a system without transport limitation ($Da << 1$). Nevertheless, core/shell morphology is observed in the CHP/Fe^{2+} initiated system. One of the likely origins of the difference in morphology between AIBN and CHP/Fe^{2+} is hydrogen abstraction from already formed PBA. The cumyloxy radical has a relatively strong tendency towards H-abstraction,[47] and the cumyloxy radicals are formed at the oil-water interface. This may lead to branched or even crosslinked polymer in the outer shell of the particle. This in turn will limit the mobility of the polymer and lead to core/shell morphology.

From the results it is thus quite clear that core/shell morphology can be obtained when radicals are formed at the oil/water interface and if diffusion to the interior of the particle is restricted.

3.5 Conclusions

Core/shell particles with liquid cores were synthesized via an *in situ* miniemulsion polymerization process. Morphology predictions were performed on the investigated system and it was found that predicted and observed morphologies did not coincide. The reason for this discrepancy is that current prediction models are only based on thermodynamic considerations and not on kinetic considerations. Deviation from the predicted morphology can be caused by the type and amount of surfactant and type of initiator used in the miniemulsion polymerization reaction. Selection of the proper initiator type can lead to anchoring of entering radicals. This will reduce the ability of radicals to diffuse to the inside of the droplet. Polymerization will therefore occur preferentially at the oil/water interface, thereby causing a phase separation between the polymer and core-oil, thus forming the desired core/shell particles with liquid cores. This

reasoning was further strengthened by changing the type of initiator. AIBN provides no surface anchoring. In this instance the thermodynamically preferred morphology, which is inverse core/shell, will dominate, thus causing solid poly(butyl acrylate) particles to form. The redox initiator (CHP/Fe^{2+}) was used to specifically create primary radicals at the water/oil interface. The fact that this way of initiation leads to core/shell particles is most likely due to branching, which leads to decreased mobility of the chains near the surface of the particle.

References

(1) Hughes, L. J.; Brown, G. L. *J. Appl. Polym. Sci.* **1961**, *V*, 580-588.

(2) Grancio, M. R.; Williams, D. J. *J. Polym. Sci., Part A-1* **1970**, *8*, 2617-2629.

(3) Arshady, R. *Polym. Eng. Sci.* **1989**, *29*, 1746-1758.

(4) Arshady, R. *Polym. Eng. Sci.* **1990**, *30*, 905-914.

(5) Frère, Y.; Danicher, L.; Gramain, P. *Eur. Polym. J.* **1998**, *34*, 193-199.

(6) Arshady, R. *Polym. Eng. Sci.* **1990**, *30*, 915-924.

(7) Jung, M. *Polymerization in bilayers*, Technische Universiteit Eindhoven, Eindhoven, 2000.

(8) Sudol, E. D.; El-Aasser, M. S. In *Emulsion Polymerization and Emulsion Polymers*; Lovell, P. A.; El-Aasser, M. S., Eds.; John Wiley and Sons Ltd.: England, 1997; pp 699-722.

(9) Kirsch, S.; Landfester, K.; Shaffer, O.; El-Aasser, M. S. *Acta Polym.* **1999**, *50*, 347-362.

(10) Schellenberg, C.; Akari, S.; Regenbrecht, M.; Tauer, K.; Petrat, F. M.; Antonietti, M. *Langmuir* **1999**, *15*, 1283-1290.

(11) Sommer, F.; Duc, T. M.; Pirri, R.; Meunier, G.; Quet, C. *Langmuir* **1995**, *11*, 440-448.

(12) Landfester, K.; Boeffel, C.; Lambla, M.; Spiess, H. W. *Macromolecules* **1996**, *29*, 5972-5980.

(13) Dobashi, T.; Yeh, F.-J.; Ying, Q.; Ichikawa, K.; Chu, B. *Langmuir* **1995**, *11*, 4278-4282.

(14) Sekine, K.; Hanai, T. *Colloid Polym. Sci.* **1991**, *269*, 880-888.

(15) Tiarks, F.; Landfester, K.; Antonietti, M. *Langmuir* **2001**, *17*, 908-918.

(16) Torza, S.; Mason, S. G. *J. Colloid Interface Sci.* **1970**, *33*, 67-83.

(17) Reiss, H. *J. Colloid Interface Sci.* **1975**, *53*, 61-70.

(18) Berg, J.; Sundberg, D.; Kronberg, B. *J. Microencapsulation* **1989**, *6*, 327-337.

(19) Sundberg, D. C.; Casassa, A. P.; Pantazopoulos, J.; Muscato, M. R.; Kronberg, B.; Berg, J. *J. Appl. Polym. Sci.* **1990**, *41*, 1425-1442.

(20) Sundberg, E. J.; Sundberg, D. C. *J. Appl. Polym. Sci.* **1993**, *47*, 1277-1294.

(21) Winzor, C. L.; Sundberg, D. C. *Polymer* **1992**, *33*, 3797-3810.

(22) Chen, Y. C.; Dimonie, V.; El-Aasser, M. S. *J. Appl. Polym. Sci.* **1992**, *45*, 487-499.

(23) Chen, Y.-C.; Dimonie, V.; El-Aasser, M. S. *Macromolecules* **1991**, *24*, 3779-3787.

(24) Waters, J. A. *Colloids Surf., A* **1994**, *83*, 167-174.

(25) Waters, J. A. In *Colloidal Polymer Particles*, Second ed.; Goodwin, J. W.; Buscall, R., Eds.; Academic Press Limited: London, 1995; pp 113-135.

(26) Loxley, A.; Vincent, B. *J. Colloid Interface Sci.* **1998**, *208*, 49-62.

(27) Chen, Y.-C.; Dimonie, V. L.; Shaffer, O. L.; El-Aasser, M. S. *Polym. Int.* **1993**, *30*, 185-194.

(28) Stubbs, J. M.; Sundberg, D. C. *Journal of Coatings Technology* **2003**, *75*, 59-67.

(29) Lee, S.; Rudin, A. In *Polymer Latexes: Preparation, Characterization and Applications*; Daniels, E. S., Ed.; ACS: Washington DC, 1992; pp 234-254.

(30) Domingue, J. *Am. Lab.* **1990**, 50-55.

(31) Wu, S. *Polymer Interface and Adhesion*; Marcel Dekker Inc., 1982.

(32) Van Krevelen, D. W. *Properties of Polymers. Their Correlation with Chemical Structure; their Numerical Estimation and Prediction from Additive Group Contributions*; Elsevier Science B.V.: The Netherlands, 1997.

(33) Lide, D. L. *CRC Handbook of Chemistry and Physics*, 76th Edition ed.; CRC Press Inc., 1995.

(34) Wu, S. *J. Macromol. Sci.-Revs. Macromol. Chem.* **1974**, *C10*, 1-73.

(35) McDonald, C. J.; Bouck, K. J.; Chaput, A. B. *Macromolecules* **2000**, *33*, 1593-1605.

(36) Jang, J.; Lee, K. *Chem. Commun.* **2002**, *10*, 1098-1099.

(37) Dimonie, V. L.; Daniels, E. S.; Shaffer, O. L.; El-Aasser, M. S. In *Emulsion Polymerization and Emulsion Polymers*; Lovell, P. A.; El-Aasser, M. S., Eds.; John Wiley & Sons Ltd: Chichester, 1997; pp 293-326.

(38) Bachtsi, A. R.; Boutris, C. J.; Kiparissides, C. *J. Appl. Polym. Sci.* **1996**, *60*, 9-20.

(39) Wang, C. C.; Yu, N. S.; Chen, C. Y.; Kuo, J. F. *J. Appl. Polym. Sci.* **1996**, *60*, 493-501.

(40) Wang, C. C.; Yu, N. S.; Chen, C. Y.; Kuo, J. F. *Polymer* **1996**, *37*, 2509-2516.

(41) Sue, H. J.; Garcia-Meitin, E. I.; Burton, B. L.; Garrison, C. C. *J. Polym. Sci., Part B: Polym. Phys.* **1991**, *29*, 1623-1631.

(42) Landfester, K.; Bechtold, N.; Tiarks, F.; Antonietti, M. *Macromolecules* **1999**, *32*, 5222-5228.

(43) Behari, K.; Tripathi, M.; Taunk, K.; Kumar, R. *Polym. Int.* **2000**, *49*, 153-157.

(44) Yurkova, I. L.; Schuchmann, H.-P.; Sonntag, C. v. *J. Chem. Soc., Perkin Trans.* **1999**, *2*, 2049-2052.

(45) Kolthoff, I. M.; Medalia, A. I. *J. Polym. Sci.* **1949**, *V*, 391-427.

(46) Van den Hoven, B.; Ostlender, P.; TU Eindhoven; Akzo Nobel Central Research Deventer, 1998.

(47) Moad, G.; Solomon, D. H. *The Chemistry of Free Radical Polymerization*; Pergamon Press: Oxford, 1995.

(48) Cho, I.; Lee, K.-W. *J. Appl. Polym. Sci.* **1985**, *30*, 1903-1926.

(49) Chern, C.-S.; Poehlein, G. W. *J. Polym. Sci., Part A: Polym. Chem.* **1987**, *25*, 617-635.

(50) Mills, M. F.; Gilbert, R. G.; Napper, D. H. *Macromolecules* **1990**, *23*, 4247-4257.

(51) Ballard, M. J.; Napper, D. H.; Gilbert, R. G. *J. Polym. Sci.: Polym. Chem. Ed.* **1984**, *22*, 3225-3253.

(52) Gilbert, R. G. *Emulsion Polymerization: A Mechanistic Approach*; Academic Press Limited: London, 1995.

(53) Croxton, C. A.; Mills, M. F.; Gilbert, R. G.; Napper, D. H. *Macromolecules* **1993**, *26*, 3563-3571.

(54) Mills, M. F.; Gilbert, R. G.; Napper, D. H.; Rennie, A. R.; Ottewill, R. H. *Macromolecules* **1993**, *26*, 3553-3562.

(55) Jönsson, J.-E.; Hassander, H.; Törnell, B. *Macromolecules* **1994**, *27*, 1932-1937.

(56) Stubbs, J.; Karlsson, O.; Jönsson, J.-E.; Sundberg, E.; Durant, Y.; Sundberg, D. *Colloids Surf., A* **1999**, *153*, 255-270.

(57) Shen, S.; El-Aasser, M. S.; Dimonie, V. L.; Vanderhoff, J. W.; Sudol, E. D. *J. Polym. Sci., Part A: Polym. Chem.* **1991**, *29*, 857-867.

(58) Muscato, M. R.; Sundberg, D. C. *J. Polym. Sci., Part B: Polym. Phys.* **1991**, *29*, 1021-1024.

(59) *Polymer Handbook*, Second ed.; Wiley Interscience: New York, 1975.

(60) Luo, Y.; Schork, F. J. *J. Polym. Sci., Part A: Polym. Chem.* **2002**, *40*, 3200-3211.

(61) Blythe, P. J.; Klein, A.; Phillips, J. A.; Sudol, E. D.; El-Aasser, M. S. *J. Polym. Sci., Part A: Polym. Chem.* **1999**, *37*, 4449-4457.

(62) Alduncin, J. A.; Forcada, J.; Barandiaran, M. J.; Asua, J. M. *J. Polym. Sci., Part A: Polym. Chem.* **1991**, *29*, 1265-1270.

(63) Thoenes, D. *Chemical Reactor Development from Laboratory Synthesis to Industrial Production*; Kluwer Academic Publishers: Dordrecht, 1994.

Chapter 4

The role of surfactant in controlling particle size and stability in the miniemulsion polymerization of polymeric nanocapsules

Abstract

The influence of surfactant concentration on particles, in particular core/shell particles with liquid cores, synthesized by an in situ miniemulsion polymerization process, was investigated. Although the role of surfactant in the synthesis of particles in the nanometer range has frequently been documented, the transition from seed to structured particles, which almost consist of a 1:1 weight ratio of liquid hydrophobe encapsulated by polymeric shell, has not received much attention. Capillary hydrodynamic fractionation (CHDF) analysis was used to evaluate particle size. These results were subsequently used to stoichiometrically calculate the area which is occupied per surfactant molecule on the particle surface. These results were compared with "classical" miniemulsion data, i.e. data generated from the synthesis of polymeric latexes in the presence of a hydrophobe, but at a much lower hydrophobe:monomer ratio as was used here. The surface coverage per surfactant molecule could be related to the surface tension of the latex, thus providing a relationship between particle size and

stability. CHDF was furthermore used to investigate particle size after grafting of the secondary shell as well as to examine the influence of MeOH addition on particle size. Data obtained from CHDF experiments were in all cases confirmed by TEM analysis of the synthesized particles. To conclude, the synthesis of core/shell particles with liquid cores could be successfully scaled-up, with retention of all the characteristics of the final latex.

4.1 Introduction

The synthetic route for core/shell particles with liquid cores differs slightly from the conventional emulsion polymerization systems because of the high hydrophobicity and low water solubility of the core oil. In a conventional emulsion polymerization no transport of the oil into micelles will take place; hence an oily layer will be present at the end of the reaction. Miniemulsion polymerization, however, has proven to be a versatile method for these types of reactions.[1]

Miniemulsion polymerization starts with the dispersion of an oil phase in a continuous aqueous phase. The size of the dispersed droplets is usually between 50 and 500 nm and the dispersion is created by applying a shear field to a system consisting of water, oil, surfactant and cosurfactant or hydrophobe. Shear can be applied by various techniques including microfluidizing, ultrasonication and high-speed agitation or mixing. Because most of the oil phase is forced into the droplets by the high shear devices, a 1:1 copy of the droplets to the particles should be obtained upon polymerization in the ideal case. However, system instabilities such as Ostwald ripening and droplet growth by collision and coalescence can occur if preventative measures are not taken.[2] Ways to overcome these problems are, for example, through the optimization of types and concentrations of surfactants and cosurfactants or hydrophobes used, which will not only avoid destabilization effects but will also influence the initial droplets by changing droplet area and consequently particle size. Landfester *et al.*[3] showed that particle size can be controlled by the ultrasonication time as well as the variation of the amount of surfactant used. At constant ultrasonication time, particle size will be dependant on the ability to increase and stabilize "newly created" interfacial areas. The ability to stabilize the "newly created" surface area is therefore solely dependant on the amount of surfactant used and hence the area of the droplet which will be covered by surfactant chains becomes an important parameter in determining particle size. The smaller the droplets are and the more collisions they undergo, the more dense the coverage of the particles with surfactant must be to keep the miniemulsion stable.[4] According to Landfester[5] only one SDS molecule per 5.5 nm^2 interfacial area is necessary to stabilize a particle with a

diameter of about 180 nm. This value will decrease with particle size to a value smaller than 0.4 nm^2 for particles with a diameter smaller than 50 nm.

Until recently, most studies involving miniemulsions focused on the influence of surfactants/cosurfactants and the mechanisms involved in creating stable particles. In this chapter the use of *in situ* miniemulsion polymerization to create core/shell particles with liquid cores, to be used as impact modifying agents, will be described. Hexadecane will be used as both core-liquid and hydrophobe. Poly(butyl acrylate) (PBA) will be used as shell polymer. Poly(methyl methacrylate) (PMMA) will be used to cap the initial particle to add physical stability and compatibility with the PMMA matrix that will be used in further impact modification studies. As very small particles are necessary for effective impact modification,[6] the influence of surfactant concentration on the particle size will be investigated. Results will be compared to "classical" miniemulsion results, i.e. particle size and stability as a function of surfactant concentration, and trends will be explained.

4.2 Theoretical background

4.2.1 Emulsion vs. miniemulsion polymerization systems

Emulsion polymerization usually comprises an aqueous continuous phase, water-soluble initiator, water-insoluble monomer as well as a suitable surfactant to facilitate micelle formation. Three main mechanisms have been proposed for particle formation in such a system, namely, *micellar*, *homogeneous* and *droplet* nucleation.[7]

In the occurrence of *micellar nucleation*, initiator radicals generated in the aqueous phase will enter the monomer swollen surfactant micelles. This will initialize polymerization to form monomer swollen polymeric particles, which will facilitate further growth by propagation reactions. Growth will continue until monomer and surfactant are depleted from unentered micelles and will cease with the disappearance of the micelles, at which point a constant number of particles will be present.

Homogeneous nucleation will occur when aqueous phase radicals propagate by adding monomer, thus forming oligomeric radical species. Addition will continue until a critical length is reached, at which point insolubility in the aqueous phase and consequent precipitation will occur. The precipitated oligomeric radicals will form primary particles and subsequently adsorb surfactant molecules, to stabilize themselves, as well as monomer for further propagation.
Droplet nucleation, on the other hand, occurs when aqueous phase radicals enters monomer emulsion droplets and propagate to form polymeric particles.

Although all three mechanisms can occur in emulsion polymerization systems, droplet nucleation is the predominant mechanism in miniemulsion polymerizations comprising monomers or macromonomers with extremely low water solubilities and where the small size of the droplet can compete effectively for the generated radicals. Whereas colloidal stability is the main concern in emulsion systems, miniemulsions require additional stabilization against coalescence of droplets as a result of collisions, as well as growing of droplets due to Ostwald ripening.

In the progress of emulsion polymerization, three distinct intervals are observed. Interval I is defined as the period of particle formation. Interval II is the period of particle growth at the expense of the monomer droplets, thus resulting in a constant rate of polymerization in this interval. In interval III only two phases remain, namely, the water phase and the monomer swollen particles. As polymerization proceeds, the concentration of monomer will decrease and therefore also the rate of polymerization.

In miniemulsion polymerization, however, interval II (i.e. the period of particle growth) is not present, as can be seen in Figure 4.1.[8] In this instance interval I is the particle nucleation interval and is the time needed to reach an equilibrium radical concentration within every droplet formed during the miniemulsification process. The low radical flux through the droplet interface will determine the rate of this interval and will proceed until the average number of radicals per particle, $\bar{n} \sim 0.5$, is established.[8,9] This will result in the droplets not being nucleated at exactly the same time so that the

evolution of conversion in each droplet is not the same. For this reason every droplet can therefore be seen as an individual nanoreactor.

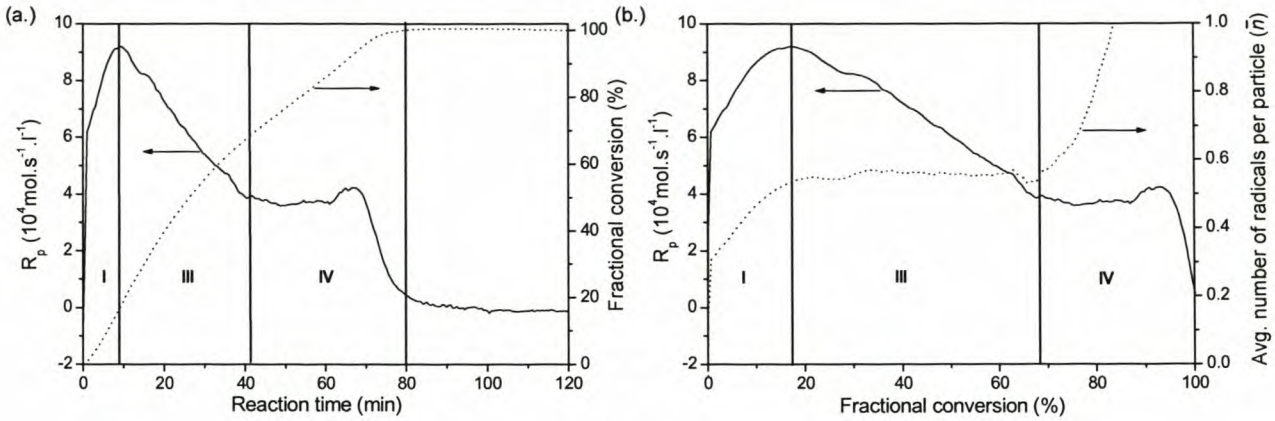

Figure 4.1: (a.) Calorimetric curve of a typical miniemulsion showing the three distinct intervals in this type of polymerization and (b.) the development of the average number of radicals per particle as a function of the fractional conversion.[4]

In interval III, only monomer in the droplet is left for polymerization, which resembles bulk or suspension polymerization, and will therefore show an exponential depletion as monomer is consumed. Interval IV can be attributed to the increase in viscosity in the droplet, which will cause a gel effect, a barrier to recombination and therefore an increase in the average number of radicals per particle ($\bar{n} > 0.5$).

Ugelstad *et al.*[10] were the first to report on miniemulsion polymerization in the 1970s and were soon followed by numerous scientists probing the many uses of this versatile technique.[11-17] However, as can be seen from the above discussion, special care must be taken to ensure stability of the submicron system. In the next few paragraphs this will briefly be highlighted and explained.

4.2.2 The formation of a miniemulsion

Miniemulsions can successfully be formed by the application of various homogenization techniques. In the earliest reports on miniemulsions, stirring was used,

but this has now made way for high-speed agitation, microfluidization as well as ultrasonication to effectively form submicron droplets.

Miniemulsification involving mechanical agitation usually starts with a pre-emulsion step, which includes the premixing of the liquid phase containing the surfactants/cosurfactants as well as the oil (monomer etc.).[18] During this step the droplets are deformed and disrupted in order to increase the specific area of the emulsion. This is subsequently followed by stabilization of the newly formed interfaces by surfactant. During break-up and deformation, nearly no surfactant will be located at the droplet interface. The reason for this is that adsorption of surfactant is slower than deformation. However, surfactant is still able to adsorb to the newly formed droplets between disruption steps.

The produced droplet size is usually determined by factors such as the monomer density, monomer solubility, aqueous density, concentration of surfactant as well as the concentration of the cosurfactant or hydrophobe. For a monomeric miniemulsion the produced droplet size is a function of the amount of shear but will undergo rapid change immediately after sonication until a pseudo steady-state is reached. The droplet size will then be independant of further shear only if a minimum amount of disruption was applied in the initial step.

Miniemulsification by ultrasound also commences with a pre-stir in order to reach droplet sizes which are about ten times the size of the desired miniemulsified droplets. Pre-stir is followed by ultrasonication, during which droplets are further broken down by unstable oscillations of the liquid-liquid interface as well as cavitation.[19] Droplet size will steadily decrease until equilibrium is reached although initial size distributions are all but uniform. Uniformity is reached after a fission/fusion process, thus reaching the preferred steady-state.[4]

4.2.3 Colloidal stability of miniemulsions

For dispersed droplets, as caused by miniemulsification, there are two mechanisms that can effectively lead to a change in the droplet size and number, and therefore droplet instability. These mechanisms are growth by Ostwald ripening (τ_1 mechanism) and growth by collision between droplets (τ_2 mechanism).[2,3,5,20] Coalescence (or growth by collision) can effectively be controlled by the addition of a surfactant of which numerous types have successfully been employed.[21-24] Ostwald ripening involves using a hydrophobe to effectively create an osmotic pressure in every droplet, which will suppress monomer diffusion from smaller to bigger droplets. Because the hydrophobe is confined in every droplet, a small decrease in droplet size (which might be due to diffusion) will cause a large increase in osmotic pressure (Π) due to the fact that $\Pi \sim R^{-3}$ (where R is the droplet radius) whereas the Laplace pressure only scales with R^{-1}. A minimum amount of hydrophobe is necessary to counteract the influence of Ostwald ripening and the effectiveness of the hydrophobe will increase with a decrease in water solubility. Employed hydrophobes include hexadecane (which is the most commonly used), silanes, siloxanes, fluorinated alkanes etc.

Other hydrophobes, which also act as costabilizers, but not necessarily by counteracting the Laplace pressure, are the addition of polymer, cetyl alcohol[25] as well as comonomers.[26-31] The addition of a monomer-soluble polymer to a miniemulsion will significantly reduce diffusion degradation of the droplets. Such a miniemulsion will, however, not be stable for long periods, as is the case for the long chain alkanes and alcohols, but will provide adequate stability to resist diffusion long enough for nucleation to occur. In this case the polymer stabilizes the droplets kinetically and not thermodynamically.[20] When using cetyl alcohol as costabilizer an unstable miniemulsion will be obtained. However, when cetyl alcohol is used in addition to a surfactant system, increased stability is observed. This is due to the formation of a liquid crystal layer at the droplet/water interface, thus increasing the droplet's shear stability.[4]

In a well-stabilized miniemulsion system, the growth of droplets (due to collisions) will be slower than the rate of polymerization, thus producing an almost 1:1 copy of droplets to particles and thereby freezing the critically stabilized state.

4.2.4 Initiators

For miniemulsion systems either a water-soluble or oil-soluble initiator can be used. In the former case the reaction is started from the continuous phase, thus involving the formation of oligomeric radicals, which will enter the droplets at a certain critical chain length. The latter case involves mixing the initiator with the oil (monomer and hydrophobe) before premixing with the surfactant/water system. In this instance initiation will commence predominantly in the oil phase although exit of radicals can occur with consequent formation of oligomeric radical species that can re-enter. The possibility of nucleation in the water phase can be minimized by using a redox initiation system of which one component is in the aqueous phase and the other is in the organic phase.[18] Initiation will then be restricted to the interfacial layer.

4.2.5 Differentiation between heterogeneous polymerization techniques

Due to the fact that miniemulsions are very similar to conventional emulsions and microemulsion systems, it is possible to differentiate between the various techniques by summarizing the discussion so far. It is easy to differentiate between emulsion and miniemulsion only when comparing the locus of polymerization and the corresponding mechanism involved. In an emulsion system the latex particle does not correspond to the primary emulsion droplet and the size of the formed particles is kinetically controlled by, *e.g.*, the amount of initiator as well as the reaction temperature. In miniemulsion polymerization almost a direct copy between the droplet and particle exist. The size of the droplet is thermodynamically controlled, by controlling dispersion and stability, and not by the polymerization processes.

Miniemulsion and microemulsion polymerization have a lot more in common and are both classified as a highly dispersed system. To enable differentiation between the two techniques, a checklist has been provided by Landfester *et al.*[3] Note that even with this checklist, crossing of borders still exist in literature.

1. Steady-state miniemulsions are osmotically stable, but critically stabilized with respect to colloidal stability. Microemulsions are in equilibrium with both the τ_1- and τ_2-process.
2. The oil/water interfacial energy is larger than 0 for a miniemulsion, thus indicating an incomplete surfactant coverage of the droplet surface. For a microemulsion the interfacial energy is close to 0, which points to complete surface coverage by surfactant molecules.
3. For a steady-state (equilibrium between fission and fusion) to be reached in a miniemulsion, a high mechanical agitation is needed. The formation of microemulsions is usually spontaneous.
4. Osmotic stability of a miniemulsion is determined by the osmotic pressure inside the droplets. This, in turn, can be varied/optimized by the addition of a hydrophobe, which will effectively increase the osmotic pressure, thus suppressing monomer diffusion. The high osmotic pressure, as introduced by the hydrophobe, will suppress droplet growth during polymerization.
5. The amount of surfactant required to produce a stable miniemulsion (between 0.005 and 0.25 surfactant to monomer weight ratio (*S*), in the case of SDS) is well below the surfactant requirements needed for a microemulsion.
6. During polymerization of a microemulsion the original droplets can grow, whereas in a miniemulsion the growth can be suppressed.

4.3 Experimental

4.3.1 Materials

Butyl acrylate (BA, Hoechst, 99.5%) and methyl methacrylate (MMA, ICI Chemicals and Polymers, 99.9%) were washed with a 0.3M potassium hydroxide (KOH, Associated Chemical Enterprises, 85%) solution followed by distillation under reduced pressure to remove the inhibitor. Monomers were stored at –12 °C prior to use. Sodium dodecyl sulfate (SDS) (BDH, 90%); potassium persulfate (KPS, 99+%), sodium metabisulfite (SMBS, 97%), cumyl hydroperoxide (CHP, 80%), sodium formaldehyde sulfoxylate (SFS), iron(II)sulfate (99+%), 1,3-diisopropenylbenzene (DIPB, 97%) (all Aldrich); methanol (MeOH, 99.8%), ethylenediaminetetraacetic acid, disodium salt (EDTA) (both ACROS); sodium bicarbonate (Saarchem, 99.5%); benzyl acrylate (Alfa Aesar, 97%), were used as received. Distilled deionized water, obtained from a Millipore Milli-Q purification system, was used. Hexadecane (HD, ACROS, 99%) was used as core oil.

4.3.2 Latex synthesis

PBA/HD core/shell particles were synthesized by a miniemulsion polymerization reaction. Butyl acrylate, benzyl acrylate, hexadecane and sodium bicarbonate were premixed with a SDS/water solution for 1 hour, after which a miniemulsion was obtained by sonicating the mixture with a Sonics & Materials Inc. Vibracell VCX 750 ultrasonicator for 5 minutes at 95% amplitude (applied energies shown in Table 4.1). Benzyl acrylate was added to facilitate staining for TEM analysis, if necessary. Sample volumes of up to 40 mL could be sonicated. Successive sonications were performed on 40 mL fractions of larger sample volumes. During this period the solution was continuously stirred in a water-cooled jacketed vessel to avoid polymerization due to heating and to facilitate homogeneous sonication. After miniemulsification the solution was transferred to a glass reactor, which was suspended in a thermostatted oil bath and

equipped with a condenser and nitrogen purge. Polymerization was achieved by adding KPS initiator and SMBS at 75 °C while continuously purging with nitrogen. DIPB (6 wt% to monomer) was added 10 minutes after the start of the reaction to give more stability to the rubbery shell via crosslinking. The reaction was allowed to continue for 3.5 hours after which it was cooled down to 50 °C. To add a second shell a redox initiator system consisting of cumyl hydroperoxide/Fe^{2+}/ethylenediaminetetraacetic acid/sodium formaldehyde sulfoxylate (CHP-Fe^{2+}-EDTA-SFS) was used in the grafting of MMA onto the PBA shell. EDTA is used as chelating agent and SFS as reducing agent[18,32] to reduce Fe^{3+} to Fe^{2+} during the redox polymerization. The MMA monomer was fed over a predetermined time. A schematic representation of the reaction can be seen in Scheme 3.5, Chapter 3. Experimental formulations are given in Table 4.1.

Table 4.1: Experimental formulations for the synthesis of PBA/HD core/shell particles with varying surfactant concentration, and with and without the addition of MeOH. Number average particle diameters, as obtained by CHDF, are shown.

	#140	#141	#142	#143	#151	#151b	#152	#152b	#153	#153b
Reactor charge										
SDS	0.7	0.35	0.175	0.0875	1.4	1.4	1.4	1.4	3.5	3.5
DDI	76	76	76	76	76	76	76	76	181	181
Pre-stir										
BA	3.66	3.66	3.66	3.66	3.66	3.66	3.66	3.66	9.15	9.15
BzA	0.19	0.19	0.19	0.19	0.19	0.19	0.19	0.19	0.5	0.5
HD	3.01	3.01	3.01	3.01	3.01	3.01	3.01	3.01	7.525	7.525
$NaHCO_3$[§]	0.2039	0.10195	0.051	0.025	0.4078	0.4078	0.4078	0.4078	1.0195	1.0195
MeOH	7mL	7mL	7mL	7mL	7mL	7mL	---	---	17.5mL	17.5mL
Sonication										
Sonication time (min)	5	5	5	5	5	5	5	5	5	5
Sonication amplitude	95%	95%	95%	95%	95%	95%	95%	95%	95%	95%
Sonication energy (kJ)										
E1	40.253	46.429	42.258	44.515	46.598	46.598	47.543	47.543	47.695	47.695
E2									51.351	51.351
E3									50.615	50.615
E4									52.516	52.516
E5									50.089	50.089
Initiator										
KPS[*]	0.05	0.05	0.05	0.05	0.05	0.05	0.05	0.05	0.25	0.25
SMBS[℘]	0.0354	0.0354	0.0354	0.0354	0.0354	0.0354	0.0354	0.0354	0.177	0.177
Crosslinker										
DIPB	0.1155	0.1155	0.1155	0.1155	0.1155	0.1155	0.1155	0.1155	0.2888	0.2888
Graft reaction										
MMA						2mL		2mL		5mL
CHP						0.5		0.05		1.25
$FeSO_4$						0.0104		0.0104		0.0260
EDTA						0.4		0.4		1
SFS						0.4		0.4		1
Feed rate (mL/min)						0.0167		0.0167		0.0250
Diameter (CHDF) (nm)	45.2	64.8	70.7	87.8	36.0	53.3	23.2	49.0	34.7	41.2

[*] 4.90mM based on DDI water; [§] 1:1 molar ratio with SDS; [℘] 1:1 molar ratio with KPS

4.3.3 Analytical techniques

Transmission electron microscopy (TEM)

Analysis of the synthesized particles by TEM was carried out as follows: 2 mL of the latex was added to an excess of MeOH to aid precipitation of the particles. The solution was first homogenized by shaking and then transferred to a copper TEM grid by pipette. The copper grid was held at an angle to try to facilitate the formation of a monolayer of particles. The grid was left to dry at ambient temperature before analyses were performed. No staining was applied to the dried particles. Contrast between the core and shell was a result of the combined effect of the difference of path length and material density of the constituting materials. This resulted in the incident e^--beam being scattered from the wall material, resulting in a darker region on the TEM images. Analyses were done on a JEM - 200CX and 2000FX (JEOL Ltd, Tokyo, Japan) TEM. Copper grids were prepared by the deposition of a thin film of carbon to increase the strength and conductivity of the film.

Capillary hydrodynamic fractionation (CHDF)

Particle size was determined by capillary hydrodynamic fractionation (CHDF). Analyses were performed on a Matec Applied Sciences CHDF 1100, which was calibrated with PS latex standards.

Surface tension measurements

Surface tension measurements were performed by using a torsion balance and platinum Du Noüy ring (White Elec. Inst. Co. Ltd.).

4.4 Results and discussion

Core/shell particles with liquid cores were synthesized by an *in situ* miniemulsion process. The morphology was controlled by strong kinetic influences, which caused deviations from predicted morphologies based on thermodynamic effects.[33] It was therefore already shown that particles with the desired morphology can be established (Chapter 3) but the influence of process parameters on particle size had yet to be investigated.

Although the accuracy of CHDF results for particles below 50 nm has been widely debated, the technique has, nevertheless, successfully been used by various researchers to study particle sizes in both emulsion and miniemulsion polymerizations.[34-37] Not only is the speed of analysis a great advantage, but the results can also be used to qualitatively compare particle sizes as a function of the surfactant concentration. For this study a particle size between 30 and 40 nm is desired for the initial core/shell particles consisting of hexadecane as core-liquid and PBA as shell polymer (see Chapter 1). This is crucial as the correct particle size and narrow size distribution play an important role in the final use of the particles as impact modifiers.

To ensure stable dispersions and reproducible results, stable miniemulsions were produced by sonicating the pre-stirred latex under optimum time and amplitude conditions. The influence of the surfactant/water ratio on particle size was evaluated by changing the surfactant to water weight percentage from 0.1 to 2% at the predetermined sonication time and amplitude. Results of the relative number intensity versus the particle size with varying surfactant concentration are shown in Figure 4.2.

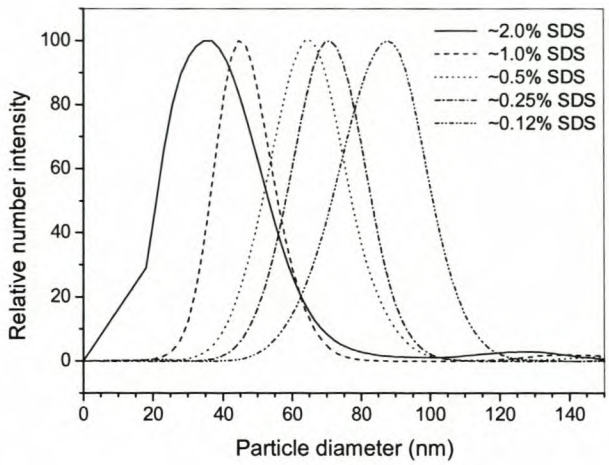

Figure 4.2: CHDF traces showing the relative number intensity versus the particle size with varying surfactant concentration.

From Figure 4.2 it follows that the particle size is dictated by the surfactant concentration at constant solids content and under steady-state miniemulsification conditions. Hence, the particle size will decrease as the amount of surfactant is increased thereby leading to critically stabilized particles. Smaller droplets (or smaller particles if a 1:1 copying of droplets to particles is assumed) will undergo more collisions and therefore need more surfactant to keep the miniemulsion stable, i.e. to critically stabilize the particles. At high surfactant to monomer weight ratios (*S*) the miniemulsion is almost translucent, which points to the presence of sub-50 nm particles. Under the applied experimental conditions it can therefore be seen, in Figure 4.3, that a plateau region will be reached if *S* is increased under the specified reaction conditions. Thus, an increase in surfactant concentration will not necessarily lead to a dramatic reduction in particle size but can also lead to the presence of free surfactant micelles in the miniemulsion. The values obtained from Figure 4.3 corresponds well with literature data in which it was shown that the amount of surfactant needed to obtain a stable polymerizable miniemulsion with SDS is between $0.005 < S < 0.25$.

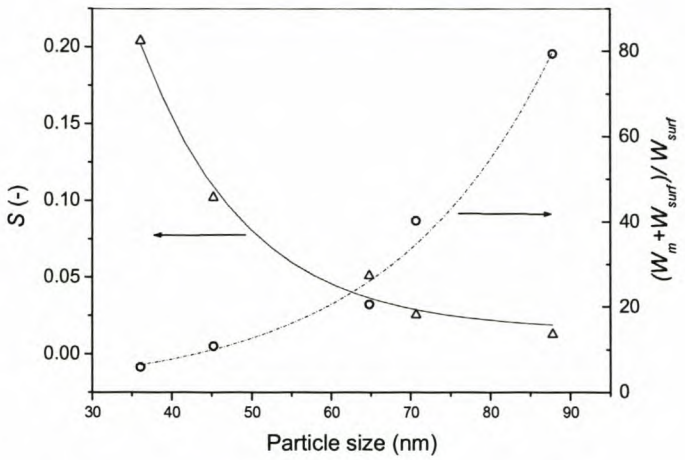

Figure 4.3: Surfactant to monomer weight ratio (*S*) and the inverse weight fraction of the surfactant plotted against the particle size.

In order to determine the stability of a miniemulsion dispersion it is therefore necessary to look at the packing density of the surfactant molecules on the droplet/particle surface.[4] Landfester[5] proposed that the surface area per molecule of SDS will increase with increasing particle size and that this will result in smaller particles requiring more surfactant per interfacial area to obtain a steady-state after miniemulsification. For particles with a diameter smaller than 50 nm the surface area that will be occupied by one surfactant molecule will therefore be less than 0.4 nm^2, which indicates that there is an almost dense packing of the surfactant on the surface.[22,38,39]

Experimental data for miniemulsion polymerization reactions with different surfactant concentrations are summarized in Table 4.2. These data were calculated from stoichiometry and assuming that all the surfactant molecules are located at the droplet surface.[22] Information on the surfactant to monomer weight ratio (*S*), number of particles (N_p), total area, number of surfactant chains ($N_{surf\ chains}$), area covered per surfactant molecule (A_{surf}) and particle size as measured by CHDF, are given.

Table 4.2: Experimental data for miniemulsion polymerization reactions of PBA/HD core/shell particles showing the influence of surfactant (SDS) concentration on the number average particle diameter and packing density (A_{surf}) of the surfactant molecules.

Experiment	#151	#140	#141	#142	#143
[SDS] (mM)	63.88	31.94	15.97	7.98	3.99
(Wm+Ws)/Ws	5.9	10.8	20.6	40.2	79.4
Ws/Wm (S)	0.2	0.1	0.05	0.025	0.013
N_p (latex)	3.35×10^{17}	1.69×10^{17}	5.75×10^{16}	4.43×10^{16}	2.31×10^{16}
Total area (nm^2)	1.37×10^{21}	1.09×10^{21}	7.59×10^{20}	6.95×10^{20}	5.60×10^{20}
$N_{surf\ chains}$	2.92×10^{21}	1.46×10^{21}	7.31×10^{20}	3.65×10^{20}	1.83×10^{20}
A_{surf} (nm^2)	0.46	0.74	1.04	1.90	3.06
Diameter (nm) (CHDF)	36.0	45.2	64.8	70.7	87.8

In Figure 4.3 the inverse weight fraction of the surfactant $(W_m+W_{surf})/W_{surf}$ versus the particle diameter can also be seen. W_{surf} and W_m are the weights of surfactant and monomer respectively. The slope of the graph (as presented in Figure 4.4) can be related to the surface coverage of the droplets by surfactant molecules and is clearly indicative of changing surface coverage with particle size as is expected in miniemulsions.[3,40]

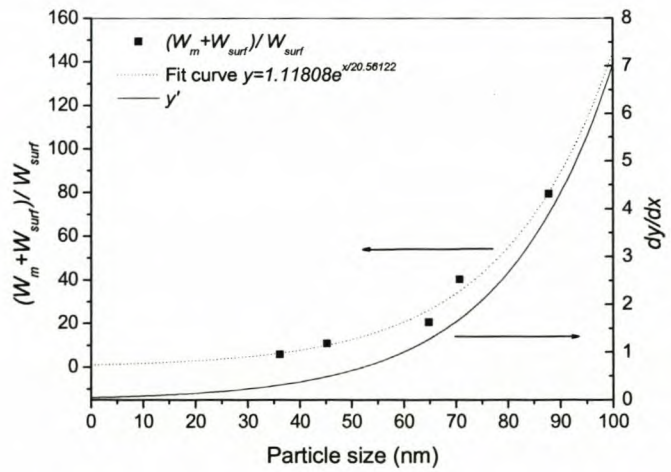

Figure 4.4: The inverse weight fraction of the surfactant, the fitted curve and the first derivative of the inverse weight fraction of the surfactant plotted against the particle size.

According to Antonietti *et al.*[40]

$$A_{surf} = \left(\frac{W_m + W_{surf}}{W_{surf}} \right) \cdot \left(\frac{3M_{surf}}{N_A \rho} \right) \cdot \left(\frac{1}{R_h} \right) \tag{4.1}$$

where M_{surf} is the molar mass of the surfactant, N_A is the Avogadro number, ρ is the average density of a droplet and R_h is the hydrodynamic radius of a droplet.

For a microemulsion the droplet size will gradually decrease with an increase in more surfactant, thus leading to a constant slope value. For a miniemulsion the initial addition of surfactant will only partially cover the droplets and further additions will therefore bring forth a large decrease in particle size. In other words, for a small increase in surfactant, a large decrease in particle size will be obtained. The slope will therefore continuously change, which is indicative of a miniemulsion. The change in slope will decrease as the miniemulsion/microemulsion boundary is neared.

The area covered per surfactant molecule, calculated stoichiometrically, as a function of particle size is shown in Figure 4.5. The obtained value for A_{surf} as a function of particle size is quite important to ensure a stable miniemulsion and, if further monomer additions are required, to eliminate the possibility of secondary nucleation and thus secondary particle formation due to the presence of free micelles.[24] The value obtained for A_{surf} for a particle with a diameter of 36 nm is 0.46 nm^2. According to this every surfactant molecule will stabilize an area of 0.46 nm^2 on the droplet interface, which is indicative of very dense surfactant packing. For further verification of the packing density surface tension measurements were conducted, which produced a value of 38.1 mN/m for a particle with a diameter of 36 nm. This value is already close to the surface tension value for the CMC plateau for a pure SDS solution.[38] If A_{surf}= 0.4 nm^2 is assumed for a dense SDS layer,[3] then the obtained value of 0.46 nm^2 shows that close packing is almost obtained and that the packing density is approximately 86%.

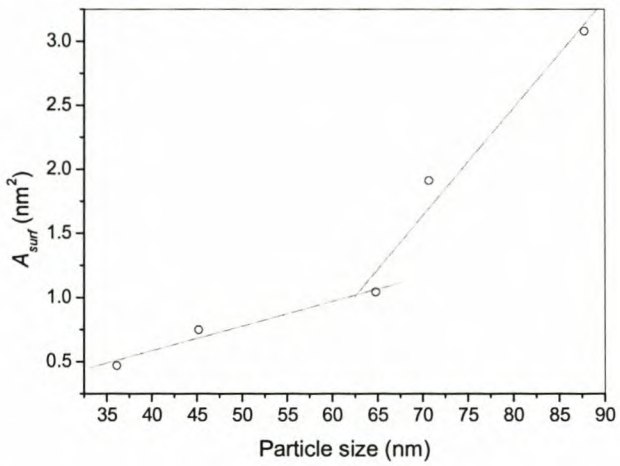

Figure 4.5: The area per surfactant molecule (A_{surf}) versus the particle size.

The amount of free SDS in the aqueous phase will therefore be approximately 7 mmol/L. This is just below the CMC of a pure SDS solution (8.2 mmol/L). As there will be an equilibrium between free surfactant in the aqueous phase and the surfactant molecules packed around the droplets, a higher concentration of surfactant in the aqueous phase is indicative of an almost completely dense packing. Note that the surfactant molecules on the droplets are in equilibrium with surfactant molecules at the air/water interface; thus an incomplete surface coverage of the droplet will also be reflected by an incompletely covered dispersion surface. For droplets approaching complete packing by surfactant molecules, the surfactant concentration of the surfactant saturated surface will approach the concentration of the critical micelle concentration. Even though particles will be completely packed at a surfactant concentration above the CMC, equilibrium will force the formation of additional free micelles, which will be present in the aqueous phase.

CHDF particle size measurements performed on the initial core/shell particles (PBA/HD) and the MMA-grafted core/shell particles synthesized with a ~2 % surfactant concentration can be seen in Figures 4.6 (a.) and (b.), respectively. Figure 4.6 (a.) represents the particle size data for the ungrafted PBA/HD core/shell particles. Figure 4.6 (b.) shows the particle size after grafting with PMMA.

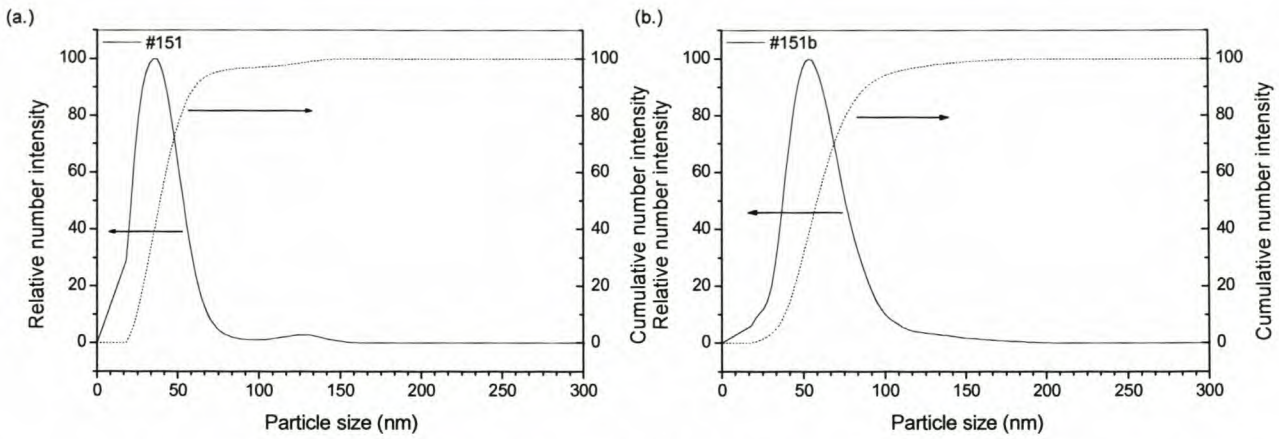

Figure 4.6: Particle size distribution of PBA/HD particles by relative number intensity: (a.) before grafting and (b.) after grafting with PMMA.

Confirmation of the particle size is obtained from TEM images, shown in Figure 4.7. The size of the grafted particles is between 50 and 60 nm, which corresponds with CHDF analysis results.

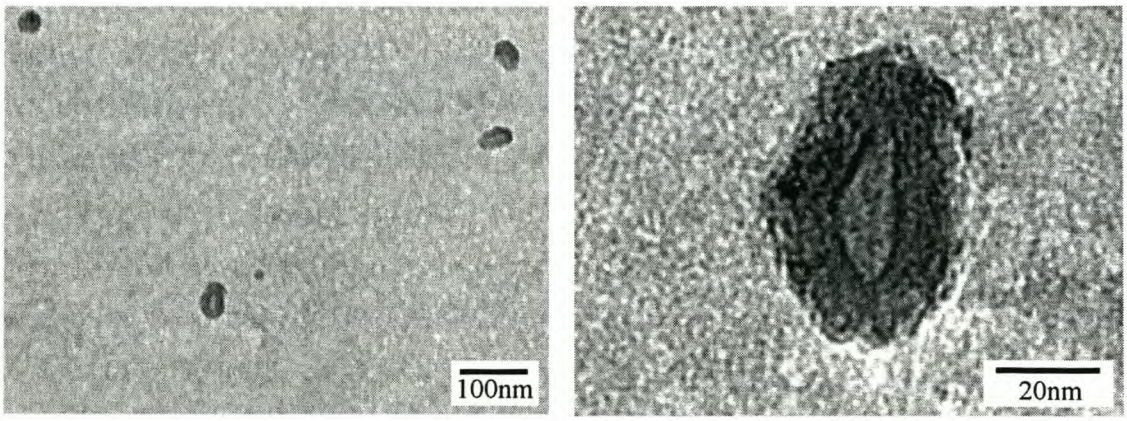

Figure 4.7: TEM images of the MMA-grafted PBA/HD core/shell particles.

Figure 4.8 shows a TEM image of core/shell particles synthesized with a ~1% surfactant solution. In this instance the grafted particles are much larger than for the ~2% surfactant solution. This is due to the larger size of the initial PBA/HD core/shell particles (Figure 4.2) as well as the higher amount of MMA that was used to obtain adequate grafting.

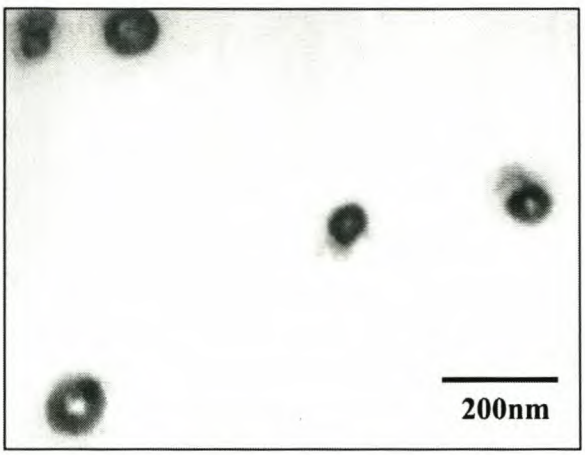

Figure 4.8: TEM image of MMA-grafted PBA/HD core/shell particles synthesized with a ~1% surfactant solution.

According to McDonald *et al.*[41] the addition of a water-miscible alcohol is one of the components necessary to control morphology and the extent of encapsulation. For this reason the influence of MeOH on particle size and stability was investigated by performing polymerizations in the presence and absence of MeOH. The addition of an alcohol will decrease the dissociation of the emulsifier, which will consequently lead to the formation of larger emulsifier aggregates and thus bigger particles.[42] The addition of polar compounds, such as alcohols, can effectively increase the oil solubilization capabilities of micelles. This is important to increase the thermodynamic stability of miniemulsions, i.e. to induce retardation of the diffusional degradation of monomer droplets, which would thus preserve the very small droplet size generated by the homogenization process. Either long- or short-chain alcohols can be used as coemulsifiers although they differ in the way they are incorporated in the micelle structure. Short-chain alcohols are adsorbed at the outer region of the micelles (close to the micelle/water interface) whereas long-chain alcohols are incorporated into the micelle. On addition of the short-chain alcohol the polarity of the continuous phase will decrease significantly, which will cause a decrease in the dissociation of the emulsifier. A high concentration of emulsifier will therefore be present at the droplet surface and will lead to the formation of droplets with a low interfacial curvature.[43] Confirmation of this can be seen when CHDF particle size results, obtained from experiments with constant surfactant concentration (2%) and in the presence and absence of MeOH, are compared.

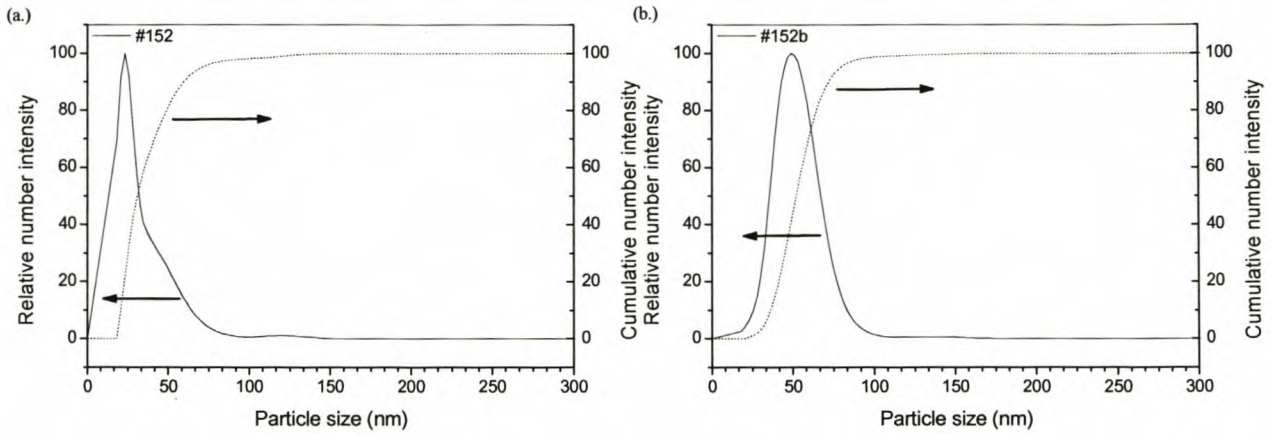

Figure 4.9: Particle size distribution by relative number intensity for (a.) non-grafted and (b.) grafted core/shell particles synthesized without the addition of MeOH.

Figure 4.9 (a.) shows the CHDF trace for the number average particle size of experiment #152 before MMA grafting. Figure 4.9 (b.) shows the CHDF trace of particles after MMA grafting. By comparing these results with the CHDF results of experiments performed with the addition of MeOH (Figure 4.6), it can be noted that the addition of MeOH leads to a slight increase in particle size (see also Table 4.1). Apart from the stabilization effect that occurs from addition of an alcohol as cosurfactant, it can also be used as a tool to fine-tune particle size. In Figure 4.9 (a.), however, the particle size does not show a clean distribution but a shoulder on the larger particle size side. This is probably due to the reduced stability effect as a result of synthesis without MeOH addition. Figure 4.10 shows TEM images of core/shell particles obtained in experiment #152b. The particles were synthesized without the addition of MeOH, thus causing the small particle size.

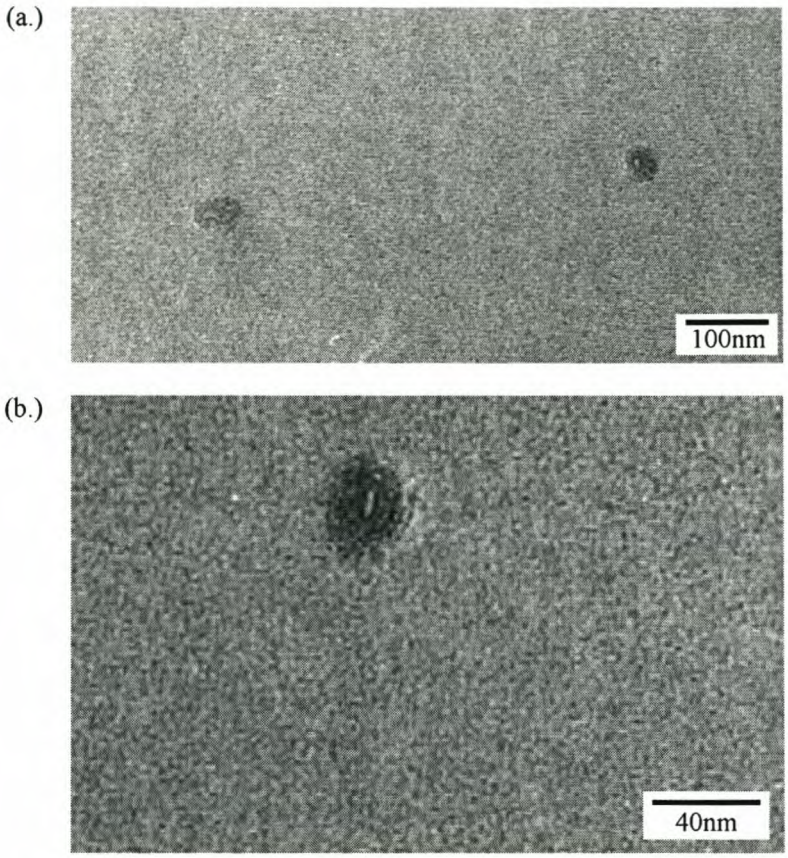

Figure 4.10: TEM images of MMA-grafted PBA/HD core/shell particles synthesized without MeOH addition.

All of the above experimental results compared well with "classical" miniemulsion data. Most of these "classical" miniemulsion polymerizations were done with the addition of a hydrophobe (hexadecane for osmotic stability), but in much smaller quantities compared to the monomer. In this study, however, the weight ratio of monomer to oil (hydrophobe) is almost 1:1. This did not influence the expected particle size and stability, thus leading to similar deductions (as mentioned in literature and already referenced in this chapter) regarding the interaction between these two factors.

To conclude this chapter, the process was scaled-up. For the experimental setup used it is only possible to sonicate fractions of larger sample volumes over a period of time. It was therefore important to evaluate the influence of time delay between successive sonications on the outcome of particle size and morphology, thus to assess the

reproducibility for different sample volumes. Figure 4.11 shows CHDF traces obtained from experiment #153 and #153b.

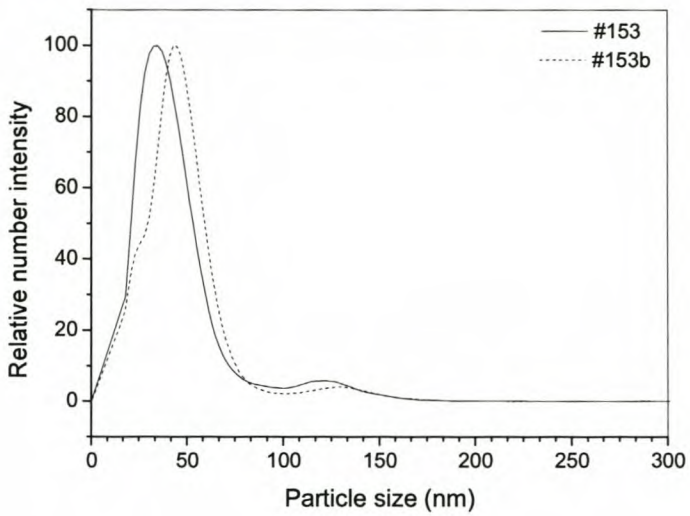

Figure 4.11: CHDF traces for non-grafted (#153) and grafted (#153b) core/shell particles obtained by scaled-up synthesis conditions.

The experimental volumes were increased 2.5 times, thus forcing the total volume to be split up into 5 equal batches for sonication. Table 4.1 shows the sonication energies applied to the consecutively homogenized batches. Particle size for the ungrafted samples (2% surfactant to water weight percentage) is 34 nm, which is in good accordance with size results of experiment #151. The grafted sample (#153b) shows an increase in particle size up to ~ 42 nm, which is slightly smaller when compared to the corresponding experiment, #151b (53.3 nm).

4.5 Conclusions

Core/shell particles with liquid cores were synthesized by an *in situ* miniemulsion polymerization process. By changing the surfactant concentration it was possible to synthesize a wide variety of particle sizes. Core/shell particles with a particle diameter of 36 nm could be synthesized by increasing the surfactant concentration from 0.1 to 2% (wt% to aqueous phase). By calculating the number of particles present in the aqueous phase and hence the total area of the particles, it was possible to calculate the surface area

that is stabilized per surfactant molecule. This was calculated from stoichiometry by assuming that all of the surfactant is adsorbed on the droplet surface. For the target particle size of 36 nm a surface coverage of 0.46 nm^2 per surfactant molecule was obtained, which indicated that the particle surface was almost completely covered. Additional surface tension measurements showed surface tension values close to the CMC plateau for a pure SDS solution. As there exists an equilibrium between the surfactant molecules on the particle surface and the surfactant molecules at the latex/air surface, the low surface tension value is indicative that most of the particle has been covered by surfactant. Plots of the particle size versus the weight ratio of surfactant to monomer as well as the inverse weight fraction of surfactant followed similar trends to those obtained by other researchers for "classical" miniemulsion experiments.

CHDF analysis revealed the particle size of the synthesized core/shell particles. The results were confirmed by TEM, which clearly showed a decrease in particle size with an increase in surfactant concentration. Particle size of MMA-grafted core/shell particles was also determined by CHDF and confirmed by TEM analysis. The influence of MeOH as costabilizer was investigated and showed that the addition of MeOH decreased the dissociation of the emulsifier, which resulted in larger organized aggregates. This in turn led to a slight increase in particle size. The difference in particle size, as a direct influence of MeOH addition, was again followed by CHDF analysis and confirmed by TEM images. To conclude, the experiments were successfully scaled-up and showed particle size data, which was in good agreement with data from the original recipe.

References

(1) Sudol, E. D.; El-Aasser, M. S. In *Emulsion Polymerization and Emulsion Polymers*; Lovell, P. A.; El-Aasser, M. S., Eds.; John Wiley and Sons Ltd.: England, 1997; pp 699-722.

(2) Soma, J.; Papadopoulos, K. D. *J. Colloid Interface Sci.* **1996**, *181*, 225-231.

(3) Landfester, K.; Bechtold, N.; Tiarks, F.; Antonietti, M. *Macromolecules* **1999**, *32*, 5222-5228.

(4) Landfester, K. *Macromol. Rapid Commun.* **2001**, *22*, 896-936.

(5) Landfester, K. *Macromol. Symp.* **2000**, *150*, 171-178.

(6) Van Melick, H. G. H.; Govaert, L. E.; Meijer, H. E. H. *Polymer* **2003**, *44*, 457-465.

(7) El-Aasser, M. S.; Sudol, E. D. In *Emulsion Polymerization and Emulsion Polymers*; Lovell, P. A.; El-Aasser, M. S., Eds.; John Wiley & Sons Ltd.: Chichester, 1997; pp 37-58.

(8) Bechtold, N.; Landfester, K. *Macromolecules* **2000**, *33*, 4682-4689.

(9) Miller, C. M.; Sudol, E. D.; Silebi, C. A.; El-Aasser, M. S. *Macromolecules* **1995**, *28*, 2765-2771.

(10) Ugelstad, J.; El-Aasser, M. S.; Vanderhoff, J. W. *Journal of Polymer Science: Polymer Letters Edition* **1973**, *11*, 503-513.

(11) Delgado, J.; El-Aasser, M. S.; Vanderhoff, J. W. *J. Polym. Sci., Part A: Polym. Chem.* **1986**, *24*, 861-874.

(12) Blythe, P. J.; Klein, A.; Phillips, J. A.; Sudol, E. D.; El-Aasser, M. S. *J. Polym. Sci., Part A: Polym. Chem.* **1999**, *37*, 4449-4457.

(13) Leiza, J. R.; Sudol, E. D.; El-Aasser, M. S. *J. Appl. Polym. Sci.* **1997**, *64*, 1797-1809.

(14) Choi, Y. T.; El-Aasser, M. S.; Sudol, E. D.; Vanderhoff, J. W. *J. Polym. Sci.: Polym. Chem. Ed.* **1985**, *23*, 2973-2987.

(15) Delgado, J.; El-Aasser, M. S.; Silebi, C. A.; Vanderhoff, J. W. *J. Polym. Sci., Part A: Polym. Chem.* **1990**, *28*, 777-794.

(16) Wang, S. T.; Schork, F. J.; Poehlein, G. W.; Gooch, J. W. *J. Appl. Polym. Sci.* **1996**, *60*, 2069-2076.

(17) Tang, P. L.; Sudol, E. D.; Adams, M.; El-Aasser, M. S.; Asua, J. M. *J. Appl. Polym. Sci.* **1991**, *42*, 2019-2028.

(18) Wang, C. C.; Yu, N. S.; Chen, C. Y.; Kuo, J. F. *J. Appl. Polym. Sci.* **1996**, *60*, 493-501.

(19) Tang, P. L.; Sudol, E. D.; Silebi, C. A.; El-Aasser, M. S. *J. Appl. Polym. Sci.* **1991**, *43*, 1059-1066.

(20) Schork, F. J.; Poehlein, G. W.; Wang, S.; Reimers, J.; Rodrigues, J.; Samer, C. *Colloids Surf., A* **1999**, *153*, 39-45.

(21) Paunov, V. N.; Sandler, S. I.; Kaler, E. W. *Langmuir* **2001**, *17*, 4126-4128.

(22) Landfester, K.; Bechtold, N.; Tiarks, F.; Antonietti, M. *Macromolecules* **1999**, *32*, 2679-2683.

(23) Chern, C. S.; Chen, T. J. *Colloid Polym. Sci.* **1997**, *275*, 1060-1067.

(24) Anderson, C. D.; Sudol, E. D.; El-Aasser, M. S. *Macromolecules* **2002**, *35*, 574-576.

(25) Blythe, P. J.; Morrison, B. R.; Mathauer, K. A.; Sudol, E. D.; El-Aasser, M. S. *Macromolecules* **1999**, *32*, 6944-6951.

(26) Miller, C. M.; Sudol, E. D.; Silebi, C. A.; El-Aasser, M. S. *Macromolecules* **1995**, *28*, 2754-2764.

(27) Miller, C. M.; Sudol, E. D.; Silebi, C. A.; El-Aasser, M. S. *Macromolecules* **1995**, *28*, 2772-2780.

(28) Lim, M.-S.; Chen, H. *J. Polym. Sci., Part A: Polym. Chem.* **2000**, *38*, 1818-1827.

(29) Landfester, K.; Bechtold, N.; Förster, S.; Antonietti, M. *Macromol. Rapid Commun.* **1999**, *20*, 81-84.

(30) Blythe, P. J.; Klein, A.; Sudol, E. D.; El-Aasser, M. S. *Macromolecules* **1999**, *32*, 4225-4231.

(31) Blythe, P. J.; Klein, A.; Sudol, E. D.; El-Aasser, M. S. *Macromolecules* **1999**, *32*, 6952-6957.

(32) Wang, C. C.; Yu, N. S.; Chen, C. Y.; Kuo, J. F. *Polymer* **1996**, *37*, 2509-2516.

(33) Moad, G.; Solomon, D. H. *The Chemistry of Free Radical Polymerization*; Pergamon Press: Oxford, 1995.

(34) Miller, C. M.; Venkatesan, J.; Silebi, C. A.; Sudol, E. D.; El-Aasser, M. S. *J. Colloid Interface Sci.* **1994**, *162*, 11-18.

(35) Ferguson, C. J.; Russell, G. T.; Gilbert, R. G. *Polymer* **2002**, *43*, 6371-6382.

(36) Ramos, J. G. D.; Silebi, C. A. *Polym. Int.* **1993**, *30*, 445-450.

(37) Silebi, C. A.; Ramos, J. G. D. *J. Colloid Interface Sci.* **1989**, *130*, 14-24.

(38) Evans, D. F.; Wennerström, H. *The Colloidal Domain: Where Physics, Chemistry, Biology, and Technology Meet*; Wiley-VCH: Toronto, 1994.

(39) Myers, D. *Surfaces, Interfaces, and Colloids: Principles and Applications*, 2nd ed.; John Wiley & Sons, 1999.

(40) Antonietti, M.; Basten, R.; Lohmann, S. *Macromol. Chem. Phys.* **1995**, *196*, 441-466.

(41) McDonald, C. J.; Bouck, K. J.; Chaput, A. B. *Macromolecules* **2000**, *33*, 1593-1605.

(42) Capek, I.; Chern, C.-S. In *Adv. Polym. Sci.*; Springer-Verlag: Berlin, 2001; Vol. 155, p 101.

(43) Capek, I. *Adv. Colloid Interface Sci.* **2001**, *92*, 195-233.

Chapter 5

Synthesis of liquid-filled polymeric nanocapsules by the use of living polymerization techniques

Abstract

Core/shell particles with liquid cores and molar mass controlled polystyrene shells were synthesized by an in situ miniemulsion polymerization reaction in the presence of a RAFT agent. The formation of structured particles with the targeted morphology is extremely dependent on the type of monomer, RAFT agent and the type of initiator used. Different RAFT agents lead to different retardation times, thus resulting in different chain lengths as a function of time. The different chain lengths will influence viscosity and consequently chain mobility and can therefore cause a deviation from the desired morphology. The type of initiator used influences the surface activity of entering oligomers and is therefore also an important factor in obtaining the targeted structure. Retardation caused by the RAFT agent can be decreased by using a monomer with a high propagation rate constant. Results showed that a RAFT agent with reduced retardation, used in conjunction with a surface-active initiating species, is able to lock the

---

Reproduced from:
Synthesis of liquid-filled polymeric nanocapsules by the use of living polymerization techniques
André J.P. van Zyl, Rutger F.P. Bosch, James B. McLeary, Ron D. Sanderson, Bert Klumperman, submitted to **Macromolecules**.

polymerization locus at the droplet/water interface. This results in entering oligomers being anchored at the droplet/water interface with consequent core/shell formation only if the RAFT agent used leads to a rapid increase in chain length with time and thus a restriction of chain mobility of the mediated species. However, a RAFT agent with high retardation time can also successfully be employed if used in conjunction with a highly reactive monomer. This will result in an increase in the rate of polymerization and a consequent increase in viscosity at the polymerization locus with consequent core/shell formation.

5.1 Introduction

Living/controlled radical polymerization techniques have been known for more than 30 years, but only in the past decade have they received broad academic and industrial interest. Although living/controlled radical polymerization all started with the use of iniferters (initiator-transfer agent-terminator),[1] techniques such as reversible addition fragmentation chain transfer (RAFT) polymerization,[2,3] atom transfer radical polymerization (ATRP)[4,5] and nitroxide mediated radical polymerization (NMP)[6,7] have led to a significant revitalization of the field of radical polymerization. These techniques provide the ability to control radical polymerizations (when compared to conventional free radical polymerization chemistry) and can also impart living properties to a polymeric species, which enables immediate or delayed chain extension by addition of more monomer units.

Homogenous media are preferred for living/controlled polymerizations. However, recent developments[8] have shown that such polymerizations can also be extended to aqueous media via different routes, some of which include miniemulsions,[9-13] emulsification of RAFT end-capped oligomers,[14] RAFT agent transport[15] and *ab initio* emulsion polymerization.[16,17] The transition from homogeneous to heterogeneous media is most welcome from an industrial point of view, where aqueous phase polymerization is preferred. The latter is not only more cost effective, but the environmental friendly aspects of polymerization without organic solvents are an added advantage. However, although living/controlled polymerizations have been performed in aqueous systems, these systems have in some cases proven to be limited to specific monomers or conditions.[18] The solubility of the mediating species used in living/controlled polymerization is invariably different to that of the monomer in the varying phases, which makes a multiphase polymerization system far more difficult to control. It is therefore very important to tailor a method when chain growth mediating agents are used. When carrying out heterophase polymerization, partitioning of the mediating species between the aqueous phase and the polymerization loci has to be optimized. This problem is partially overcome by the use of predispersion or homogenization.

The focus of many research groups involved in polymer synthesis has recently shifted due to the development of living/controlled polymerization techniques that are able to control chain architecture in aqueous media. Products which are dependant on multiphase systems, such as core/shell particles, can now potentially be prepared with polymers of controlled chain architecture. Core/shell particles are used in many applications, ranging from impact modifiers and toughening agents,[19] opacifiers, gloss enhancers for paper coatings, polymeric nanocapsules for controlled and sustained drug delivery[20,21] to encapsulation of volatile solvents or toxic substances. The ability to combine such versatile techniques, i.e. complete control of encapsulating and core material, with the added versatility of core/shell particles, is opening new horizons on the scientific front, including revolutionary applications such as the possibility of adapting the molar mass of the encapsulating species to a patient's weight or type of illness in drug delivery.

As a result of earlier research (Chapter 3), it was found that the desired core/shell morphology can be locked-in by choice of surfactant and initiating species in the *in situ* miniemulsion polymerization of core/shell particles with liquid cores. Thus, when the correct initiating species (which will facilitate adequate immobilization at the droplet/water interface) is added to a miniemulsified oil containing monomer, core-oil and RAFT agent, the initiator radicals will anchor themselves at the interface, leading to preferential polymerization at the droplet/water interface. Unfortunately, degenerative transfer is the basis of the RAFT process and will result in small radical species being generated. This problem must therefore be addressed by the reaction kinetics, thus, the type of RAFT agent used. In addition, the choice of RAFT agent will also influence the chain lengths produced as a function of time and thereby chain mobility.[22] When all conditions are met, polymerization will occur at the droplet/water interface as a result of monomer depletion from the inside of the droplet, causing phase separation and leaving an oily core.

In this chapter, core/shell particles were synthesized by using RAFT agents to control the molar mass of the shell polymer. Styrene was initially used as the encapsulating

monomer and isooctane as the core-oil. The influence of different RAFT agents was investigated as well as the influence of different initiating species. It was found that the production of core/shell particles is controlled by the selection of initiator and RAFT agent. To conclude this chapter, butyl acrylate was used to encapsulate hexadecane. The reason for this was twofold: to investigate the influence of monomer on the core/shell formation capabilities in a RAFT/miniemulsion system and to synthesize core/shell particles with the same chemical reagents initially set out to synthesize particles, which adheres to the criteria for impact modification.

5.2 RAFT – a theoretical overview

In 1998 a new living free radical polymerization process was patented and published by Rizzardo *et al.*[2,3] and consequently coined RAFT due to the fact that the mechanism involved a reversible addition chain transfer procedure. The main advantage of this process over other living polymerization techniques is that a wide range of monomers can be used under different reaction conditions, yet still ensuring controlled molar mass and narrow polydispersities of the synthesized polymers. An additional advantage is the possibility to predetermine the molar mass of the polymers to be synthesized by using the reagent concentrations as well as conversion. Due to the living nature of the system, existing polymer chains can also be reactivated, thus providing possibilities for further chain extensions, *e.g.* additional extension with the same monomer, block formation,[23] i.e. extension by addition of a different monomer, as well as other exotic architectures, *e.g.* stars,[24,25] grafts and brushes.

The first species used as RAFT agents were methacrylate macromonomers (Scheme 5.1).

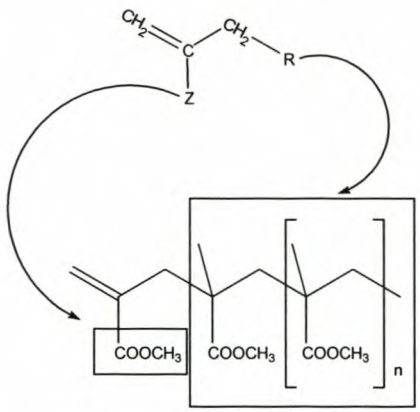

Scheme 5.1: Methacrylate macromonomers used as chain transfer agents.

These macromonomers could be used as chain transfer agents due to their ability to perform the necessary addition-fragmentation process.[18] However due to low reactivity of these "agents", propagation dominated transfer at high monomer concentration, thereby causing the loss of controlled characteristics. Other macromonomers were used but they resulted in a loss of the reversible character due to poor leaving groups, again causing loss of control and living properties. These initial results were nonetheless useful; they facilitated the understanding and optimization of transfer agents to be used in the RAFT process. The latter were in the form of dithioesters, subsequently followed by dithiocarbamates, trithiocarbonates and xanthates.

In the case of the dithioesters, the more reactive double bond provided improved transfer over propagation, thus resulting in far better control if compared to macromonomers. Fast transfer is necessary to ensure a rapid exchange rate between the active and dormant species, which would result in chains growing at the same rate and therefore decreasing the polydispersity of the formed polymer. In Scheme 5.2 a schematic representation of a RAFT agent can be seen.

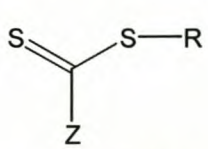

Scheme 5.2: Simplified structure of a RAFT agent where R and Z denote the leaving and activating groups, respectively.

The effectiveness of a RAFT agent is determined by the substituents R and Z, the free radical leaving and activating group, respectively. The importance of these groups will be discussed in Sections 5.2.3 and 5.2.4.

5.2.1 The RAFT mechanism

The RAFT mechanism is depicted in Scheme 5.3.

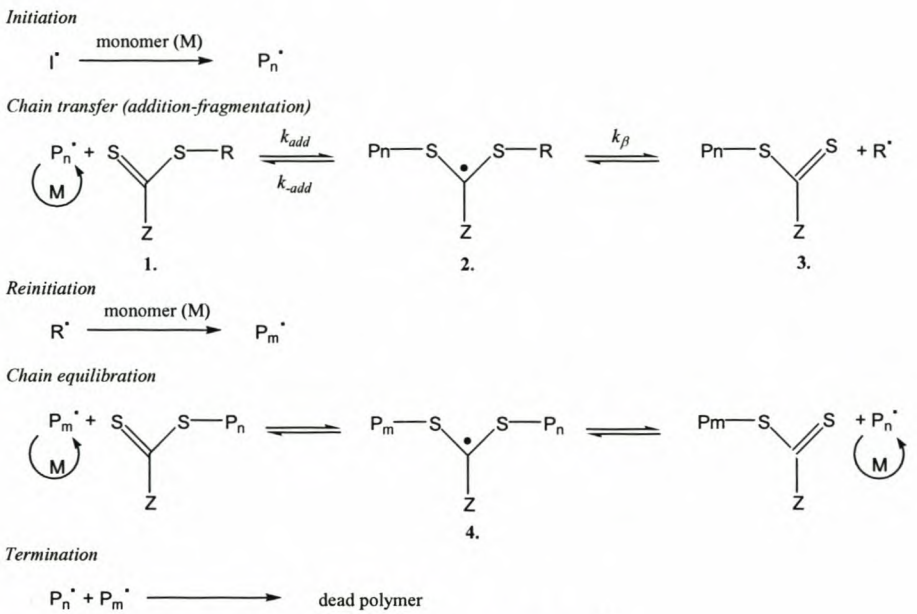

Scheme 5.3: The mechanism for the RAFT procedure.[26]

Initiator decomposition will lead to initiator fragment radicals which can add to monomer, thus being able to form oligomeric radical species ($P_n^{\cdot}$). These species will add (addition step) to the carbon-sulfur double bond (thiocarbonyl double bond) and will consequently form the labile intermediate species (**2.**) (see Scheme 5.3). Upon fragmentation (fragmentation step) of the intermediate species two possibilities exist; 1.) fragmentation into the two species that it was formed by or 2.) fragmentation into a dormant polymeric RAFT species and a radical species ($R^{\cdot}$). This radical species can initiate monomer (reinitiation step), thus again forming polymeric radicals which are able to react with the dormant polymeric RAFT agent (**3.**).

The formation of the dormant polymeric RAFT agent is the most important step in the RAFT mechanism due to the fact that the dormant chain can act as a transfer agent. This will ensure that the radical species will react with the dormant RAFT agent, thus forming a dormant species itself, while releasing the previously dormant polymer chain as a radical, which is again capable of further growth by monomer addition. This step is called the equilibration step because it allows an equilibrium to establish among all the propagating radicals and all the dormant chains, subsequently resulting in all the chains growing at the same rate. This is of utmost importance for achieving polydispersity values <1.5, which is one of the criteria for a living/controlled polymerization system. Note that the rate of addition to the thiocarbonyl double bond must be fast in comparison to the propagation step and termination must be suppressed by keeping the radical concentration low. Failure to achieve this will lead to the presence of dead chains which will ultimately result in tailing of the molar mass distribution and hence an increase in polydispersity.

The reason why the rate of addition to the transfer agent, alternatively the transfer constant (C_{tr}), must be high can be related back to the polydispersity (provided that termination can be neglected), as reported by Müller *et al.*[27]. According to them

$$\overline{M}_w / \overline{M}_n = 1 + 1/C_{tr} \tag{5.1}$$

, which suggests that a transfer constant >2 will give a polydispersity <1.5. For a transfer constant <2 a narrow polydispersity can still be obtained under feed conditions. By applying feed conditions the monomer to RAFT agent ratio is kept low and transfer is therefore favored. Although the transfer constant is low, a propagating radical is forced to undergo transfer, since the ratio between transfer and propagation rate is determined by both the transfer constant and the concentration of RAFT agent and monomer.[28] Note that

$$C_{tr} = k_{tr} / k_p \tag{5.2}$$

where k_{tr} and k_p are transfer and propagation rate coefficients, respectively. A transfer constant >2 therefore indicates that transfer is predominant in the reaction. If Scheme 5.3 is considered, it follows that the transfer rate is[18]

$$R_{tr} = k_{tr} \cdot [radical] \cdot [RAFT] \tag{5.3}$$

where the transfer rate coefficient is given by

$$k_{tr} = k_{add} \cdot \frac{k_\beta}{k_\beta + k_{-add}} \tag{5.4}$$

In the chain equilibrium of the RAFT process there is no preference for fragmentation during the chain transfer step owing to similarities in chain lengths and structures (see Scheme 5.3). This results in k_β being equal to k_{-add} and Equation 5.4 can thus be simplified to

$$k_{tr} = 0.5 \cdot k_{add} \tag{5.5}$$

Because transfer is fast, addition or radical exchange must also be fast, resulting in chains having equal chance to add to monomer and thereby contributing to the narrow polydispersity.

The number of polymer chains produced during a RAFT polymerization can be equated as follows:[18]

$$[chains] = [RAFT] + 2 \cdot f \cdot ([I] - [I]_0) \tag{5.6}$$

where $[RAFT]$ is the initial RAFT concentration (if assumed that all the RAFT agent is rapidly transformed into dormant species, then $[RAFT]$ is the concentration of the dormant species), $[I]_0$ is the initial initiator concentration and f is an efficiency factor.

The second term of the equation will therefore produce the number of chains being formed by initiator radicals, hence the factor 2 to account for the fact that two radicals are produced per initiator molecule.

The number of chains produced in a RAFT reaction must be constant. Termination, as well as delayed starting of polymer chains will cause the presence of a population of chains, thereby strongly influencing the polydispersity of the formed polymer. To ensure a constant number of chains, the initiator term in Equation 5.6 must be kept to a minimum by minimizing the amount of initiator used. This will ensure that termination is kept at a minimum. If it is assumed that termination occurs through recombination then the number of dead chains will be equal to the amount of initiator consumed; conversely, the number of dormant chains will be equal to the amount of RAFT agent consumed. To ensure a high fraction of dormant species the ratio of initiator to RAFT agent must therefore be very low ~ [initiating radicals]/[*RAFT*] < 0.2.[2] As a rule of thumb, the molar ratio between the initiating and RAFT species should be chosen as 1:5, however, due to differences in reaction conditions and species this ratio might have to be increased to achieve better control. Note that limits do exist, below which insufficient initiating radicals will be present in the system and above which a too large number of initiator derived chains are formed, in both cases leading to a loss of control and living properties.

5.2.2 Retardation in RAFT polymerization

Rate retardation plays a significant role when certain RAFT agents are used in living/controlled polymerizations.[26] However, when it is considered that most of the agents still behave like ideal chain transfer agents then it becomes apparent that certain factors must be inducing and controlling retardation. Moad *et al.*[26] based their studies on a cumyl dithiobenzoate and showed that deviation from the ideal case is observed in the early stages of polymerization and if a high concentration of the RAFT agent is used. Possible reasons for this are given as:

1. slow fragmentation of the intermediate species formed by the initial RAFT agent in the chain transfer step,

2. slow fragmentation of the intermediate species formed by the polymeric RAFT agent in the chain equilibration step,
3. slow reinitiation of the radical $R^{\cdot}$,
4. preferential addition of the expelled radical $R^{\cdot}$ to the RAFT agent rather than to reinitiate monomer,
5. preferential addition of the propagating radical species $P_n^{\cdot}$ to the RAFT agent rather than to monomer.

De Brouwer used models to test the hypotheses as proposed by Moad *et al.*[26] and concluded that it could not be used (except at unrealistic values) to explain the particular behavior observed in styrene solution polymerization. He therefore proposed a different mechanism in which termination of the intermediate radical takes place.[29] This allowed him to change the polymerization rate equation, thus indicating the dependence on the addition and fragmentation rate constants

$$R_p = k_p \cdot [M] \cdot \left(\frac{2 \cdot f \cdot k_d \cdot k_{frag} \cdot [I]}{k_t \cdot (k_{frag} + k_{add} \cdot [SR])} \right)^{0.5} \tag{5.7}$$

where [SR] is the concentration of the transfer agent (the other terms have already been defined). De Brouwer showed that the intermediate species concentration will be high if fragmentation is slow, thus increasing the termination between these species. He concluded his study by looking at the incorporation of different substituents on the phenyl ring of the RAFT agent, thereby allowing him to study the effect of the stability of the intermediate radical. By reducing the stability, the intermediate radical is likely to fragment faster, thereby reducing intermediate radical termination and causing a reduction in retardation.

Although De Brouwer suggested that the hypotheses made by Moad *et al.*[26] were not conclusive enough, they did manage to support their hypotheses by experimental verification. This author therefore concludes that although the termination of the

intermediate radical might be the predominant effect, the hypotheses made by Moad *et al.* will also play a role, albeit to a lesser extent.

5.2.3 Effect of the free radical leaving group, R[30]

The effectiveness of a RAFT agent depends strongly on the nature of the Z and R groups, the monomer and polymerization conditions (see Scheme 5.4). The major factor determining the transfer coefficient, which can again be related to the efficacy of the RAFT species, is the partitioning of the intermediate species into either the starting materials or products. This ability is determined by the free radical leaving group, R, whose properties are established by steric and polar factors as well as radical stability. More stable, more electrophilic and more bulky radicals make better leaving groups and will also contribute to the ability of the R group to partition between adding to monomer and adding to polymeric RAFT agent, which can have an effect on the rate of RAFT consumption. To simplify, if the RAFT agent has a poor leaving group then the growing radical has to add more often to the RAFT agent before effective transfer will take place. In this case the intermediate will revert back into its originating species.

(a.)

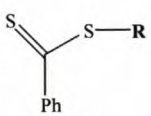

MMA polymerization

R =

$-C(CH_3)(CH_2CH_2CH_2OH)CN > -C(Me)_2CN \sim -C(Me)_2Ar >$

$-C(Me)_2C(=O)OEt > -C(Me)_2C(=O)NH-(alkyl) >$

$-C(Me)_2CH_2C(Me)_3 > -C(Me)HPh > -C(Me)_3 \sim -CH_2Ph$

Styrene polymerization

R =

$-C(Me)_2Ph$

$-C(Me)_2CO_2Et$

$-C(Me)_2CH_2C(Me)_3$

(b.)

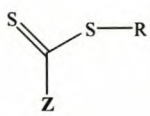

Z =

$Ph > SCH_2Ph \sim SMe \sim$ *N*-pyrrolo $>> OC_6F_5 >$ *N*-lactam $> OC_6H_5 > O(alkyl) >> N(alkyl)_2$

Scheme 5.4: The effect of the leaving group (R) and activating group (Z) on RAFT polymerization.

In Scheme 5.4 (a.) the ability of the dithiobenzoate derivatives to produce narrow polydispersities and molar mass control decrease in the order as shown for MMA polymerization. For styrene polymerizations, however, all the dithiobenzoates shown produces controlled molar masses and narrow polydispersities.

5.2.4 Effect of the activating group, Z[31]

The Z group, or activating group, is able to modify the reactivity of the dithiocarbonyl compound as well as the desired intermediate radical. This group will modify the rate of free radical addition to the C=S double bond, thus also influencing the transfer coefficient and thereby the effectivity of the RAFT agent. RAFT agents with electrophilic Z substituents with lone pairs directly conjugated to the C=S double bond have lower transfer coefficients. Electron withdrawing groups on O or N (in particular, groups able to delocalize the nitrogen lone pair in the case of the dithiocarbamates), on the other hand, can significantly enhance the efficiency of the RAFT agents. In Scheme 5.4 (b.) the chain transfer coefficient will decrease for the series shown for the activating group.

5.2.5 Following the RAFT reaction quantitatively

Due to the trademark characteristics of living/controlled polymerizations, it is well known that the molar mass will increase in a linear manner with monomer conversion. This therefore allows quantification of the molar mass of a proposed reaction if the monomer and RAFT agent concentrations are known.[18] By substituting these values in

$$\overline{M}_{n,theory} = \frac{x[M]_0}{[RAFT]_0} \times FW_M + FW_{RAFT} \qquad (5.8)$$

where $[M]_0$ and $[RAFT]_0$ are the initial concentration of the monomer and the RAFT agent, FW_M is the molar mass of a monomer unit, FW_{RAFT} is the molar mass of the RAFT agent, x is the fractional conversion, $\overline{M}_{n,theory}$, which is the theoretical number average molar mass of the formed polymer, can be calculated.

For miniemulsion polymerization reactions the above equation was modified by De Brouwer *et al.*[32] The deviation from solution polymerization was attributed to two factors: 1.) exit of the transfer radical into the aqueous phase, which consequently leads to termination with a radical in the aqueous phase or termination with a growing chain upon re-entering the droplet, 2.) termination of the entering radical with the intermediate radical. However, the influence of the first factor should be small due to the fact that re-initiation with monomer will be very high, thus decreasing the probability of exit. The consumption of RAFT is also very high, therefore leading to longer chains, which will have a profound effect on the hydrophobicity as well as the diffusion capabilities of the chains, hence lowering exit. Deviation from predicted molar mass is therefore most likely caused by the termination reaction with the intermediate radical species. Equation 5.8 was therefore modified to allow for these effects, thus giving

$$\overline{M}_{n,theory} = FW_{RAFT} + \frac{x \cdot [M]_0 \cdot FW_M}{[RAFT]_0 + 2f_I \cdot f_{entry} \cdot [I]_0 \cdot \left(1 - e^{-k_d t}\right)} \tag{5.9}$$

$$\text{with } f_{entry} = \left(\frac{\sqrt{k_d \cdot [I]_w \cdot k_{t,aq}}}{k_{p,aq} \cdot [M]_w} \right)^{1-z} \tag{5.10}$$

The equation accounts for termination reactions that can occur by including the amount of initiator decomposed over the reaction, which is corrected by two efficiency factors f_I and f_{entry},[33] and assuming termination by combination. FW_{RAFT} and FW_M have the same meaning as in Equation 5.8, x is the fractional monomer conversion and $[M]_0$ is the initial monomer concentration, $[I]_0$ is the initial initiator concentration, k_d is the initiator decomposition rate in the aqueous phase, t is the time in seconds, $[RAFT]_0$ is the initial concentration of the RAFT agent, f_I is the initiator efficiency for addition to monomer and f_{entry} is the efficiency for radical species in the aqueous phase to enter before aqueous phase termination occurs. f_{entry} can further be explained by Equation 5.10 in which $k_{t,aq}$ and $k_{p,aq}$ are the termination and propagation rate coefficient in the aqueous phase, respectively, $[I]_w$ and $[M]_w$ the initiator and monomer concentration in the aqueous

phase, respectively, and z is the lowest number of monomer units needed for the oligomer to be surface active. f_{entry} was taken as 1 and f_1 as 0.7, which are similar to values for solution experiments. For very small initiator concentrations the second term of the denominator can be neglected, thus converting back to Equation 5.8.

5.3 Experimental

5.3.1 Materials

Styrene (Sty, Protea Chemicals, 99.5%), butyl acrylate (BA, Hoechst, 99.5%) and methyl methacrylate (MMA, ICI Chemicals and Polymers, 99.9%) were washed with a 0.3M potassium hydroxide (KOH) solution followed by vacuum distillation to remove the inhibitor. The monomer was stored at –12 °C prior to use. Sodium dodecyl sulfate (SDS, BDH, 90%); isooctane (99.5%), diethyl ether (99.5%) (both Merck); chloroform (Labchem, 99%); HCl (ACE, 32%); α-methyl styrene (99%), n-hexadecane (both ACROS); potassium persulfate (KPS, 99+%), n-dodecyl mercaptan (98%), sodium hydroxide (50% solution in H_2O), phenyl magnesium bromide (3.0M in ether), benzyl magnesium chloride (1.0M in diethyl ether), bromobenzene (99%), CS_2 (99.9%), CCl_4 (99.9%) (all Aldrich); Aliquot 336 (Fluka); acetone (99.5%), ethyl acetate (99%), isopropanol (99%), pentane (99%), heptane (99%) (all Saarchem); 4,4'-azobis(4-cyanovaleric acid) (75%) and *p*-toluene sulfonic acid (98.5%) (both Sigma-Aldrich) were used as received. 2,2'-Azobis(isobutyronitrile) (AIBN, Delta Scientific, 98%) was recrystallized from methanol. Distilled deionized water, obtained from a Millipore Milli-Q purification system, was used throughout.

5.3.2 Synthesis of RAFT agents

Synthesis of 4-cyano-4-((thiobenzoyl)sulfanyl)pentanoic acid (1, CVADTB)

The synthesis of 4-cyano-4-((thiobenzoyl)sulfanyl)pentanoic acid was carried out according to the method of Rizzardo *et al.*[2] and purified by liquid chromatography over a

silica column using a 3:3:4 ratio of pentane:heptane:ethyl acetate. The product was crystallized with the help of a drop of chloroform and dried under vacuum to provide the product with a NMR purity estimated at ~ 98%, 62% yield based on bis(thiobenzoyl) disulfide.

Synthesis of phenyl 2-propyl phenyl dithioacetate (2, PPPDTA)

Phenyl 2-propyl phenyl dithioacetate was prepared according to the method of Quinn *et al.*[22] with the following modifications. Phenyl magnesium bromide was purchased and used as reagent. The Grignard agent was added to CS_2, in an equimolar amount, in a dropwise fashion under nitrogen while the reaction temperature was maintained below 20 °C by using an ice bath. After the addition was completed, the reaction was terminated by pouring the reactor contents into ice water and extracting the organic by-products with diethyl ether. The aqueous layer was then acidified with 32% HCl and extracted with diethyl ether. The organic layer was concentrated and a molar equivalent of α-methyl styrene was added. *p*-Toluene sulfonic acid catalyst was added and the mixture was allowed to reflux in CCl_4 overnight. The product was then concentrated and crystallized from cold methanol. NMR purity was estimated at 99%, 15% yield based on carbon disulfide.

Synthesis of S-1-dodecyl-S'-(R,R'-dimethyl-R-acetic acid) trithiocarbonate (3, DIBTC)

S-1-Dodecyl-S'-(R,R'-dimethyl-R-acetic acid) trithiocarbonate was prepared according to the method of Lai *et al.*[34]. n-Dodecyl mercaptan, acetone (~ 6 times molar excess) and catalytic Aliquot 336 (tricaprylylmethylammonium chloride) were mixed in a reactor, cooled in an ice bath, under a nitrogen atmosphere and stirred with an overhead stirrer. An equimolar amount of sodium hydroxide solution (50%) was added dropwise. After the base addition, an equimolar amount of carbon disulfide in acetone (40%) was added dropwise, during which time the color turned yellow and the mixture became viscous. After the addition was complete, a 1.5 times molar excess of chloroform was added to the reaction mixture in one portion, followed by dropwise addition of 5 times

molar excess 50% sodium hydroxide solution. The reaction was stirred overnight and added to 600 mL of water in a 2L beaker that was vigorously stirred while 100 mL of concentrated HCl was added. After coagulation the solid was collected by filtration and then stirred in 1L of isopropanol. The insoluble S,S'-bis(1-dodecyl) trithiocarbonate was filtered and discarded. The isopropanol solution was concentrated and poured into ice-cold hexane from which crystallization took place. NMR purity was estimated at 99%, 60% yield based on dodecyl mercaptan.

Synthesis of cumyl dithiobenzoate (4, CDB)

The synthesis of cumyl dithiobenzoate was, in a similar fashion, carried out according to the method of Le *et al.*[2] and purified by successive liquid chromatography on silica and alumina using hexane as an eluent system. The product crystallized after vacuum removal of solvent and storage below -10 °C. The purity was estimated by ^{1}H NMR to be >95%, 25% yield based on dithiobenzoic acid.

All of the above RAFT agents are shown in Scheme 5.5.

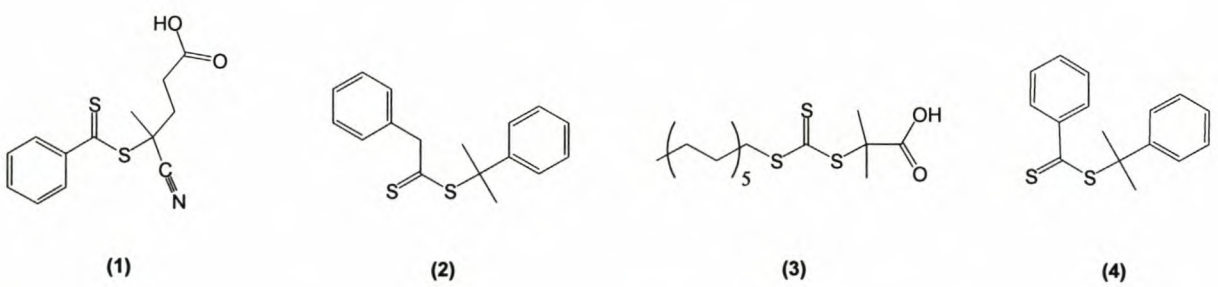

(1) (2) (3) (4)

Scheme 5.5: RAFT agents (**1**) 4-cyano-4-((thiobenzoyl)sulfanyl)pentanoic acid (CVADTB), (**2**) phenyl 2-propyl phenyl dithioacetate (PPPDTA), (**3**) S-1-Dodecyl-S'-(R,R'-dimethyl-R-acetic acid) trithiocarbonate (DIBTC) and (**4**) phenyl 2-propyl dithiobenzoate (cumyl dithiobenzoate) (CDB).

5.3.3 Preparation of core/shell particles

Core/shell particles were synthesized by a miniemulsion polymerization reaction. Styrene, hexadecane, isooctane and the RAFT agent were premixed with a SDS/water solution for 1 hour after which a miniemulsion was obtained by sonicating the mixture with a Sonics & Materials Inc. Vibracell VCX 750 ultrasonicator for 10 minutes at 95% amplitude (sample volumes of up to 40 mL can be sonicated). Successive sonications were performed on 40 mL fractions of larger sample volumes. The average energy input per sample was 95 kJ. During the sonication period the solution was continuously stirred in a water-cooled jacketed vessel to avoid polymerization due to heating and to facilitate homogeneous sonication. After miniemulsification, the solution was transferred to a glass reactor, equipped with a condenser and nitrogen purge, and suspended in a thermostatted oil bath. Polymerization was achieved by adding KPS or AIBN initiator at 75 °C, under continuous nitrogen purging. For formulations for particle syntheses with different RAFT agents, monomer and initiators, refer to Table 5.1.

For the synthesis of PBA/HD core/shell particles the styrene and isooctane, as used in the above reactions, were substituted with butyl acrylate and hexadecane, respectively. Samples were sonicated for 5 minutes at 95% amplitude, resulting in an energy input of ~50 kJ. Table 5.2 shows the formulations for PBA/HD core/shell particles as well as the additional block copolymerizations with MMA.

Table 5.1: Formulations for the synthesis of PS/isooctane particles using different RAFT agents and initiators.

	RAFT agent									
	PPPDTA		PPPDTA		CVADTB		CDB		DIBTC	
	(g)	(mmol)	(g)	(mmol)	(g)	(mmol)	(g)	(mmol)	(g)	(mmol)
styrene	10.98	105	10.98	105	10.98	105	10.98	105	13.18	126
isooctane	8.55	74.8	8.55	74.8	8.55	74.8	8.55	74.8	10.31	90.3
MeOH	10	312	10	312	10	312	10	312		
hexadecane	1.14	5	1.14	5	1.14	5	1.14	5	1.37	6
SDS	4	13.9	4	13.9	4	13.9	4	13.9	2.75	9.5
DDI	93		93		93		93		105	
KPS	0.01	0.037			0.02	0.074	0.02	0.074	0.01	0.037
AIBN			0.01	0.061						
RAFT agent	0.106	0.37	0.106	0.37	0.106	0.38	0.106	0.39	0.1616	0.44

5.3.4 Block copolymerization in miniemulsion

PBA/HD miniemulsions were polymerized for 6 and 3 hours respectively (Section 5.3.3) in order to synthesize the initial core/shell particles. CDB and PPPDTA were used as RAFT agents. After polymerization the latexes were stirred for 12 hours before block copolymerization, at which point the latex was heated to 80 °C under continuous nitrogen purging. MMA was added over a 2 hour period and KPS (0.037 mmol) was added immediately after the start of the feed. Samples of the crude reaction mixture were taken for SEC measurements at regular time intervals.

Table 5.2: Formulations for the synthesis of PBA/HD core/shell particles as well as subsequent chain extensions with MMA.

	RAFT agent			
	PPPDTA		CDB	
	(g)	(mmol)	(g)	(mmol)
butyl acrylate	11	85.8	11	85.8
MeOH	9.3	290	9.3	290
hexadecane	10	44.2	10	44.2
SDS	2.5	8.7	2.5	8.7
DDI	93		93	
KPS	0.01	0.037	0.01	0.037
RAFT agent	0.106	0.37	0.106	0.39
Block formation				
MMA	3.69	36.8	3.51	36.8
KPS	0.0034	0.0125	0.0032	0.0118
Feed rate (mL/min)		0.0438		0.042

5.3.5 Analytical techniques

Size-exclusion chromatography (SEC)

Molar mass distributions were measured via size-exclusion chromatography (SEC). Dried latex samples were dissolved in THF (8 mg/mL) and filtered through a 0.45 μm nylon filter. Analyses were carried out with a SEC system comprising a Waters 610 Fluid Unit, Waters 410 Differential Refractometer at 30 °C, a Waters 717_{plus} Autosampler and Waters 600E System Controller. Two PLgel 5 μm Mixed-C columns and a pre-column (PLgel 5 μm Guard) were used and the column oven was set at 30 °C.

Millennium[32] was used for data acquisition and data analysis. THF was used as solvent and the flow rate was 1.0 mL/min. The volume of the injected samples was 100 μL. The system was calibrated with narrow polystyrene standards ranging from 800 to 2×10^6 g/mol.

Transmission electron microscopy (TEM)

Analysis of the synthesized particles by TEM was carried out as follows: 2 mL of the latex was added to an excess of MeOH to aid precipitation of the particles. The solution was first homogenized by shaking and then transferred to a copper TEM grid by pipette. The grid was left to dry at ambient temperature before analyses were performed. No staining was applied to the dried particles. Contrast between the core and shell was a result of the combined effects of the different path lengths and material densities of the constituting materials. This resulted in the incident e^--beam being scattered more from the wall material than the core-oil, resulting in a darker region on the TEM images. Analyses were done on a JEM - 200CX and 2000FX (JEOL Ltd, Tokyo, Japan) TEM. Copper grids were prepared by the deposition of a thin film of carbon on them to increase the strength and conductivity of the film.

5.4 Results and discussion

From Chapter 3 it was shown that particle morphology can be controlled by the initiating species, which will manipulate interfacial activities, and rate of polymerization, which in turn will influence the viscosity of the polymerized phase and thus chain mobility. By using a suitable surfactant/initiator pair in a miniemulsion reaction it is possible for the oligomeric radicals entering the stabilized droplets to be anchored at the water/droplet interface, thus directing polymerization to take place at the interface. When this is combined with fast polymerization kinetics the polymerization locus can be locked-down at the interface, with monomer diffusion taking place from the inside of the droplet.[35-38] For the formation of core/shell particles this is very important, especially when the difference in hydrophobicities of the constituting core and shell material

produces undesired morphologies.[39] When the core material is a liquid, encapsulation becomes even more difficult.

The successful development of the ability to produce particles with desired core/shell structures (Chapter 3) led to the introduction of additional goals of this study to now include control of the molar mass of the encapsulating shell. One of the advantages of a controlled radical polymerization is that the molar mass of the polymer formed increases in a uniform manner. Unfortunately, the advantage in controlling molar mass becomes a disadvantage in controlling morphology. Stubbs *et al.*,[40] however, reported that this is not the case for highly effective conventional chain transfer agents, except at very high chain transfer agent concentrations In RAFT polymerization, on the other hand, all the chains will grow at the same rate, which is dependent on the particular RAFT agent used. Long chains, which lock-in the morphology, are not formed rapidly with many RAFT agents. The shorter chains result in a higher degree of chain mobility and thus a loss of control of particle morphology. This means that it becomes important to use a RAFT agent that allows for rapid polymerization to chain lengths that will provide a high viscosity within the particles and, in that way, lock-in the morphology. In this work, three classes of RAFT agents are used, namely dithiobenzoates, trithiocarbonates and phenyl dithioacetates. The kinetics that accompany the different agents have been and are still under investigation. It is, however, known that dithiobenzoates lead to a large retardation in polymerization rate and, for that reason, the molar mass distribution of polymer that is formed using a dithiobenzoate will develop more slowly than that formed using a phenyl dithioacetate, even though the target molar masses may be of the same order. This factor is of particular relevance to this investigation as we have a mechanism by which chain growth can be slowed. This allows the kinetic effect of the increasing viscosity of a latex particle to be examined more thoroughly.

The second critical factor is the degree of surface activity that is present in the oligomeric radical that enters the particle. If no surface activity is present, i.e. in the case of an oil-soluble initiating species such as AIBN, then there is no driving force for interfacial initiation or surface stabilization via the functional endgroup, which would

have been present in the case of a water-soluble initiator such as KPS. This means that there is a very good probability that an inverted system will be formed. Such a system is predicted to be thermodynamically stable (for this specific monomer/oil combination) during the formation of high molar mass polymer.[41,42] However, when initiation takes place from the water phase and if the anchoring effect occurs, entering radicals will (1.) lead to the reduction in the interfacial tension between the entering oligomers and the water phase, (2.) facilitate the presence of the mediated species at the droplet/water interface and (3.) if the RAFT agent used allows very little retardation, rapid polymerization can occur at the interface, which will result in an increase in viscosity. Polymerization will therefore take place mainly at the interface, leading to the desired core/shell morphology.

The use of RAFT in miniemulsion has been controversial due to the problems that have been encountered as far as latex stability and molar mass control are concerned. The early work by de Brouwer *et al.*[43] with SDS is an excellent example. Low conversions and colloidal instabilities led to a change in direction and to the use of polymeric surfactants. Butté *et al.*[44] and Lansalot *et al.*[9] were able to show that polymeric RAFT agents that exceed the critical length for water solubility were suitable for miniemulsion polymerizations using SDS. However, the degree of control that was obtained typically lead to PDIs > 1.5 and some classes of RAFT agents were unable to provide control in miniemulsion polymerization. Work in our group[45] has shown that excellent control can be obtained in miniemulsion polymerization with no loss of latex stability, using RAFT agents that have not been polymerized in homogeneous media,[9,14,44] and being independant of the class of RAFT agent used.

The expansion of the RAFT technique to structured particles was, for this reason, the logical next step for investigation.

5.4.1. Influence of the type of initiator

As a starting point for the synthesis of structured particles, an "intermediate" RAFT agent (PPPDTA), i.e. exhibiting moderate retardation, was used together with KPS as initiating species. KPS was chosen for its interfacial effects when combined with SDS as surfactant. This will provide surface anchoring of the entering oligomeric species, thus polymerization at the interface as caused by the radicals produced by the mediating species. SEC traces for the above system can be seen in Figure 5.1, clearly indicating the living nature of the system, as evidenced by the steady increase in molar mass as a function of conversion.

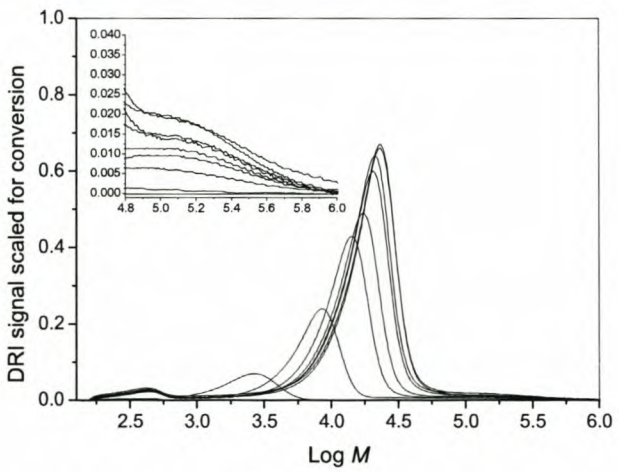

Figure 5.1: SEC traces showing the living/controlled nature of particles synthesized with PPPDTA and KPS as initiating species.

Note the very small peak (magnified in insert), which can be attributed to secondary nucleation and which will be explained in more detail later. The predicted number average molar mass was calculated according to De Brouwer[32] and this, as well as the experimentally acquired $\bar{M}_n$ and polydispersity data, plotted against the conversion, can be seen in Figure 5.2. The experimental $\bar{M}_n$ values almost coincide with the theoretically calculated $\bar{M}_n$ values. This is a strong indication of the controlled nature of the system and is strengthened by the low polydispersity index values obtained. The small secondary nucleation peak was not taken into account when the polydispersity and $\bar{M}_n$

values were calculated. The polymer contributing to this peak was formed by a different mechanism in this compartmentalized system.[46] When this peak is excluded, excellent correlation with predicted values is obtained, which shows us that the percentage of the polymer mass contained within this peak is negligible.

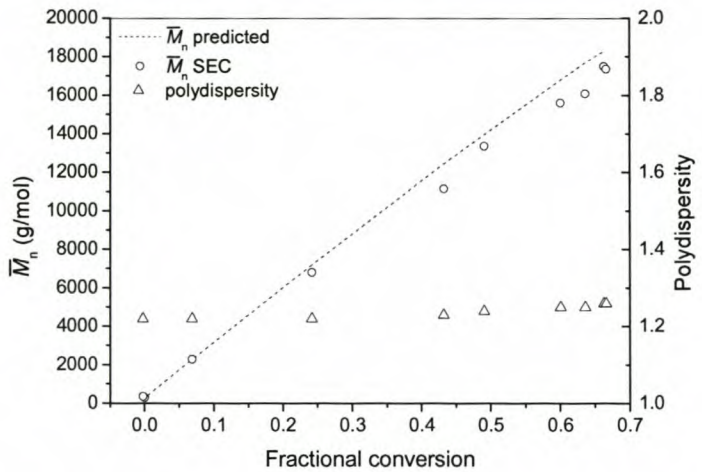

Figure 5.2: Predicted $\overline{M}_n$, experimental $\overline{M}_n$ (SEC) and polydispersity values versus the fractional conversion for the miniemulsion polymerization of PS/isooctane core/shell particles in the presence of PPPDTA and KPS.

Figure 5.3 shows a TEM image obtained from the synthesized core/shell particles.

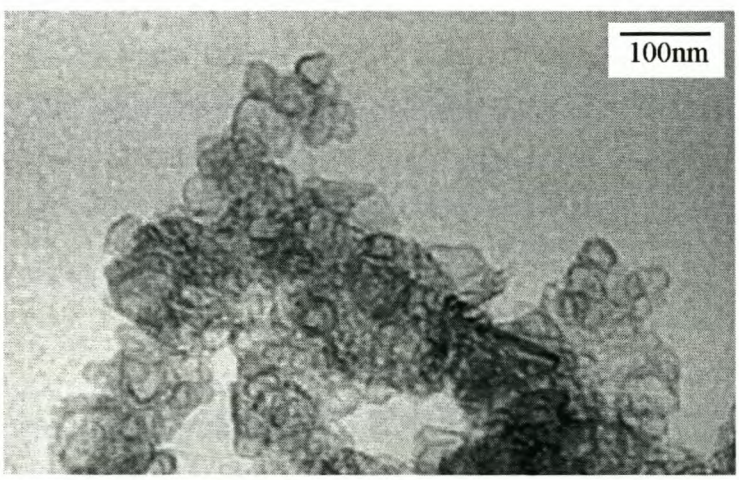

Figure 5.3: TEM image of PS/isooctane core/shell particles synthesized in the presence of PPPDTA and KPS under controlled conditions.

The image shows core/shell particles clumped together thus causing overlapped shapes. Some of the obtained particles show deformed structures. This is quite normal when considering the low molar mass values obtained for the synthesized particles together with the fact that no crosslinkers were added. The particles will therefore easily deform if no further strengthening (crosslinking) is performed and lead to visually flattened or deformed particles. Figure 5.4 shows a high-magnification image of the synthesized particles. Figure 5.5 shows a close-up of individual particles along with a scale bar indicating the average particle size.

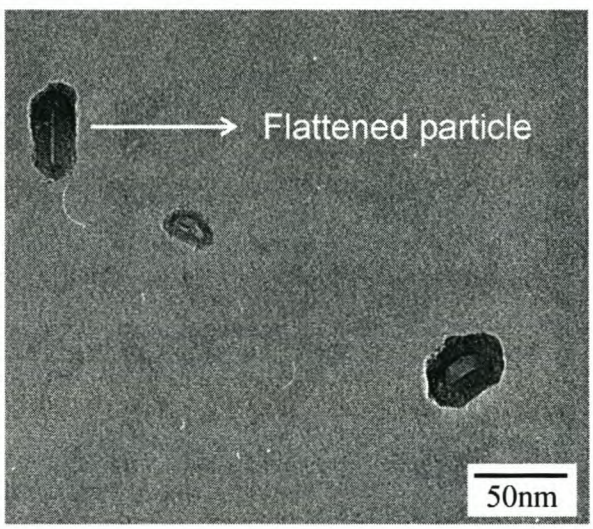

Figure 5.4: Higher magnification of core/shell particles synthesized in the presence of PPPDTA and KPS. In the top-left corner a flattened core/shell particle can be seen.

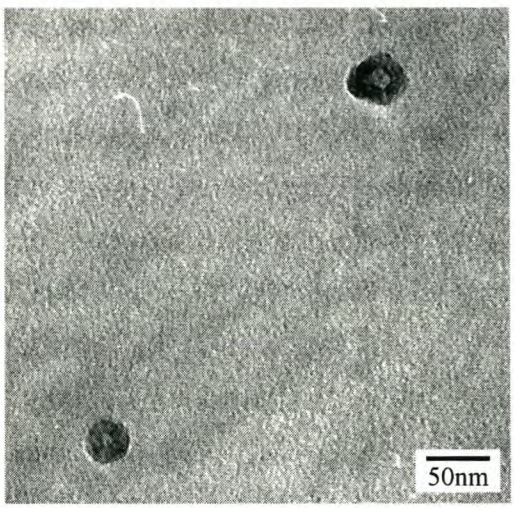

Figure 5.5: High-magnification TEM image of individual core/shell particles synthesized in the presence of PPPDTA and KPS.

Although the predominant particle morphology is core/shell, Figure 5.6 shows the existence of a population of solid spherical particles.

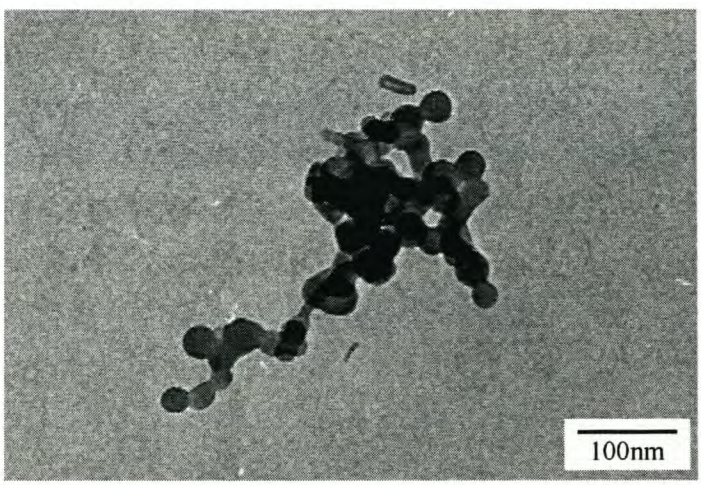

Figure 5.6: TEM image showing the presence of solid particles that were caused by secondary nucleation. Note the flattened particle at the top of the image that has core/shell morphology.

These particles are most likely caused by secondary nucleation (note that three particle nucleation mechanisms can occur for heterophase polymerizations namely

micellar nucleation, homogeneous nucleation and heterogeneous nucleation),[47] which will result in the formation of particles that do not contain core material. Due to the fact that virtually no RAFT agent is present in the aqueous phase, or for that matter the free micelles, polymerization will continue under conventional free radical conditions thus leading to uncontrolled polymerization and hence high molar mass. This is confirmed in the SEC traces (Figure 5.1). Up to now the confirmation of secondary nucleation has been rather difficult in miniemulsion polymerization of RAFT-initiated species. This is because nucleated species are usually homogeneous, thus leading to solid spherical particles and therefore making it impossible to differentiate between controlled particles and particles produced under conventional free radical conditions.

For initiator comparison the same RAFT agent (PPPDTA) was used but with the oil-soluble initiator (AIBN) as initiating species. SEC traces for the miniemulsion polymerization can be seen in Figure 5.7.

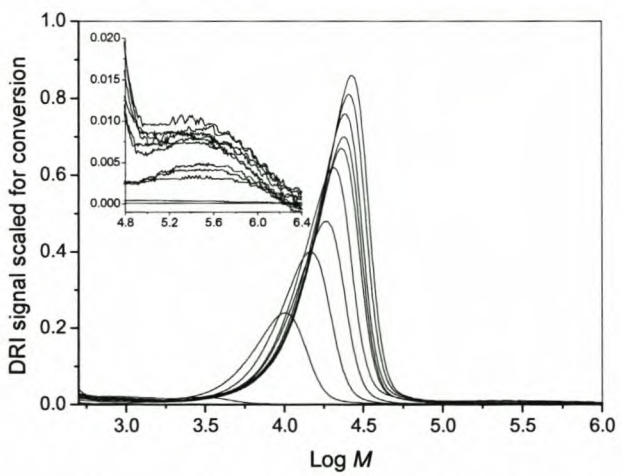

Figure 5.7: SEC traces showing the living/controlled nature of particles synthesized with PPPDTA and AIBN as initiating species.

As with the KPS (Figure 5.1), it can be seen that the polymer grows in a controlled fashion. The inlay is again a magnification of the secondary nucleation part which was not taken into consideration when $\bar{M}_n$ and polydispersity index values were calculated. Figure 5.8 shows theoretical $\bar{M}_n$ values, SEC $\bar{M}_n$ values and polydispersity index values

versus conversion for the system, and confirms that the criteria for living polymerization are met. A slight deviation between the theoretical and experimental $\bar{M}_n$ values is observed at high fractional conversion. This is caused by tailing of the MMD towards lower molar mass. Figure 5.9 shows the TEM image of the obtained particles. All synthesized particles show solid structures and thus no core/shell morphology.

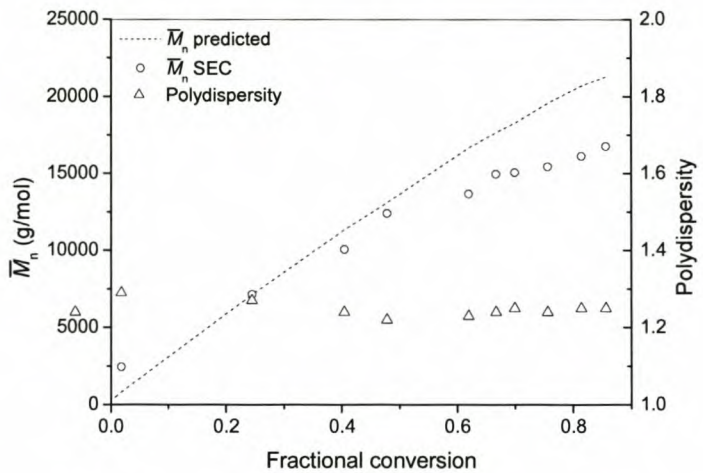

Figure 5.8: Predicted $\bar{M}_n$, experimental $\bar{M}_n$ (SEC) and polydispersity values versus the fractional conversion for the miniemulsion polymerization of PS/isooctane in the presence of PPPDTA and AIBN.

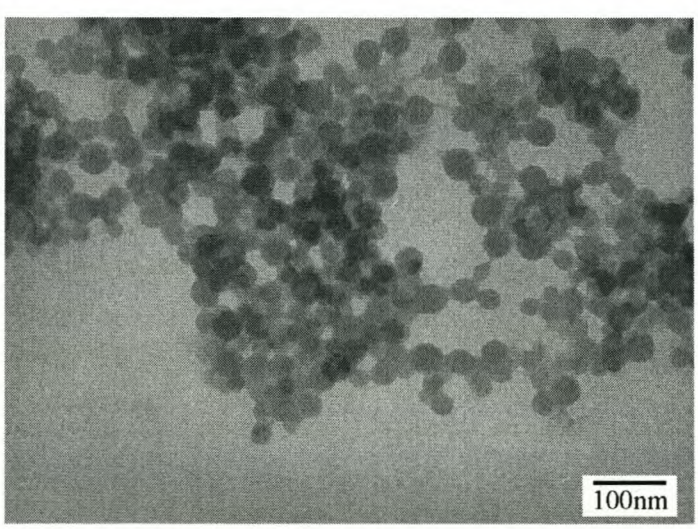

Figure 5.9: TEM image of solid particles synthesized under controlled conditions in the presence of PPPDTA and AIBN.

In this case the anchoring effect will not be present as a result of the fact that AIBN does not possess any ionic groups that will interact with the surfactant molecules stabilizing the droplet surface. Thus, although AIBN has a degree of water phase initiation[48] the entering radicals will not be able to anchor themselves at the water/droplet interface and therefore polymerization due to mediated species will not preferentially take place at the oil/water interface. In addition AIBN, also shows higher rates of dissociation when compared to KPS.[49] Higher dissociation rates will lead to an increased number of radicals entering the droplet at any given moment, which will cause a higher rate of monomer conversion. The rate of chain growth is, however, still determined by the type of RAFT agent present in the system. Further propagation and transfer will all take place inside the droplet without any necessity for the more hydrophobic oligomers to migrate to the interfacial layer to form the desired core/shell morphology. Controlled polymerization will therefore take place in the entire volume of the droplet and not only at the water/droplet boundary, thus causing solid particles. Polymer encapsulation is limited due to the polarity difference between the polystyrene and water and will therefore rather result in an inverse morphology due to the lack of kinetic influences, which causes thermodynamics to dominate.

From the above it is therefore quite obvious that the type of initiator used will play a crucial role in establishing core/shell morphology.

5.4.2 Influence of the type of RAFT agent

In this instance the type of RAFT agent used will be compared. For this experiment a "slower" RAFT agent, i.e. an agent that provides greater polymerization rate retardation, was chosen, namely CVADTB. This RAFT agent is kinetically slower than PPPDTA. See Figure 5.10 for a first-order kinetic comparison between the different RAFT agents used.

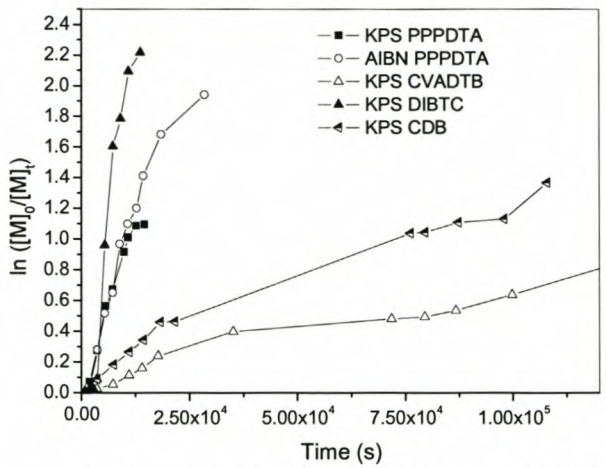

Figure 5.10: First-order kinetic plots for reactions done with PPPDTA, CVADTB and DIBTC using KPS and AIBN as initiating species.

KPS was used as initiating species, facilitating the presence of mediated species at the oil/water interface. Figure 5.11 shows the MMDs for the miniemulsion polymerization reaction with CVADTB as RAFT agent and KPS as initiating species.

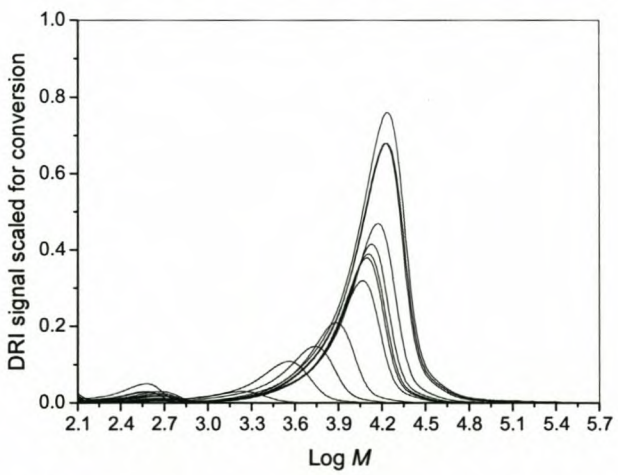

Figure 5.11: SEC traces showing the living/controlled nature of particles synthesized with CVADTB and KPS as initiating species.

Again it is quite obvious that controlled polymerization could be achieved, as is confirmed from the plots in Figure 5.12. Here the $\bar{M}_n$ values obtained from SEC follow the theoretically predicted $\bar{M}_n$ values and the polydispersity values are acceptable.

Although it is expected that the use of KPS as initiating species would increase the chances of core/shell formation, Figure 5.13, showing TEM images of the obtained particles, proves the opposite. Keep in mind that CVADTB is a much slower (higher retardation) RAFT agent than PPPDTA. Thus, even though KPS will provide surface anchoring of the entering oligomers, polymerization at the droplet interface, caused by radicals produced by mediating species, is rather slow, which will lead to a slow increase in viscosity as a function of time.

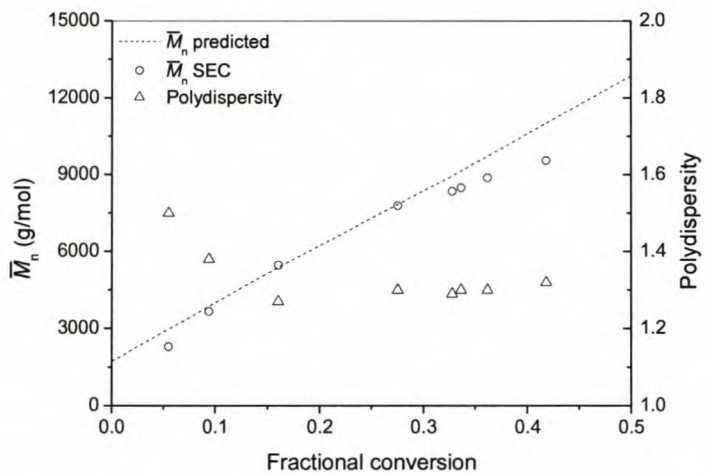

Figure 5.12: Predicted $\overline{M}_n$, experimental $\overline{M}_n$ (SEC) and polydispersity values versus the fractional conversion for the miniemulsion polymerization of PS/isooctane in the presence of CVADTB and KPS.

There is now no driving force for the formation of an interfacial polymer layer. The slow formation of chains will allow diffusion due to the low viscosity of the polymerization locus. Hence, the thermodynamically preferred morphology, which is inverse core/shell, will dominate, thus causing solid particles to be formed. This is quite different from the case of PPPDTA, where the rapid formation of polymer does not allow thermodynamically predicted (inverse morphology) phase separation between the core-oil and the polymer, leading to two separate phases, i.e. core/shell morphology. KPS has a documented influence on the pH of emulsion polymerization and for this reason heterogeneous systems are normally buffered against major pH changes, which could affect surfactant efficiency in the case of ionic surfactants.[36] In this study no buffer was

used in the experimental procedures using CVADTB, which will, at high pH values, provide ionic endgroups. These endgroups should then increase the degree of surface anchoring in the system. However, the experimental data suggest that even if a substantial increase in surface anchoring has occurred, the rate of interfacial polymerization is unaffected and thus no extreme viscosity increase occurs in the interfacial region of the particles. This means that even though enhancement of the surface anchoring might be expected in the system, it does not increase the possibility of establishing a polymer phase at the droplet/water interface. Establishment of the interfacial polymer phase is due to the increase in viscosity, which is dependant on the radical stabilizing group of the RAFT agent and is not a function of the nature of the chain end. Experimental data showed no major effect of pH on particle size or latex stability and for that reason any variation that might occur in the pH of the system is deemed to have a minimal impact on the interpretation of the data. The hydrolytic stability of dithioesters in aqueous media with time has been studied and it has been shown that degradation of the dithioester moiety is minimal on the timescale of these polymerizations.[50] The typical pH value of the studied latexes was 5.4.

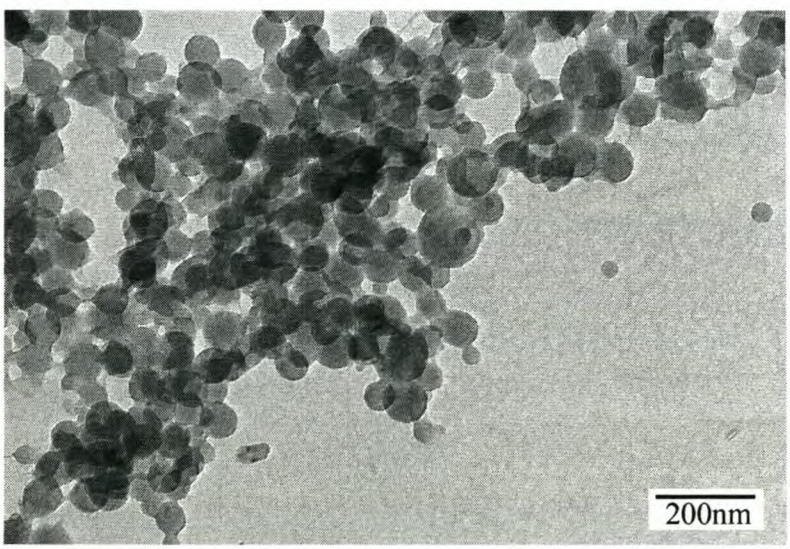

Figure 5.13: TEM image of solid particles synthesized under controlled conditions in the presence of CVADTB and KPS.

In the above section miniemulsion polymerizations with CVADTB and PPPDTA as RAFT agents were compared, using different initiating species, AIBN and KPS. As an additional proof for the investigation, it was therefore decided to minimize variables, thus to substitute the CVADTB RAFT agent in order to compare the influence of RAFT species, consisting of similar leaving groups (R), on morphology. This was done by substituting CVADTB with CDB and comparing again with PPPDTA. The justification in changing the CVADTB to CDB lies in the fact that these two RAFT agents have similar transfer constants (C_{tr}) but different leaving groups. From Figure 5.10 it follows that the retardation for the CVADTB is slightly higher than for the CDB. This is because of the nature of the leaving groups, which can facilitate exit into the continuous phase, thus reducing the rate of polymerization.[28,51,52] The effect of exit also becomes significant at very small droplet/particle size due to the fact that exit (or the probability of exit, *P(exit)*) is inversely proportional to the radius of the droplet/particle as can be seen in Equation 5.11

$$P(exit) = \frac{k_{dm}}{k_{dm} + k_p^1 C_p}, \quad k_{dm} = \frac{3D_w}{r_s^2}\frac{C_w}{C_p} \tag{5.11}$$

where D_w is the diffusion coefficient in water, C_w and C_p are the concentrations of the leaving free radical in the aqueous phase and particle, respectively, r_s is the swollen radius of the droplet/particle, k_{dm} is the coefficient for the desorption of a monomeric free radical and k_p^1 is the propagation rate coefficient for free radical species to monomer.

Although the above was presented for seed particles, it will still hold true for *in situ* polymerization of miniemulsion droplets. The exited radical species can undergo several termination reactions, *viz.* termination in the aqueous phase via initiator-derived radicals or termination with a growing radical upon re-entering of the droplet. The net effect is that some of the droplets will loose their propagating radicals and they therefore need to be re-initiated to again become loci of polymerization.[9]

Both CDB and PPPDTA contain a phenyl 2-propyl leaving group, although the activating groups are different (Scheme 5.5). The Z group in CDB contains a phenyl ring which is able to delocalize electrons more readily than the benzyl substituent in PPPDTA. The benzyl substituent is able to change the intermediate radical into a less stable radical which will increase the rate of fragmentation of the intermediate radical species and thus result in faster establishment of the RAFT equilibrium. This will therefore determine the degree of retardation as can be seen in Figure 5.10. Because of the higher stability of the CDB macroradicals, lower conversion will be achieved in the same reaction time as for PPPDTA.

Figures 5.14 and 5.15 again confirm the living/controlled nature of the polymerization reaction with CDB. Thus, even though the influence of the type of R-group, as variable, has been removed, similar retardation rates are achieved when compared to the CVADTB and TEM results (Figure 5.16) again confirm the deviation from the desired core/shell morphology.

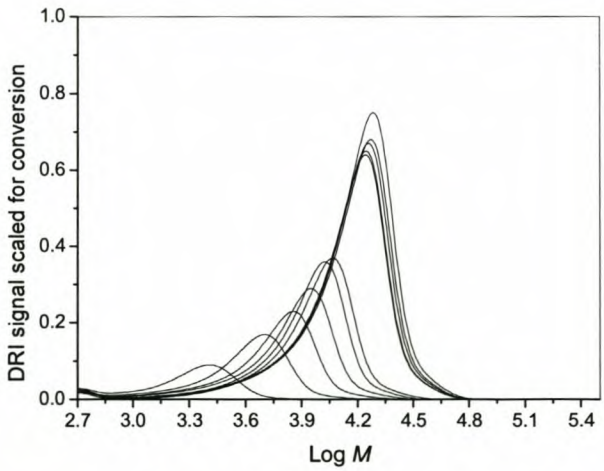

Figure 5.14: SEC traces showing the living/controlled nature of particles synthesized with CDB and KPS as initiating species.

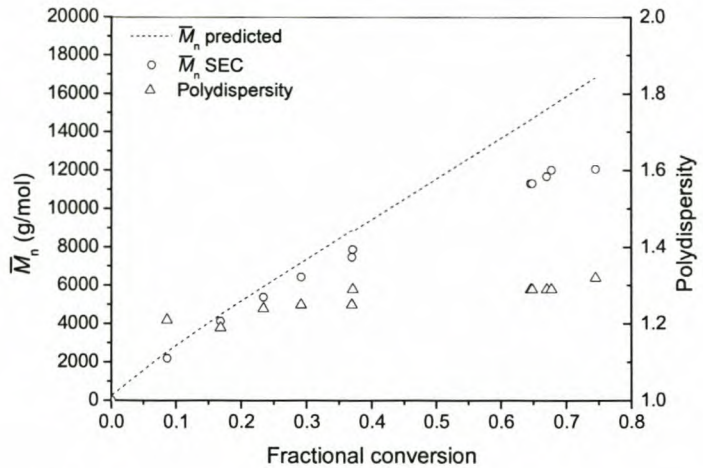

Figure 5.15: Predicted $\overline{M}_n$, experimental $\overline{M}_n$ (SEC) and polydispersity values versus the fractional conversion for the miniemulsion polymerization of PS/isooctane in the presence of CDB and KPS.

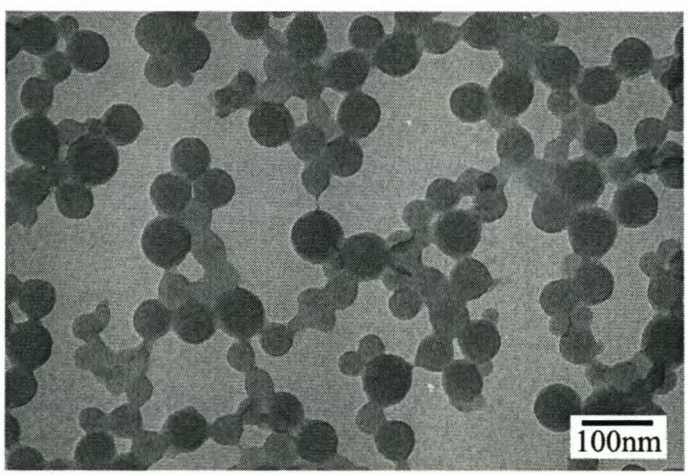

Figure 5.16: TEM image of solid particles synthesized under controlled conditions in the presence of CDB and KPS.

The final RAFT agent that was introduced to the system was a trithiocarbonate, DIBTC (Scheme 5.5). The advantage of the trithiocarbonates is that they can be prepared with one or two good homolytic leaving groups, thus Z = SR in the latter case. DIBTC has very interesting properties, one of which is the ability to act as a surface active agent, i.e. surfactant molecule, due to the fact that an alkyl chain is attached to one of the thio-

groups and an acid to the other. DIBTC exhibits very little retardation and is therefore classified as a "fast" RAFT agent, as can be seen in Figure 5.10. The dodecyl chain attached to the one thio group does not exhibit any leaving group capabilities. However, dimethyl acetic acid, which is attached to the other thio group does make a very good leaving group. Upon fragmentation of the intermediate species this group (which is water soluble) is much more prone to exit to the water phase, which can consequently cause secondary nucleation in the water phase due to the presence of free micelles and monomer. This can quite clearly be seen in Figure 5.17, where two molar mass distributions are present. As indicated, the two distributions can be associated with controlled polymerization due to the RAFT agent present in the droplet, and uncontrolled polymerization due to secondary nucleation and particle formation in the aqueous phase. Note that secondary nucleation is not the only mechanism active in this polymerization system but that re-entry can also take place. If this happens, transfer can occur inside the droplet via the RAFT mechanism or termination with an already present radical species inside the droplet.

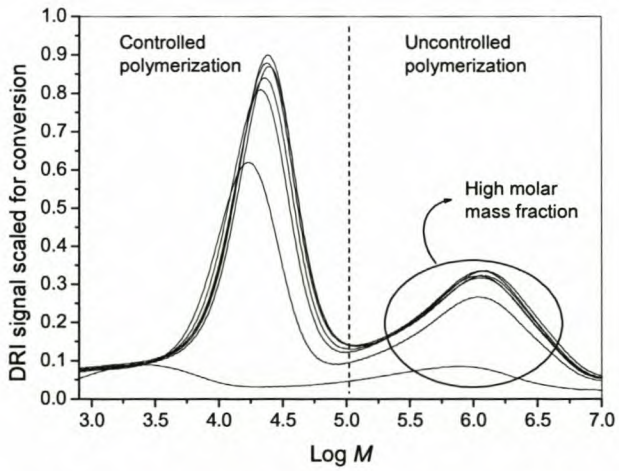

Figure 5.17: SEC traces showing bimodal molar mass distribution for particles synthesized with DIBTC and KPS.

To further evaluate the controlled nature of the first peak, the experimentally obtained $\bar{M}_n$ values were compared with theoretically calculated $\bar{M}_n$ values for the low molar mass peak, as can be seen in Figure 5.18. Again it is clear that SEC values follow the predicted

values although complete correlation is not possible due to the bimodality of the molar mass plots, which causes skewing of experimental data. Peak separation and hence peak selection is therefore not adequate, which results in deviation from predicted $\bar{M}_n$ values as well as an increase in polydispersity values.

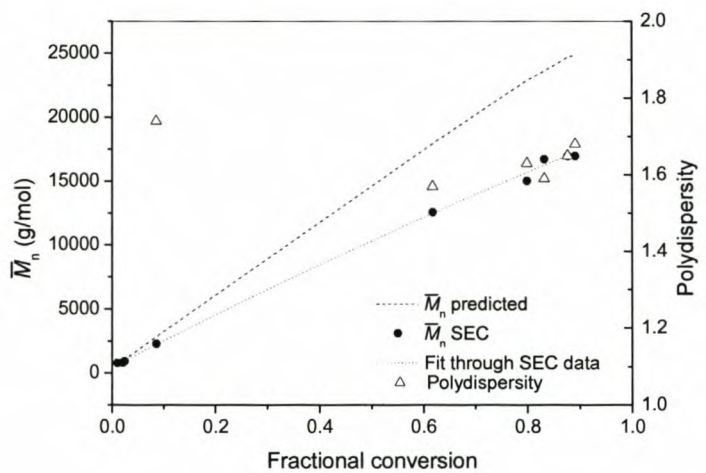

Figure 5.18: Predicted $\bar{M}_n$, experimental $\bar{M}_n$ (SEC) and polydispersity values versus the fractional conversion for the miniemulsion polymerization of PS/isooctane in the presence of DIBTC and KPS.

A TEM image of the synthesized particles can be seen in Figure 5.19.

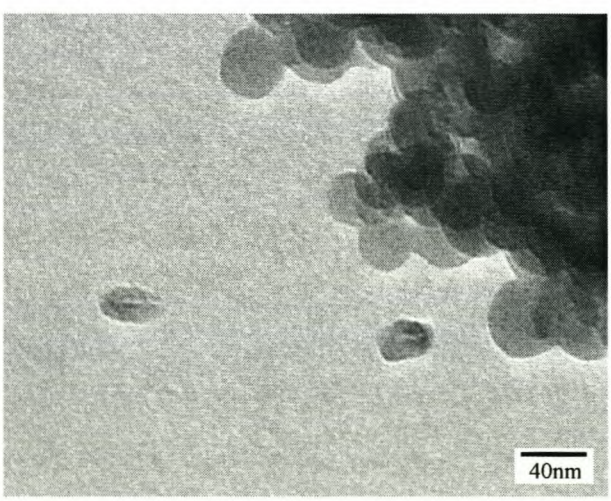

Figure 5.19: TEM image of particles synthesized in the presence of DIBTC and KPS.

Note the abundance of solid particles and the two possible core/shell particles at the bottom. The polymerization reaction possesses all the right attributes to be able to form the desired core/shell morphology, i.e. very low retardation and surface activity. However, in this instance, exit of the leaving group dominates, which will lead to secondary nucleation and therefore the formation of solid polymer particles.

5.4.3 Influence of monomer

To conclude this chapter the influence of monomer was evaluated by reverting back to the butyl acrylate/hexadecane system as previously described (Chapters 3&4). Synthesis conditions were identical to the conditions used for the styrene/isooctane system (Section 5.3.3) and two RAFT agents, CDB and PPPDTA, in conjunction with KPS as initiator were used. When comparing the propagation rate coefficients of styrene and butyl acrylate it is found that $k_p(\text{BA}) >> k_p(\text{Sty})$.[49] The faster rates increase the propagation step (increase in propagating radicals) in the RAFT mechanism (due to the fact that the equilibrium constant will be faster), ultimately leading to an increase in the polymerization rate (Equation 5.7). Thus, by changing the monomer it is also possible to change the polymerization kinetics and therefore the outcome of the particle morphology. By looking at the first-order kinetic plots (as seen in Figure 5.20) for the butyl acrylate system, compared to the styrene system, it is easy to see that retardation becomes less important for the CDB/BA system. The possibility therefore exists to force the correct morphology, by decreasing retardation, through the introduction of a "fast" monomer.

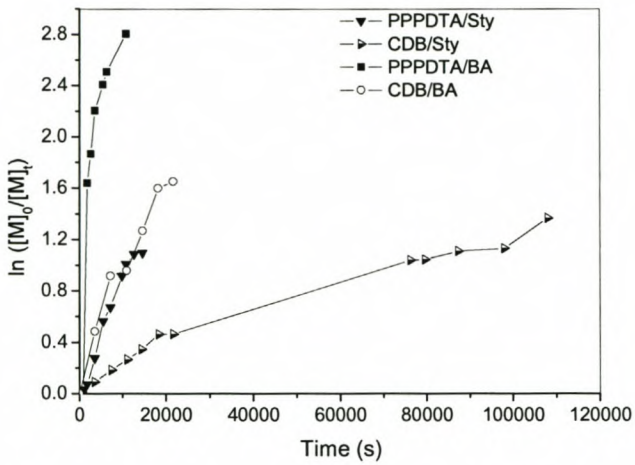

Figure 5.20: The influence of monomer on polymerization rates as confirmed by first-order kinetic plots for reactions done with PPPDTA and CDB, using KPS as initiating species.

Care must be taken when a high k_p monomer is used with a RAFT agent with limited retardation; Figure 5.21 shows the incredibly fast rate at which conversion is achieved for the BA/PPPDTA system.

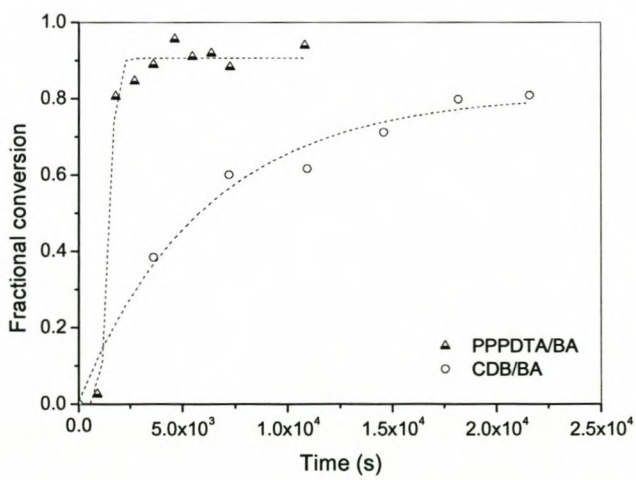

Figure 5.21: Fractional conversion versus time for the synthesis of poly(butyl acrylate)/hexadecane core/shell particles with PPPDTA and CDB and using KPS as the initiating species.

Figure 5.22 shows the SEC traces obtained for the polymerization of BA/HD core/shell particles with CDB and PPPDTA, respectively. Figure 5.23 shows the predicted versus experimentally obtained $\overline{M}_n$ values for the aforementioned reactions. It is quite clear that both reactions follow living and controlled conditions, although the polydispersity of the particles synthesized with PPPDTA is a bit high.

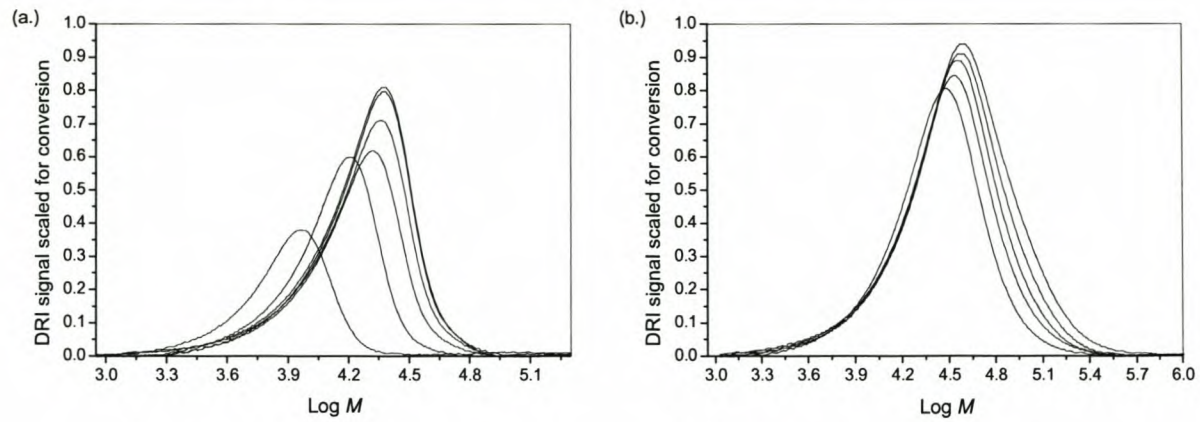

Figure 5.22: MMDs showing the living/controlled nature of particles synthesized with (a.) CDB and KPS and (b.) PPPDTA and KPS.

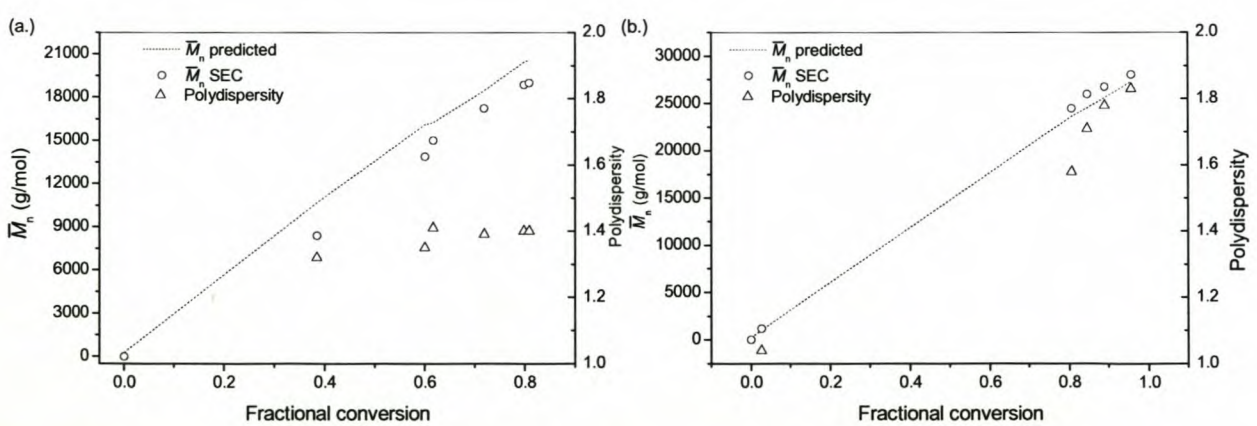

Figure 5.23: Predicted $\overline{M}_n$, experimental $\overline{M}_n$ (SEC) and polydispersity values versus the fractional conversion for the miniemulsion polymerization of PBA/HD in the presence of (a.) CDB and KPS and (b.) PPPDTA and KPS.

This might be caused by the increase in the propagation step, which will result in many monomer additions per activation/deactivation cycle, hence leading to a slight increase in molar mass and subsequent increase in polydispersity.

For TEM analysis of the synthesized nanoparticles it was necessary to strengthen the particles by grafting them with a glassy polymer. Polybutyl acrylate has a T_g of -55 °C and will therefore undergo film formation when dried at ambient temperature, even at the high conversion that was achieved. This will therefore result in spreading, and will subsequently lead to the destruction of particles. Methyl methacrylate was again chosen as secondary shell polymer but the method of addition, as was used in Chapter 3, was not followed here. In Chapter 3 methyl methacrylate was grafted onto the PBA as a result of hydrogen atom abstraction from the polymer backbone. However, when this was applied to the PBA/HD core/shell particles as synthesized by CDB, the latex system underwent a sudden color change from pink (which is the original latex color as a result of the RAFT agent used) to bright yellow to white. This change took place in a matter of seconds and is a clear indication that the redox reaction used in the grafting procedure destroys the RAFT agent and therefore the possibility for further monomer additions as a result of the living nature of the polymer.

The formation of a glassy secondary shell was therefore attempted through the living character of the polymer. The formation of a block polymer with living characteristics in solution has already been documented, but the transformation to a heterogeneous system proved to be more complex. Reasons for this are the high amount of surfactant used in the miniemulsion system, which could lead to the formation of homopolymer, as well as the difficulties in trying to achieve block growth on the particle surface and not homogeneously throughout the particle. Results will therefore only be briefly discussed as the above problems have posed numerous questions which are currently being investigated by our group.[53]

Different monomer additions can be performed during block synthesis, *viz.* shot addition, where all the monomer is added at once and allowed to swell the seed particles,

and feed addition, where monomer is fed over a predetermined time. Both methods have merits and can therefore be used for specific applications. Due to the fact that miniemulsions are used, the possibility of secondary nucleation must be minimized and therefore a starve-feed addition was used. Results of this can be seen in Figure 5.24.

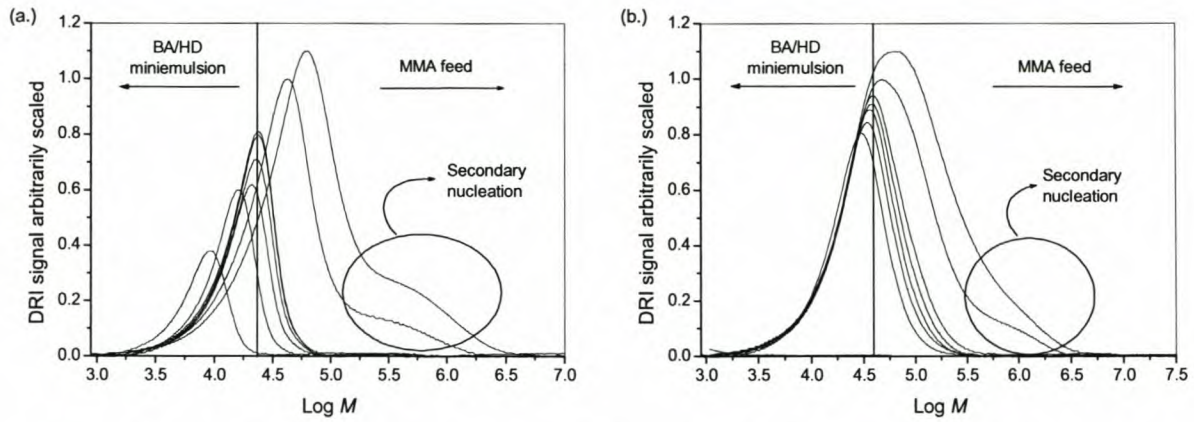

Figure 5.24: Chain extensions of PBA/HD core/shell particles with MMA in the presence of (a.) CDB and KPS and (b.) PPPDTA and KPS.

In Figure 5.24 (a.) block copolymer formation is evident from the shift of the complete MMD towards higher molar mass in a controlled manner. This is not as clear when looking at Figure 5.24 (b.) which shows no movement of the low molar mass material in the peaks. This is most likely caused by excessive termination of the radical species which will result in inactive chains, especially on the low molar mass side of the distribution. For PPPDTA there will be more propagating species when compared to the CDB. More termination can therefore occur, which will lead to the formation of low molar mass terminated species. This will result in the low molar mass side of the peak not moving as prominently in the case of the faster RAFT agent, PPPDTA.

In a RAFT system the order of monomer addition in the formation of block copolymers is very important, *e.g.* better defined blocks can be obtained when the seed is PMMA and styrene is fed. From a solution polymerization viewpoint this makes (perfect) sense as the PMMA group will be a better leaving group, thus facilitating better block formation. In heterogeneous media (miniemulsions) the above is also true as the droplet can be seen as a minireactor.[35] This, as well as the fact that the low water

solubility of the styrene monomer will impart increased transfer of monomer through the aqueous phase to the droplet, will increase formation of a block copolymer and result in less secondary nucleation.

In the PBA/HD system that was used, butyl acrylate was used to synthesize the first block with the secondary block originating from an MMA feed. MMA has substantially higher water solubility (15 g/L at 25 °C) than most monomers and is therefore more prone to secondary nucleation in the aqueous phase. This will result in the formation of an uncontrolled high molar mass fraction, which can be seen in Figure 5.24.
Block formation was nevertheless possible, which resulted in adequate strengthening of the particles and thereby allowing TEM analyses. Results of the analyses can be seen in Figure 5.25.

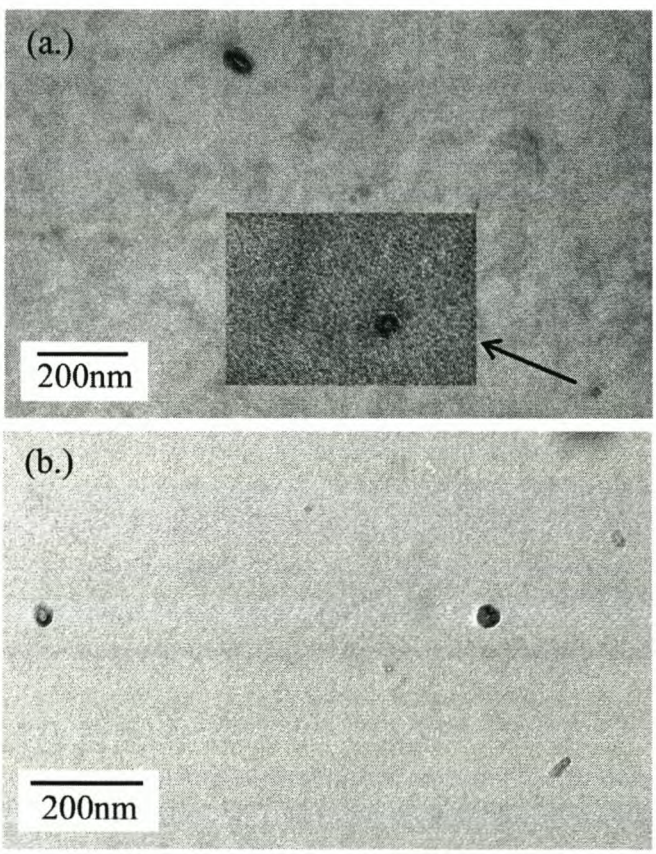

Figure 5.25: TEM images showing the successful strengthening of PBA/HD core/shell particles with PMMA.

Figure 5.25 confirms the existence of core/shell particles. Results therefore prove that it is possible to synthesize core/shell particles consisting of a rubbery shell and liquid core. Butyl acrylate is, however, not the easiest monomer to work with due to its low film formation temperature, and thus the necessity of chain extensions, as well as the fact that backbiting can occur more readily. The latter might lead to peak fronting on the high molar mass side and therefore broadening of the molar mass distribution. The addition of methyl methacrylate to the synthesized core/shell particles also proved to be a bit troublesome. Nevertheless it was still possible to successfully synthesize particles with the desired morphology, dimensions and composition, as was originally set out to do, but with the added advantage of having living characteristics. Although the results to date show that improvements to the system can still be made, such a system has never been documented and is therefore in itself already a great achievement and therefore merely a beginning of greater things to follow.

5.5 Conclusions

Chain architecture and morphology of structured particles can be controlled by using living/controlled polymerization techniques in conjunction with surface active initiating species. In this study, core/shell particles consisting of an isooctane core and polystyrene shell were synthesized with additional control of the molar mass of the shell polymer. The formation of particles with the desired morphology is made possible by controlling the kinetic effects of the reaction, i.e. polymerization kinetics as well as surface effects, i.e. anchoring of the entering oligomeric species. To study these two effects, two different RAFT agents were used to study the influence of retardation times, which are inherent to the nature of the agent used. An intermediate agent (low retardation time) as well as a slow agent (high retardation time), PPPDTA and CVADTB respectively, were used in conjunction with two initiating species, KPS and AIBN. The latter were chosen for their difference in surface activities. When the intermediate agent was used in conjunction with KPS, the entering radicals could be anchored at the droplet/water interface. This, together with the fact that PPPDTA leads to a rapid increase in chain lengths and therefore a decrease in chain mobility, resulted in the polymerization locus

being locked at the droplet/water interface, causing the formation of core/shell particles. When AIBN was used, on the other hand, no surface activity was present, allowing entering radicals to transfer into the droplet without being anchored at the surface. Even though an intermediate RAFT agent was used, there is no thermodynamic driving force for the hydrophobic oligomers to migrate to the droplet/water interface. This consequently results in polymerization across the total volume of the droplet, resulting in solid particles. A slow RAFT agent (CVADTB) was used in conjunction with a surface active initiating species, KPS. In this case entering oligomers could be anchored at the droplet/water interface. However, due to the high retardation times, no rapid increase in chain lengths took place and consequently no related increase in viscosity and decrease in chain mobility. Diffusion of transferred species into the droplet can therefore take place, causing polymerization over the entire volume of the droplet, leading to the formation of solid particles.

To minimize the number of variables, CVADTB was changed to CDB. The reason for this was to compare RAFT agents with similar R groups. Similar results to those observed with CVADTB were achieved. To conclude, the influence of monomer was investigated by reverting back to the original BA/HD system. BA dramatically increased the polymerization rate and could therefore be used in conjunction with a "slow" RAFT agent to synthesize core/shell particles. Chain extensions were also possible in this system, which was necessary for adequate TEM analysis of the formed particles.

References

(1) Šebenik, A. *Prog. Polym. Sci.* **1998**, *23*, 875-917.

(2) Le, T. P.; Moad, G.; Rizzardo, E.; Thang, S. H. In *PCT International Application*; wo98/01478, 1998.

(3) Chiefari, J.; Chong, Y. K.; Ercole, F.; Krstina, J.; Jeffery, J.; Le, T. P.; Mayadunne, R. T. A.; Meijs, G. F.; Moad, C. L.; Moad, G.; Rizzardo, E.; Thang, S. H. *Macromolecules* **1998**, *31*, 5559-5562.

(4) Wang, J.-S.; Matyjaszewski, K. *J. Am. Chem. Soc* **1995**, *117*, 5614-5615.

(5) Matyjaszewski, K.; Gaynor, S.; Wang, J.-S. *Macromolecules* **1995**, *28*, 2093-2095.

(6) Moad, G.; Rizzardo, E.; Solomon, D. H. *Macromolecules* **1982**, *15*, 909-914.

(7) Georges, M. K.; Veregin, R. P. N.; Kazmaier, P. M.; Hamer, G. K. *Macromolecules* **1993**, *26*, 2987-2988.

(8) Qiu, J.; Charleux, B.; Matyjaszewski, K. *Prog. Polym. Sci.* **2001**, *26*, 2083-2134.

(9) Lansalot, M.; Davis, T. P.; Heuts, J. P. A. *Macromolecules* **2002**, *35*, 7582-7591.

(10) Matyjaszewski, K.; Qiu, J.; Tsarevsky, N. V.; Charleux, B. *J. Polym. Sci., Part A: Polym. Chem.* **2000**, *38*, 4724-4734.

(11) Cunningham, M. F.; Xie, M.; McAuley, K. B.; Keoshkerian, B.; Georges, M. K. *Macromolecules* **2002**, *35*, 59-66.

(12) Kukulj, D.; Davis, T. P.; Gilbert, R. G. *Macromolecules* **1997**, *30*, 7661-7666.

(13) Lansalot, M.; Farcet, C.; Charleux, B.; Vairon, J.-P. *Macromolecules* **1999**, *32*, 7354-7360.

(14) Vosloo, J. J.; De Wet-Roos, D.; Tonge, M. P.; Sanderson, R. D. *Macromolecules* **2002**, *35*, 4894-4902.

(15) Prescott, S. W.; Ballard, M. J.; Rizzardo, E.; Gilbert, R. G. *Macromolecules* **2002**, *35*, 5417-5425.

(16) Ferguson, C. J.; Hughes, R. J.; Pham, B. T. T.; Hawkett, B. S.; Gilbert, R. G.; Serelis, A. K.; Such, C. H. *Macromolecules* **2002**, *35*, 9243-9245.

(17) Bon, S. A. F.; Bosveld, M.; Klumperman, B.; German, A. L. *Macromolecules* **1997**, *30*, 324-326.

(18) De Brouwer, H. *RAFT memorabilia: living radical polymerization in homogeneous and heterogeneous media*, Technische Universiteit Eindhoven, Eindhoven, 2001.

(19) Parker, D. S.; Sue, H.-J.; Yee, H.; Yee, A. F. *Polymer* **1990**, *31*, 2267-2277.

(20) Scholes, P. D.; Coombes, A. G. A.; Illum, L.; Davis, S. S.; Vert, M.; Davies, M. C. *J. Controlled Release* **1993**, *25*, 145-153.

(21) Davis, S. S.; Illum, L. *Biomaterials* **1988**, *9*, 111-115.

(22) Quinn, J. F.; Rizzardo, E.; Davis, T. P. *Chem. Commun.* **2001**, 1044-1045.

(23) De Brouwer, H.; Schellekens, M. A. J.; Klumperman, B.; Monteiro, M. J.; German, A. L. *J. Polym. Sci., Part A: Polym. Chem.* **2000**, *38*, 3596-3603.

(24) Feng, X.-S.; Pan, C.-Y. *Macromolecules* **2002**, *35*, 4888-4893.

(25) Mayadunne, R. T. A.; Jeffery, J.; Moad, G.; Rizzardo, E. *Macromolecules* **2003**, *36*, 1505-1513.

(26) Moad, G.; Chiefari, J.; Chong, Y. K.; Krstina, J.; Mayadunne, R. T. A.; Postma, A.; Rizzardo, E.; Thang, S. H. *Polym. Int.* **2000**, *49*, 993-1001.

(27) Müller, A. H. E.; Zhuang, R.; Yan, D.; Litvenenko, G. *Macromolecules* **1995**, *28*, 4326-4333.

(28) Smulders, W. *Macromolecular Architecture in Aqueous Dispersions: 'living' free radical polymerization in emulsion*, Technische Universiteit Eindhoven, Eindhoven, 2002, 187.

(29) Monteiro, M. J.; De Brouwer, H. *Macromolecules* **2001**, *34*, 349-352.

(30) Chong, Y. K.; Krstina, J.; Le, T. P. T.; Moad, G.; Postma, A.; Rizzardo, E.; Thang, S. H. *Macromolecules* **2003**, *36*, 2256-2272.

(31) Chiefari, J.; Mayadunne, R. T. A.; Moad, C. L.; Moad, G.; Rizzardo, E.; Postma, A.; Skidmore, M. A.; Thang, S. H. *Macromolecules* **2003**, *36*, 2273-2283.

(32) De Brouwer, H.; Tsavalas, J. G.; Schork, F. J.; Monteiro, M. J. *Macromolecules* **2000**, *33*, 9239-9246.

(33) Maxwell, I. A.; Morrison, B. R.; Napper, D. H.; Gilbert, R. G. *Macromolecules* **1991**, *24*, 1629-1640.

(34) Lai, J. T.; Filla, D.; Shea, R. *Macromolecules* **2002**, *35*, 6754-6756.

(35) Sudol, E. D.; El-Aasser, M. S. In *Emulsion Polymerization and Emulsion Polymers*; Lovell, P. A.; El-Aasser, M. S., Eds.; John Wiley and Sons Ltd.: England, 1997; pp 699-722.

(36) Gilbert, R. G. *Emulsion Polymerization: A Mechanistic Approach*; Academic Press Limited: London, 1995.

(37) Park, H. S.; Chang, T.; Lee, S. H. *J. Chem. Phys.* **2000**, *113*, 5502-5510.

(38) Griffiths, M. C.; Strauch, J.; Monteiro, M. J.; Gilbert, R. G. *Macromolecules* **1998**, *31*, 7835-7844.

(39) Van Zyl, A. J. P.; Sanderson, R. D.; De Wet-Roos, D.; Klumperman, B. *Macromolecules* **2003**, *36*, 8621-8629.

(40) Stubbs, J. M.; Sundberg, D. C. *Journal of Coatings Technology* **2003**, *75*, 59-67.

(41) Jang, J.; Lee, K. *Chem. Commun.* **2002**, *10*, 1098-1099.

(42) McDonald, C. J.; Bouck, K. J.; Chaput, A. B. *Macromolecules* **2000**, *33*, 1593-1605.

(43) Tsavalas, J. G.; Schork, F. J.; de Brouwer, H.; Monteiro, M. J. *Macromolecules* **2001**, *34*, 3938-3946.

(44) Butté, A.; Storti, G.; Morbidelli, M. *Macromolecules* **2000**, *33*, 3485-3487.

(45) McLeary, J. B.; Tonge, M. P.; De Wet-Roos, D.; Sanderson, R. D.; Klumperman, B. *J. Polym. Sci., Part A: Polym. Chem.* **2003**, *Accepted.*

(46) Li, M.; Matyjaszewski, K. *Macromolecules* **2003**, *accepted.*

(47) Bechtold, N.; Landfester, K. *Macromolecules* **2000**, *33*, 4682-4689.

(48) Luo, Y.; Schork, F. J. *J. Polym. Sci., Part A: Polym. Chem.* **2002**, *40*, 3200-3211.

(49) *Polymer Handbook*, Second ed.; Wiley Interscience: New York, 1975.

(50) Thomas, D. B.; Sumerlin, B. S.; Lowe, A. B.; McCormick, C. L. *Macromolecules* **2003**, *36*, 1436-1439.

(51) Monteiro, M. J.; Hodgson, M.; De Brouwer, H. *J. Polym. Sci., Part A: Polym. Chem.* **2000**, *38*, 3864-3874.

(52) Smulders, W.; Gilbert, R. G.; Monteiro, M. J. *Macromolecules* **2003**, *36*, 4309-4318.

(53) Grumel, V.; McLeary, J. B.; Van Zyl, A. J. P.; Sanderson, R. In *Reversible Addition Fragmentation Chain Transfer MMA-STY Block Investigation: Comparison of Miniemulsion and Solution Polymerizations*, Waters International GPC 2003 and ISPAC-16 Symposium, 2003.

Chapter 6

Physical evaluation and testing of core/shell nanoparticles with liquid cores embedded in a glassy polymer matrix

Abstract

In this chapter the influence of modifier particles, as synthesized in Chapters 3 and 4, on the macroscopic properties of a suitable matrix polymer is investigated. Modifier particles with particular morphology, dimensions and composition were synthesized according to certain recommendations as proposed by previous researchers. The synthesized modifier particles were successfully incorporated into the matrix polymer by compression moulding and were effective in modifying the tensile properties of the matrix polymer.

6.1 Introduction

Plastics have a tendency to undergo brittle failure especially under conditions of impact loading. This is particularly true for amorphous polymers, *e.g.* polystyrene and poly(methyl methacrylate), as well as crosslinked resins as in the case of epoxy[1] and polyester resins, which lead to significant limitations in the development of the synthetic plastics industry. Rubber toughening was successfully introduced in the late 1940s to increase the fracture resistance of plastics.[2] The essence of rubber toughening is that it can be done by standard emulsion polymerization techniques,[3] or chemically-induced phase separation,[4] thereby producing discrete micron or submicron particles for effective dispersion in the polymer matrix to be toughened.

Before considering the different classes of rubber-toughened plastics, it is important to have a very good understanding of the fracture behavior of rigid polymers. A fracture usually starts in highly localized regions and initiates at points of stress concentrations arising from molecular heterogeneities or, more usually, from impurities, *e.g.* dust or scratches. Deformation in these highly localized regions can very rapidly lead to a fracture because all the mechanical energy is focused on a very small area of material with a very low resistance to crack propagation. The two deformation processes that can consequently take place are shear yielding and crazing.[5]

Shear yielding is the local shear deformation and involves the molecular orientation in the plane of the applied stress. Crazing, however, involves the local fibrillation of the polymer and consequently produces a planar yield zone known as crazes. Crazes are formed perpendicular to the axis of stress. The advantage of a craze is that the craze fibrils have very high load-bearing capacity due to the strain hardening of the polymer in the fibrils and this acts to stabilize the craze by the resistance of further opening of the faces as the craze propagates. Crazes are crack–like entities between 100 nm and 1 μm thick and consist of 50% void and 50% fine fibrils, which are between 5 to 20 nm thick.

The interface between the bulk polymer and the craze is known as the craze active zone and contains strain softened polymers, usually between 10 to 25 nm thick. In Figure 6.1 a representation of a craze can be seen.

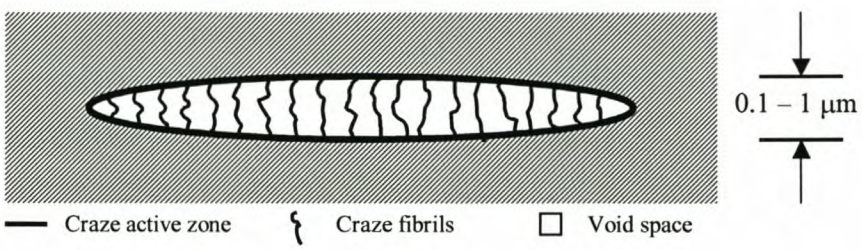

Figure 6.1: Representation of a craze.[5]

As mentioned, rubber toughening was introduced in the late 1940s with the launch of high-impact polystyrene as well as acrylonitrile butadiene styrene (ABS). In the former case the styrene was bulk polymerized in the presence of styrene-butadiene rubber. In the case of ABS, acrylonitrile-styrene copolymer was melt-blended with butadiene rubber. In the mid 1970s core/shell particles were introduced for effective toughening of glassy polymers.[5] The reason for this is, first of all, if a core/shell particle is prepared with a glassy shell and rubbery core, the glassy outer will prevent coalescence of the latex particles during film formation, which will lead to very good dispersions of the particles. Secondly, if the glassy shell can be made of the same substance as the matrix that needs reinforcement, then a very strong interface is ensured which will facilitate efficient transfer of stress from the matrix to the core/shell particles.

In this chapter the route which can be followed to improve impact modification will be explained by summarizing work done in the group of Han Meijer.[1,6-14] Synthesized MMA-grafted PBA/HD core/shell particles will be mixed with a polymer matrix and it will be shown that matrix properties can be modified successfully, thus increasing impact strength. It will also be shown that the introduction of flaws during the moulding process can seriously degrade results and future recommendations regarding this will be made.

6.2 Rationale for liquid-filled nanoparticles for impact modification of glassy polymers

In the mid 1990s, the materials technology (Ma*Te*) group at the Faculty of Mechanical Engineering, Technical University of Eindhoven (TUE), looked at modelling the toughening of heterogeneous polymeric systems.[15-17] By doing this they could define certain key-points which could lead to an increased impact modification of these systems. First of all they looked at the localization phenomena in glassy polymers, *e.g.* polystyrene (PS), poly(methyl methacrylate) (PMMA) and polycarbonate (PC). As can be seen in Figure 6.2 these polymers all have different strain to breaks with $\varepsilon_b(PS)<\varepsilon_b(PMMA)<\varepsilon_b(PC)$. This results in PS breaking brittly and PC being tough. Localization on the microscopic level plays an important role in macroscopic mechanical properties. Consider the general stress-strain behavior of a homogeneously deforming zone in an amorphous polymer network as depicted in Figure 6.3. Initial elastic response transforms into plastic deformations as (a.) the nominal yield stress (σ_y) is approached. With further deformation, stress first decreases and increases again, which is known as (b.) strain softening and (c.) strain hardening.[4]

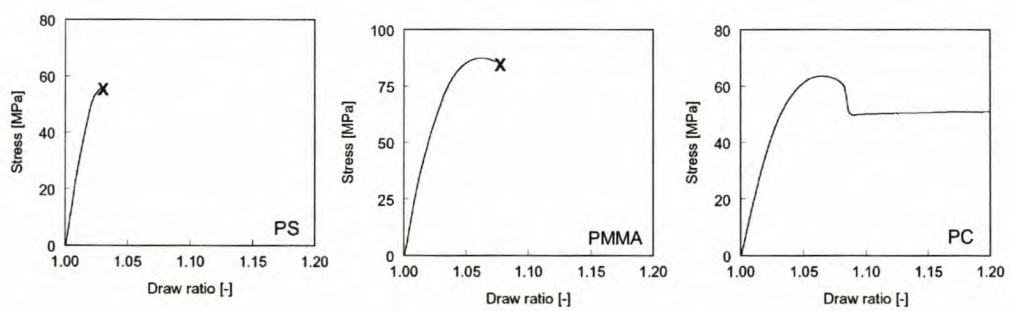

Figure 6.2: The influence of localization on the strain to break in different glassy polymers.

As stress reaches the yield point, strain localization will occur since deformation proceeds at a lower stress. Deformation can only be transferred or delocalized if the local strain hardening process results in a stress which exceeds the yield stress. Strain

localization is therefore determined by the interplay of the three parameters: yield stress, strain softening and strain hardening.

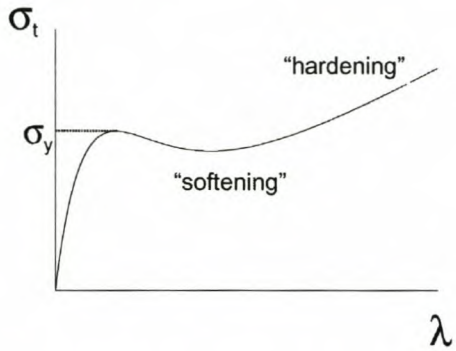

Figure 6.3: A stress-strain curve showing the yield stress (σ_y) as the elastic response transforms into plastic deformations as well as strain softening and strain hardening, which can occur with further deformation.

When comparing stress-strain curves for PS and PC, the stress-strain curve for PS shows pronounced softening, thus strong initiation as well as weak strain hardening, as shown in Figure 6.4. It is therefore quite obvious that localization will preferentially take place resulting in low cavitation stress (40 MPa). PC on the other hand shows moderate softening and therefore moderate initiation. In this case delocalization is possible due to the strong strain hardening that takes place under deformation and therefore high cavitation stress (90 MPa).[18] Note that it is compressive strain that is being presented in Figure 6.4.

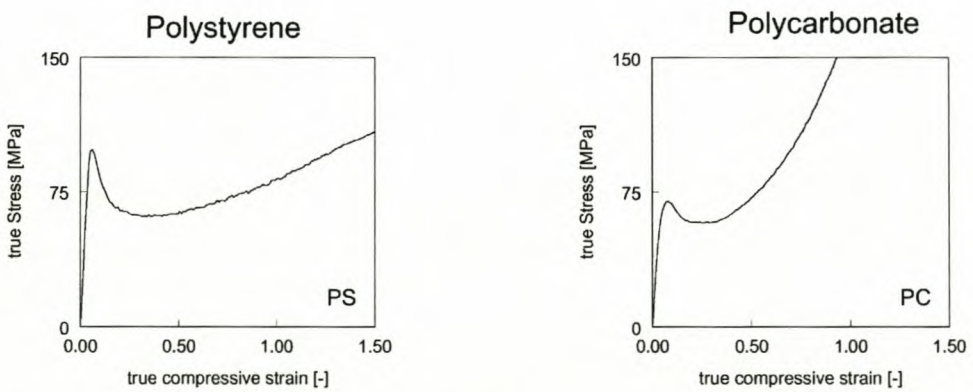

Figure 6.4: Comparisons of the stress-strain curves for PS and PC showing the characteristic differences between strain hardening and strain softening.

6.3 Influence of pre-conditioning on intrinsic mechanical behavior

The intrinsic mechanical properties of PS and PC can be changed by pre-conditioning the polymers.[19] In the case of PC, torsion cycling was applied to the polymer resulting in the reduction of strain softening as shown in Figure 6.5. Similarly, in the case of PS, which was subjected to rolling on a twin mill roll, a decrease in strain softening is observed to such an extent that PS will exhibit a ductile deformation. Note that the ductility is time dependant and will return to a brittle deformation in 30 minutes. From this it is therefore obvious that mechanical properties of polymeric materials can be changed by changing the microstructure (orientation) of the polymer. However, to investigate microstructure variables as well as to optimize this selection, it was considered necessary to model inclusions in a representative volume element (RVE)[14,20,21] and evaluate the macroscopic response.

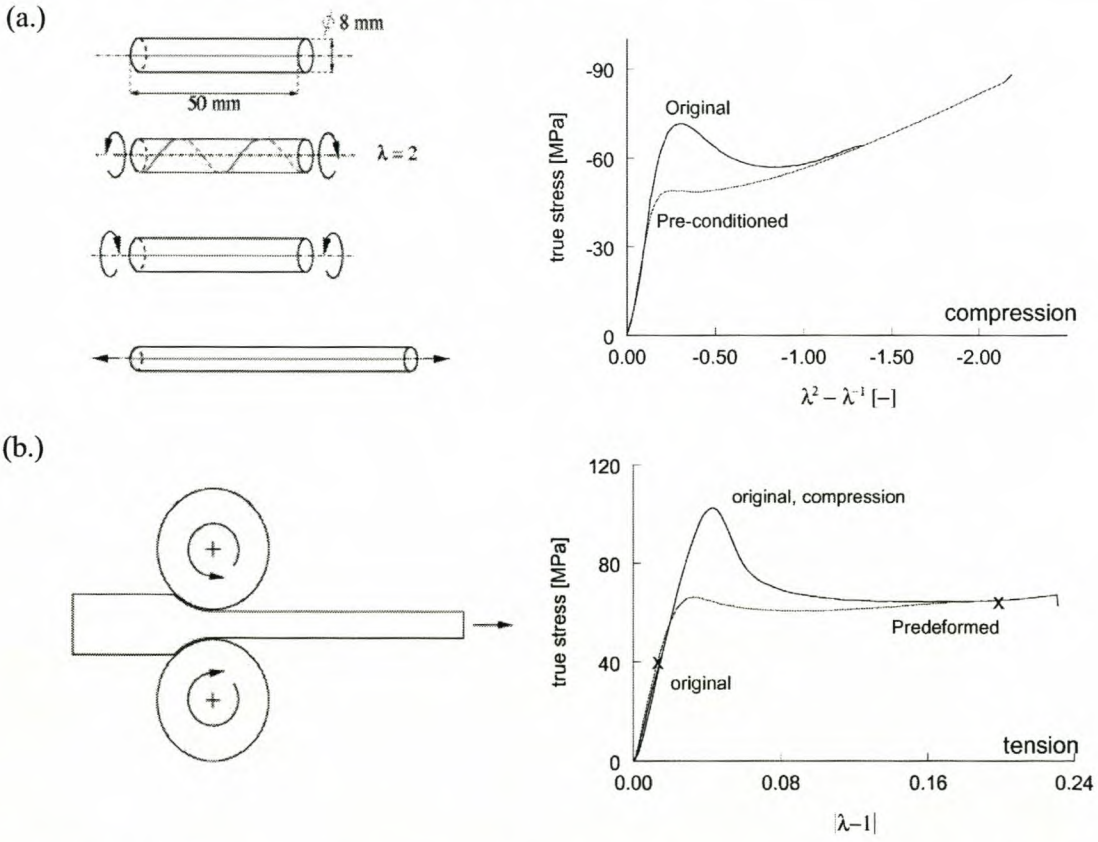

Figure 6.5: The influence of pre-conditioning on the intrinsic mechanical properties of (a.) PC and (b.) PS.

6.4 Representative volume element and the consequent relation to core/shell particles

Spherical particles are randomly packed inside a 3D representative volume element (RVE), a cutting plane is defined through the RVE and the net result is a 2D RVE from the cutting plane. This procedure can be summarized in Figure 6.6. The influence of voids on the stress-strain behavior of PC was investigated by introducing voids into a RVE followed by a cut through the plane of the sample to reveal a 2D image of the void-filled polymer.

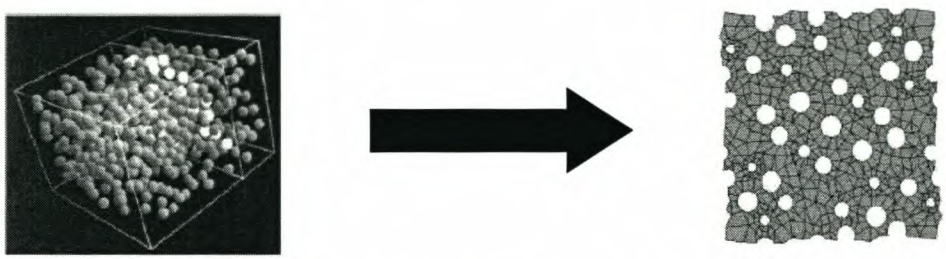

Figure 6.6: A representative volume element showing the cutting plane and consequent 2D representative volume element.

Next, the compressible Leonov model[14] was applied which showed the influence of voids on the stress strain behavior of the polymer. As can be seen in Figure 6.7 a decrease in yield stress and stiffness will occur as well as an increase in volume. This is all due to the reduction of the intrinsic softening.

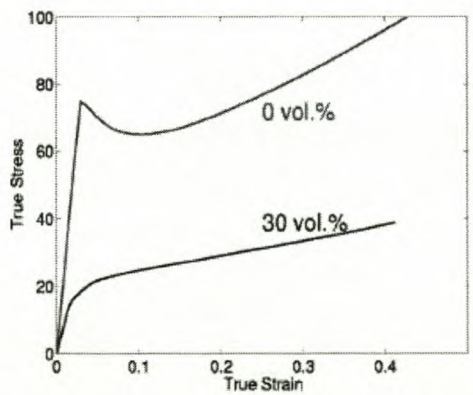

Figure 6.7: The influence of the inclusion of voids on the yield stress of PC.

It is therefore quite obvious that to improve the toughness of a polymeric material one needs to reduce the intrinsic strain softening and/or improve strain hardening. Strain softening is closely related to yield because of a shared origin and can therefore be manipulated by modifying the yield stress. The yield stress can be reduced by predeformation, creation of surface as well as the addition of low-modulus heterogeneities. Heterogeneities will cause sequential yielding, which will consequently result in a reduction of the strain softening. However, if sufficient strain hardening is not present then the local yield zone will not be sufficiently stabilized, resulting in failure of this mechanism.

Strain hardening can be improved by crosslinking, preorientation, blending as well as the incorporation of rubber particles, which must be cavitated or have easily cavitating inclusions, *e.g.* core/shell particles.

Further simulations were performed comparing the inclusion of voids, thin- and thick-shelled core/shell particles, as shown in Figure 6.8, which evidently resulted in a reduction of strain softening.

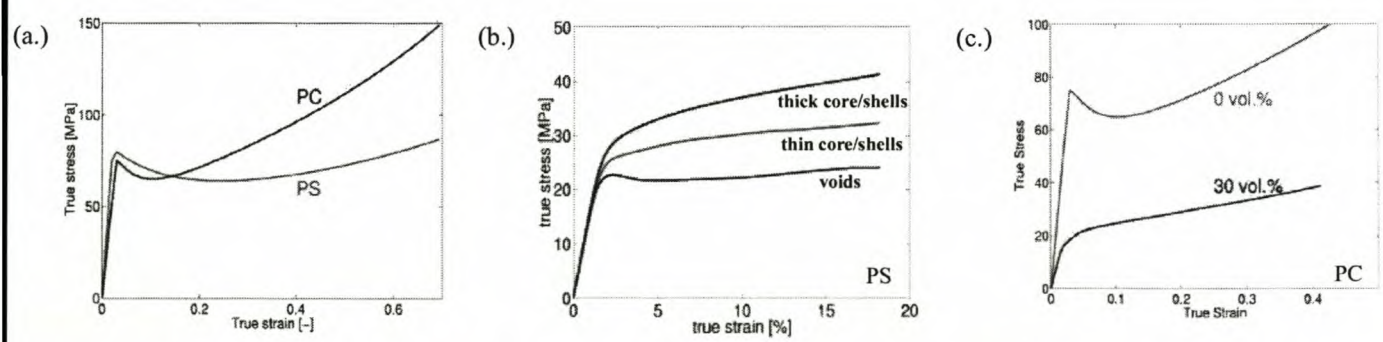

Figure 6.8: The influence of voids and core/shell particles on the stress-strain behavior of PS and PC: (a.) is the compressive stress-strain behavior of PS and PC without voids or core/shell particles, (b.) is the influence of voids and core/shell particles on the stress-strain behavior of PS and (c.) is the influence of voids on the stress-strain behavior of PC.

The influence of voids can be seen in Figure 6.9 where the deformation of a representative volume element of voided PS can be seen. Note the localization and "craze formation". It is therefore clear that although there was an improvement in the tensile behavior, this was not adequate.

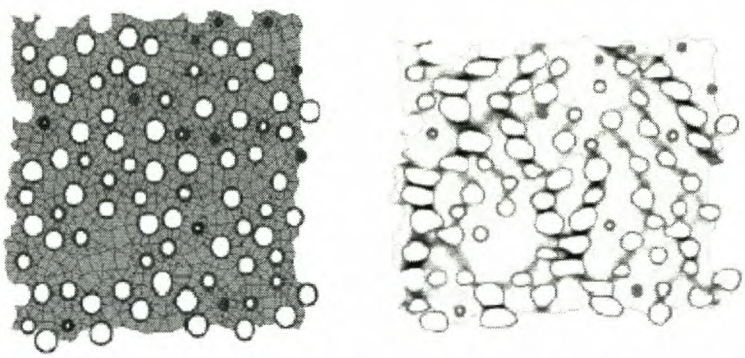

Figure 6.9: A representative volume element showing the effect of voids on the deformation.

This was therefore followed by the introduction of core/shell particles – thin- and thick-walled, with the influence visible in the Figures 6.8 and 6.10. Figure 6.10 represents filling the void in PS with load-bearing rubber shells that support the stretching filament. This will produce enough extra strain hardening and the deformation spreads uniformly in the total volume of the RVE.

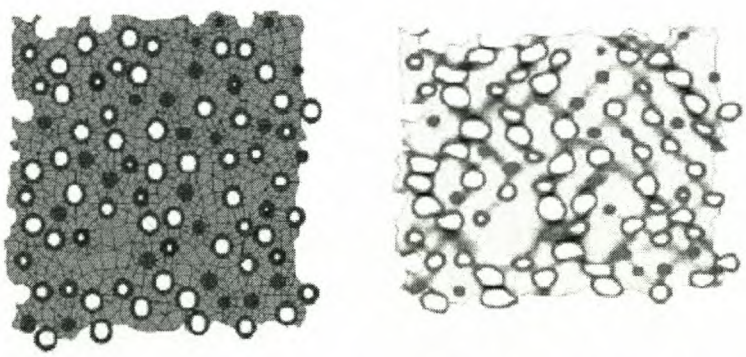

Figure 6.10: A representative volume element showing the effect of thick-walled core/shell particles on the deformation.

To conclude, the effect of particle size and inter particle distance were evaluated.[21]

Simulations therefore predicted that improved toughness can be achieved if:[14]

1. an easily cavitating nano-sized modifier with E < 30MPa is used,
2. the modifier is encapsulated by a rubber shell with E ~ 300MPa,
3. the interparticle distance < 50 nm,
4. only 5% filler is used,
5. the particle size ~ 30 nm.

6.5 Experimental

6.5.1 Preparation of core/shell particles

PBA/HD core/shell particles were synthesized according to the method described in Chapter 4. A ~2% (wt% relative to the water phase) surfactant concentration was used to obtain initial core/shell particles with a diameter of 30-40 nm. Further grafting with MMA was performed to strengthen the particles as well as to increase matrix mixing capabilities, which resulted in a total diameter of the filler/modifier particles of 50-60 nm. For initial impact tests a 3% filler to matrix weight ratio was used. A PMMA latex, synthesized in-house, was used as matrix ($\bar{M}_w$ = 112 867 g/mol, $\bar{M}_w/\bar{M}_n$ = 4.64). The filler and matrix latices were blended and stirred for 10 minutes to ensure homogeneity. To eliminate the influence of surfactant on the impact tests the blend was dialyzed for 1 week by continuous flow of distilled water. Pierce SnakeSkin™ (10,000 MWCO) was used as dialysis tubing and the degree of surfactant removal was monitored by periodic conductivity measurements. The dialyzed blend was subsequently dried and the obtained powder was used for further tests. Commercially available PMMA pellets ($\bar{M}_w$ = 262 543 g/mol, $\bar{M}_w/\bar{M}_n$ = 4.38, Atohaas VO52) were compression moulded to form a polymer matrix. The matrix was used to evaluate the physical properties of a pure PMMA polymer and results were compared to the physical properties of the above mentioned blend.

6.5.2 Compression moulding of powders and pellets and manufacturing of test pieces

Compression moulding of the blends and matrix polymers were done on a PERS hydraulic compression press, with 600 bar pressure limit and equipped with water cooling, at the Laboratory of Polymer Technology (SKT) at the University of Eindhoven. Stainless-steel moulds were used with dimensions 20 × 20 × 2 mm^3. A thin film of tin-foil, Teflon or PET (polyethylene terephthalate) was placed on top of a stainless steel plate after which the mould was directly placed on the film. The purpose of the film is to promote release after the test pieces were formed. The mould cavities were subsequently filled with polymer and again covered with a layer of film and a stainless steel top plate. The packed mould was subsequently transferred to the press, which was slowly closed until contact between the top heating plate of the press and top stainless steel plate of the mould were made. The pre-heated (160 °C) press was left in contact with the mould for 5 minutes to facilitate melting and fusion of the polymer sample, after which the press was completely closed and again left for 5 minutes. After this period the press was repeatedly opened and closed to degas the sample. After degassing, pressure was applied in increments, first to 50 bar, at which point it was again degassed and left for 2 minutes. The pressure was then increased to 100 bar, the sample degassed, and left for 5 minutes. The samples were finally cooled with cold water and removed from the mould.

6.5.3 Test conditions and equipment

Tensile tests were performed at room temperature on a Zwick Z010 universal tensile tester. Dumbbell-shaped test specimens were machined at the Faculty of Mechanical Engineering, Technical University of Eindhoven, and tensile tests were performed at a strain rate of 2 mm/min. For impact tests, notched bars were machined at the Laboratory of Polymer Technology (SKT) at the University of Eindhoven. Fast tensile tests (1 m/s) were performed at room temperature on a Zwick Rel hydraulic tensile machine to obtain sufficient impact data. The piston displacement and force were measured at a sampling rate of 250 kHz using a piezo-electric force transducer. The impact toughness energy

was calculated by integration of the measured force-displacement curve, divided by the initial cross-sectioning area behind the notch.

6.5.4 Analytical techniques

Transmission electron microscopy (TEM)

Samples for TEM were prepared by microtoming the compression moulded blend with a Reichart Ultracut S (Leica, Vienna, Austria) ultramicrotome, with a diamond knife, at ambient temperature, to produce slices with a thickness of 100 nm. The slices were placed on a copper TEM grid and placed on the edges of a Petri dish filled with ruthenium tetroxide. Staining was allowed to continue for 1 hour after which the copper grids were removed and placed in a fume hood to remove excess ruthenium tetroxide vapor. TEM was performed on a JEM - 200CX (JEOL Ltd, Tokyo, Japan) TEM.

6.6 Results and discussion

For physical tests 3 wt% filler to matrix was used to evaluate the toughness enhancement capabilities of the synthesized particles. A comparison between the compression moulded blend (filler and matrix polymer) and matrix polymer can be seen in Figure 6.11.

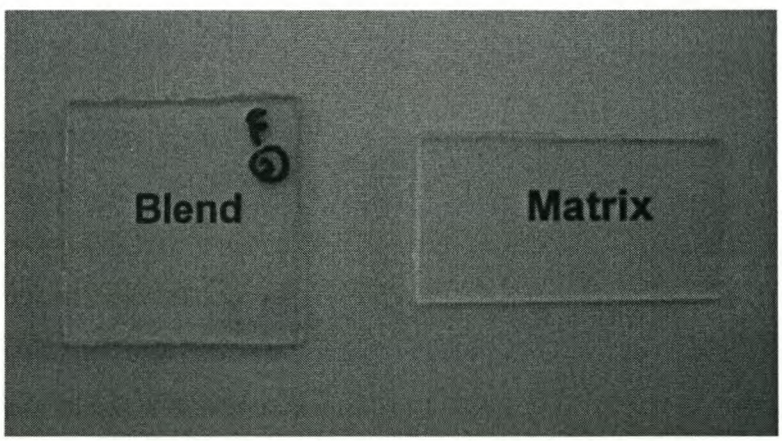

Figure 6.11: Comparison of a compression moulded blend of matrix with 3 % filler particles and compression moulded matrix polymer.

As can be seen from Figure 6.11 the blend sample is completely clear and exhibits similar optical properties to that of the matrix polymer. The degassing step is of vital importance as negligence will lead to the inclusion of tiny air bubbles, which will act as flaws and ultimately lead to catastrophic fractures.

To confirm the inclusion of the filler particles as well as to evaluate the damage to the particles during the compression moulding process, TEM was performed on a slice obtained from the blend test piece. To ensure that the fillers are not just a surface phenomenon, the sample was microtomed continuously to remove the first few microns of surface polymer. Results of this can be seen in Figure 6.12.

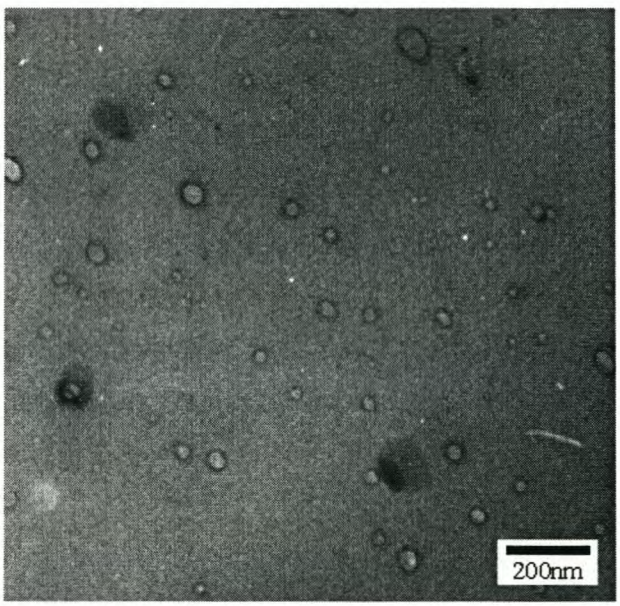

Figure 6.12: TEM image of embedded filler particles in a PMMA matrix.

From the above image it is quite clear that the majority of particle sizes are between 30 and 40 nm, thus in the target size range required for adequate impact modification (Section 6.4). However, larger particles are also present, resulting from the miniemulsion process used to achieve the small particle size. CHDF results described in Chapter 4 confirmed this, as a small fraction of bigger particles was visible in most of the traces.

Interparticle distance can be calculated by

$$ID = D\left[\left(\frac{\alpha\pi}{6V_f}\right)^{\frac{1}{3}} - 1\right] \tag{6.1}$$

where D is the diameter and V_f the volume fraction of the inclusions. α accounts for the stacking of rubber spheres within the matrix and equals 1 (for volume fractions $V_f <$ 40%). This gives an interparticle diameter of 57 nm if the total filler particle size (initial PBA/HD core/shell particle) is taken as 36 nm. According to Van Melick *et al.*[21] this is not the optimum interparticle distance although an improvement in impact resistance is still possible.

Results of tensile tests performed on the matrix and blend are shown in Figure 6.13, with corresponding data values in Table 6.1.

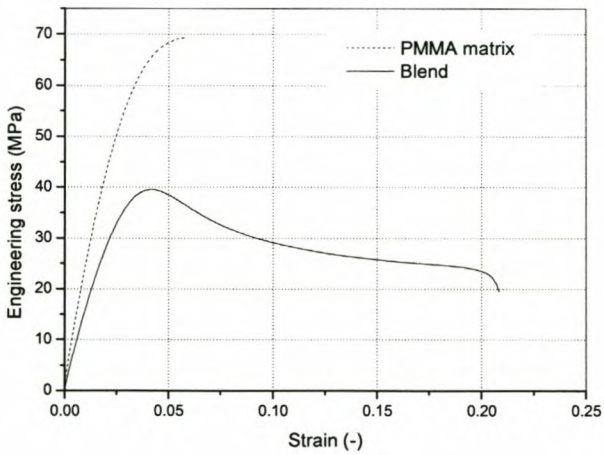

Figure 6.13: Stress-strain curves showing the improved tensile behavior of impact-modified PMMA.

Table 6.1: Numerical values for the stress-strain curves observed in Figure 6.13.

	Matrix	Blend
E mod (MPa)	2065.2559	1383.6786
Stress at yield (MPa)	69.3129	37.8522
Strain at yield	0.057853	0.04123
Strain at break	0.057853	0.20817

From this it is quite clear that the inclusion of the modifier particles has led to a dramatic reduction in the yield stress, from ~69 MPa for the matrix to ~39 MPa for the blend, thus lowering of the strain softening. As a result of this, neck drawing occurs and a ductile deformation is possible. However, insufficient increase in strain hardening is visible, which might be due to inadequate crosslinking of the initial poly(butyl acrylate) rubber shell or the large interparticle distance. In the case of the matrix polymer, no ductile behavior is visible, resulting in brittle failure.

The result of inadequate degassing can be seen in Figure 6.14 for the tensile behavior of the PMMA matrix as well as the blend material. Even though both matrix and blend show premature breakage when compared to Figure 6.13, the ductile behavior of the blend, as a result of the inclusion of the modifier, is still visible. This can be distinguished by the onset of plasticity, which would ultimately have led to a decrease in strain softening and thus an increase in toughening.

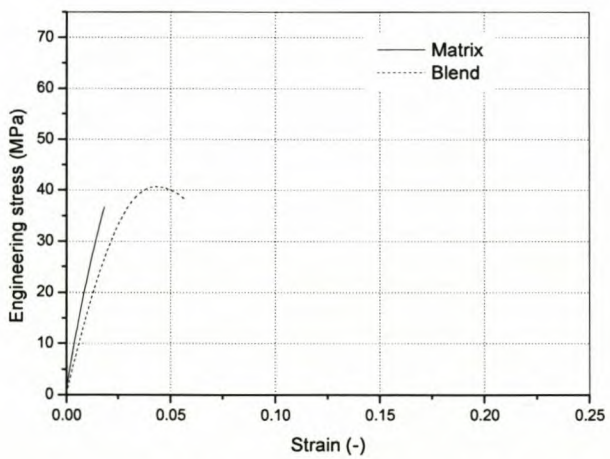

Figure 6.14: The influence of inadequate degassing on the tensile behavior of the PMMA matrix as well as the blend material.

Results of impact tests performed on the PMMA matrix as well as the blend material can be seen in Figures 6.15 and 6.16, respectively, with accompanying data sets in Table 6.2.

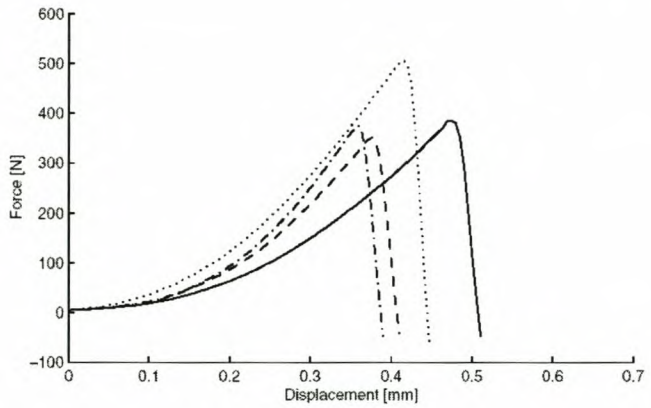

Figure 6.15: Impact tests performed on the PMMA matrix.

From the curves it is quite clear that the inclusion of small defects, as a result of the compression moulding process, plays an important role in obtaining reproducible data. However, although scattering of data exists it is still included to give an indication of the overall trend, which results from impact modification. In both types of samples very low impact energies are obtained. The average value for the blend is only slightly higher compared to that of the matrix, as is the value for the maximum stress.

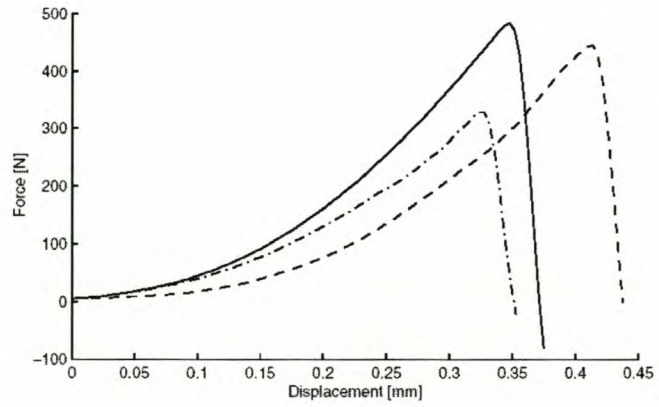

Figure 6.16: Impact tests performed on the blend material.

Table 6.2: Comparison of data obtained from impact tests performed on the matrix polymer and blend.

	Matrix			
	l (mm)	w (mm)	V (m/s)	Is (kJ/m^2)
matrix1	8.15	1.76	1.28	4.8
matrix2	13.55	1.72	1.07	2.1
matrix3	10.77	1.66	1.07	2.67
matrix4	10.86	1.62	1.12	4.73
Avg				3.575
Max stress ~ 22.945 MPa				
	Blend			
	l (mm)	w (mm)	V (m/s)	Is (kJ/m^2)
blend1	10.91	1.63	0.97	3.65
blend2	9.68	1.62	0.99	3.97
blend3	8.28	1.63	1.04	3.15
Avg				3.59
Max stress ~ 26.6133 MPa				

Due to an insufficient number of impact tests performed as well as the presence of defects, the author would not like to make any decisive conclusions on the improvement of impact, of the investigated systems, before more tests can be carried out. However, from the initial experiments carried out, although few, it is quite certain that a direct influence on the macroscopic properties of the matrix material is evident as a result of the inclusion of the modifier particles. True impact improvement is only expected if optimum spacing of the particles can be obtained.

6.7 Conclusions

Modifier particles can successfully be included in the matrix polymer as shown by visual images of the processed material as well as TEM images of microtomed samples. This proved that the inclusions did not affect the optical clarity of the matrix polymer and that particles were still intact. Additionally, the TEM images confirmed the interparticle distance, which showed that the percentage of modifier particles used could be increased. However, inclusion into a brittle polymeric matrix proved to be successful as this polymer showed ductile behavior under tensile stress, thus effectively lowering the yield stress and consequently resulting in neck drawing taking place. However, impact tests

showed a scattering of data, which is a result of the inclusion of defects (*e.g.* air bubbles as well as the method of sample preparation). Nevertheless, the average impact strength data, as obtained from the modified matrix, still showed the possibility of increased impact resistance and toughening. Thus, although there is still room for improvement, initial results already show a significant improvement in polymer properties, which can therefore form the basis to establish novel research projects carrying on from the foundations that have been laid by this present research initiative.

References

(1) Jansen, B. J. P.; Tamminga, K. Y.; Meijer, H. E. H.; Lemstra, P. J. *Polymer* **1999**, *40*, 5601-5607.

(2) Bucknall, C. B. *Toughened Plastics*; Applied Science: London, 1977.

(3) Lovell, P. A.; McDOnald, J.; Saunders, D. E. J.; Young, R. J. *Polymer* **1993**, *34*, 61-69.

(4) Jansen, B. J. P. *Toughening of Glassy Amorphous Polymers via Chemically-induced Phase Separation*, Technische Universiteit Eindhoven, Eindhoven, 1998, 104.

(5) Lovell, P. A.; Pierre, D. In *Emulsion Polymerization and Emulsion Polymers*; Lovell, P. A.; El-Aasser, M. S., Eds.; John Wiley & Sons Ltd.: Chichester, 1997; pp 657-695.

(6) Meijer, H. E. H. Eindhoven University of Tehnology, Mechanical Engineering, Materials Technology (ma*te*), PO Box 513, 5600 MB Eindhoven, The Netherlands. http://www.mate.tue.nl/mate/showemp.php/4.

(7) Jansen, B. J. P.; Rastogi, S.; Meijer, H. E. H.; Lemstra, P. J. *Macromolecules* **1999**, *32*, 6290-6297.

(8) Van Melick, H. G. H.; Govaert, L. E.; Meijer, H. E. H. *Polymer* **2003**, *44*, 3579-3591.

(9) Van Melick, H. G. H.; Bressers, O. F. J. T.; Den Toonder, J. M. J.; Govaert, L. E.; Meijer, H. E. H. *Polymer* **2003**, *44*, 2481-2491.

(10) Van Melick, H. G. H.; Govaert, L. E.; Meijer, H. E. H. *Polymer* **2003**, *44*, 2493-2502.

(11) Jansen, B. J. P.; Rastogi, S.; Meijer, H. E. H.; Lemstra, P. J. *Macromolecules* **2001**, *34*, 3998-4006.

(12) Jansen, B. J. P.; Rastogi, S.; Meijer, H. E. H.; Lemstra, P. J. *Macromolecules* **1999**, *32*, 6283-6289.

(13) Jansen, B. J. P.; Rastogi, S.; Meijer, H. E. H.; Lemstra, P. J. *Macromolecules* **2001**, *34*, 4007-4018.

(14) Smit, R. J. M. *Toughness of Heterogeneous Polymeric Systems: A Modeling Approach*, Technische Universiteit Eindhoven, Eindhoven, 1998, 103.

(15) Smit, R. J. M.; Brekelmans, W. A. M.; Meijer, H. E. H. *J. Mater. Sci.* **2000**, *35*, 2855-2867.

(16) Smit, R. J. M.; Brekelmans, W. A. M.; Meijer, H. E. H. *J. Mater. Sci.* **2000**, *35*, 2869-2879.

(17) Smit, R. J. M.; Brekelmans, W. A. M.; Meijer, H. E. H. *J. Mater. Sci.* **2000**, *35*, 2881-2893.

(18) Ishikawa, M.; Sato, Y.; Higuchi, H. *Polymer* **1996**, *37*, 1177-1181.

(19) Govaert, L. E.; Van Melick, H. G. H.; Meijer, H. E. H. *Polymer* **2001**, *42*, 1271-1274.

(20) Meijer, H. E.; Govaert, L. E.; Smit, R. J. M. In *ACS Symposium series*; Pearson, R. A.; Sue, H.-J.; Yee, A. F., Eds.; American Chemical Society: Washington DC, 2000; Vol. 759, pp 50-70.

(21) Van Melick, H. G. H.; Govaert, L. E.; Meijer, H. E. H. *Polymer* **2003**, *44*, 457-465.

Chapter 7

Conclusions and recommendations

7.1 Conclusions

The requirements to effectively impact modify glassy amorphous polymers led to the original proposal of this thesis. The macroscopic behavior of a glassy polymer is related to its microstructure, thus leading to preconceived ideas of what an effective modifier particle should look like. This ultimately led to the suggestion to synthesize nanoparticles with specific dimensions, morphology and composition, i.e. a 30 nm core/shell particle with a rubbery shell and liquid core. The main focus of this work was therefore to predict particle morphology based on the chemical precursor selection, to synthesize structured nanoparticles, to determine the morphological structure, *e.g.* core/shell, acorn or inverted core/shell, to control the molecular architecture of the shell polymer and to test the ability of the synthesized particles to strengthen glassy amorphous polymers.

In Chapter 3 the synthesis of core/shell particles with liquid cores is described. The actual syntheses were preceded by morphology predictions of polymer/oil combinations as proposed by previous researchers.[1-3] This revealed the inability of the morphology prediction models to predict the correct morphology, which was a direct effect of the thermodynamic considerations that these models were based on. Due to the fact that structured particles were being formed *in situ*, the selected polymerization conditions and precursors lead to the escalation of kinetic influences. This dominated the thermodynamic aspects of the polymerization reaction and caused thermodynamically unfavorable structures to exist. To evaluate this further, the influence of initiating species on the outcome of particle morphology was studied. This showed that surface anchoring, which is dictated by the interaction between initiating species (chains that carry a sulfate

endgroup, which will exhibit surfactant-like properties) and surfactant, plays a significant role in establishing the locus of polymerization. Furthermore, the rate of polymerization, and the subsequent viscosity of the polymerized media, will determine the ease with which these anchored species can diffuse into the droplet and therefore the ability to confine the locus of polymerization. At high interfacial viscosity, monomer depletion will take place from the inside of the droplet to form the polymeric shell and ultimately result in the core-liquid to be encapsulated. To confirm the above, a redox initiator was used to induce initiation as well as a rapid increase in viscosity and compared with AIBN. AIBN, which is not surface active, showed that the thermodynamically predicted particles, i.e. particles which have inverted core/shell morphology, can be obtained. However, the redox species produced core/shell structures, which pointed to and confirmed kinetic influences. Reasoning for kinetic influences was further strengthened by various literature reports on the diffusional resistance of long- versus short-chains, distribution of free radicals in a droplet and the influence of the repulsive wall effect.

It was also shown that a secondary polymeric shell could be grafted onto the initially synthesized particles, thus enabling the particles to be strengthened for destructive analyses, to prevent coalescence during processing and to obtain sufficient interaction with the matrix material. TEM and AFM confirmed the existence of core/shell particles with the required morphology. The work described in this chapter, most particularly the encapsulation of a liquid core with a primary rubber and secondary glassy shell, is considered as reasonably novel.

In Chapter 4 the preferred particle size for the core/shell particles was established by using a miniemulsion polymerization reaction. By changing the surfactant concentration it was found that the desired particle size and stability could be obtained. Particle size of the initial as well as the grafted core/shell particles were measured by CHDF and showed excellent comparison with particle size as obtained from TEM. Furthermore, the stability of the particles was investigated by stoichiometrically calculating the droplet area, which is being stabilized per surfactant molecule. Additional surface tension measurements also confirmed the stoichiometric results for a nearly dense surfactant packing. Results

obtained, i.e. particle size and stability as a function of surfactant concentration, showed excellent comparison with those of "classical" miniemulsion experiments and thus meets the criteria for a miniemulsion reaction. The addition of a short-chain alcohol (as costabilizer) to the miniemulsified dispersion was also investigated. Results showed that it can influence the particle size by decreasing the dissociation of the emulsifier, therefore altering the aggregate size. To conclude this chapter, the possibility of scaling up the reaction volume was investigated and proved to be successful for the investigated system by retaining the particle morphology and dimensions.

As a consequence of the results obtained in Chapter 3, the merging of controlled morphology and living/controlled polymerization was considered possible. In Chapter 5 RAFT agents were used to impart living/controlled characteristics to a core/shell latex system consisting of model compounds (styrene as shell material and isooctane as core material). However, as the RAFT agents are chain transfer agents, transfer, albeit to monomer or RAFT agent, would take place inside a monomeric droplet. This would result in polymerization taking place throughout the entire volume of the droplet, resulting in the thermodynamically predicted morphology. However, by effectively controlling the rate of polymerization as well as the anchoring of the entering oligomeric species it was shown that the kinetically favored morphology could also be obtained. To evaluate this, RAFT species that show different extents of retardation were used in conjunction with KPS, as surface-active initiating species, and AIBN, as surface inactive initiating species. Results of the miniemulsion experiments with the aforementioned RAFT/initiator combinations showed that in order to obtain the kinetically favored morphology, surface anchoring of the entering oligomeric radical species must take place by using a surface-active initiating species. This must, however, be done in conjunction with a RAFT agent exhibiting low retardation in chain growth rate, i.e. a RAFT agent that will show fast polymerization kinetics. The high polymerization rate will ensure that a rapid increase in viscosity will take place at the droplet/water interface, thus locking in the polymerization locus and therefore leading to the desired core/shell morphology.

As a result of the synthesis of core/shell particles with living characteristics in a miniemulsion system, the influence of secondary nucleation could, for the first time, be visualized by TEM. The morphology of the secondary nucleated particles was thermodynamically controlled (solid particles), thus allowing them to be differentiated from the kinetically controlled particles, which had core/shell morphology.

This chapter was concluded by changing back to the monomer/oil system as used in Chapter 3. Due to the fact that a monomer with a high propagation rate was now used, it was found that RAFT agents with increased retardation in chain growth could be used. The combination (slower RAFT and faster monomer) would still be sufficient to establish a rapid increase in viscosity and preferential polymerization of the mediated species at the droplet/water interface. Chain extensions were also successfully performed to be able to cap the initial PBA/HD core/shell particles with a glassy shell consisting of PMMA. This allowed characterization by destructive analytical techniques and the visualization of the formed core/shell particles to be carried out. This chapter is in its entirety completely novel.

Chapter 6 described the physical testing of the PBA/HD core/shell particles as synthesized in Chapter 3. Particles were successfully incorporated into a glassy polymeric matrix (PMMA), by compression moulding, as was shown by TEM of microtomed samples. The compression moulded blend showed optical clarity and compared well with the compression moulded matrix. Tensile tests performed on the blend indicated a ductile behavior of the sample, which is a result of the decrease in strain softening and yield stress. This pointed to an improvement over the matrix polymer, which showed brittle failure. Impact tests pointed to an improvement in the impact behavior of the blend sample. These initial results showed that improvement in the impact behavior of glassy polymers is possible with the inclusion of nanoparticles with the desired morphology.

7.2 Recommendations

Although the research goals of this study were achieved, the routes followed during the research initiative led to quite a number of possible recommendations. These recommendations can lead to an increase in the commercial value of the project as well as to contribute to future research efforts based on this or similar work.

As mentioned in Chapter 3, various morphology prediction models have evolved based on either thermodynamic or kinetic considerations. Few attempts have been made to unite these two, equally important, considerations in order to establish a prediction model for all types of reaction methods. Such a model should include surface activity of species, viscosity of the investigated system as a function of reaction time, diffusion or diffusional resistance and exit of species, transfer effects and repulsive wall effects. However, it should also include the influence of interfacial tensions of the chemical precursors, thus including the thermodynamic component.

If the commercial value of the synthesized nanoparticles is considered, then the synthesis procedure will have to be adapted. Particle size and morphology was established by ultrasonication of the latex sample. However, this is usually associated with a few disadvantages, *e.g.* excessive heat generated, broad polydispersities and limited sample quantities. These problems can be overcome by the use of a microfluidizer where larger sample quantities are easily handled without heat build-up. This also leads to a dramatic reduction in the polydispersity of the particles.

Seeing that Chapter 5 is entirely novel, quite a few aspects have evolved from this study although only two will be mentioned here. First of all the presence of secondary nucleation must further be investigated. This can be done by comparing the size distribution of the particles with the molar mass of the evolved polymer. This will give accurate evidence of the nature of secondary nucleation. However, to do this, intricate coupling techniques will have to be developed in order to thoroughly analyze samples in

both size and mass respects. Chain extensions, i.e. the formation of a secondary block, in heterogeneous media are also still being investigated.

As only initiatory tests were performed on the synthesized structured particles, more definite experiments can be planned in future studies. These include the investigation of the percentage of incorporated filler particles on impact and tensile modifications, more experiments to eliminate unnecessary data scattering, variation of the speed of testing, study of the influence of the cavity oil, effect of the degree of crosslinking of the PBA shell and SANS/SAXS studies on the deformation process. All of the above will ensure that more information is obtained about the deformation process, which will definitely benefit future studies in impact modification of glassy polymers.

References

(1) Torza, S.; Mason, S. G. *J. Colloid Interface Sci.* **1970**, *33*, 67-83.

(2) Waters, J. A. In *Colloidal Polymer Particles*, Second ed.; Goodwin, J. W.; Buscall, R., Eds.; Academic Press Limited: London, 1995; pp 113-135.

(3) Waters, J. A. *Colloids Surf., A* **1994**, *83*, 167-174.